

UNIVERSITÄTSKLINIKUM HAMBURG-EPPENDORF

Klinik und Poliklinik für Unfallchirurgie und Orthopädie
Experimentelle Unfallchirurgie

Prof. Dr. Karl-Heinz Frosch

Roles of Calcitonin Family of Peptides in Degenerative Musculoskeletal Diseases

Dissertation

zur Erlangung des Doktorgrades PhD
an der Medizinischen Fakultät der Universität Hamburg.

vorgelegt von:

Shan Jiang
aus Zibo, China

Hamburg 2024

**Angenommen von der
Medizinischen Fakultät der Universität Hamburg am: 13.12.2024**

**Veröffentlicht mit Genehmigung der
Medizinischen Fakultät der Universität Hamburg.**

Prüfungsausschuss, der/die Vorsitzende: Prof. Dr. Dr. Johannes Keller

Prüfungsausschuss, zweite/r Gutachter/in: Prof. Dr. Thorsten Schinke

Table of Contents

Table of Contents	3
1. Introduction	6
1.1. Bone.....	6
1.1.1. Bone modeling and remodeling	6
1.1.2. Osteoblast.....	9
1.1.3. Osteoclast.....	12
1.2. Calcitonin family of peptides in bone	15
1.2.1. Calcitonin and procalcitonin	16
1.2.2. Calcitonin gene-related peptide alpha.....	20
1.2.3. Amylin	22
1.3. Degenerative musculoskeletal diseases and calcitonin family of peptides ..	25
1.3.1. Osteoarthritis.....	25
1.3.2. Role of <i>CALCA</i> -encoded peptides in OA	28
1.3.3. Osteoporosis.....	29
1.3.4. Role of calcitonin family of peptides in osteoporosis.....	32
2. Hypothesis and Objectives	34
3. Material and Methods	35
3.1. Material	35
3.1.1. Chemical and reagents	35
3.1.2. Buffers and solutions	37
3.1.3. Equipment.....	39
3.1.4. Consumables.....	41
3.1.5. Primers.....	42
3.1.6. Commercial Kits.....	43
3.1.7. Softwares	43
3.2. Methods	43
3.2.1. Mice	43
3.2.2. Study design	46
3.2.3. Sample preparation.....	47
3.2.4. X-ray microtomography (μ CT) evaluation	47

3.2.5. Histology	48
3.2.6. Gene expression analysis	54
3.2.7. ELISA.....	54
3.2.8. Primary osteoclast isolation and differentiation	55
3.2.9. Cell culture	55
3.2.10. RNA sequencing and transcriptome analysis.....	55
3.2.11. Statistics.....	56
4. Results.....	57
4.1. <i>PCT/CT</i> transcripts protect from cartilage deterioration and subchondral bone loss, while α CGRP is a potent driver of osteophyte formation.....	57
4.1.1. The expression of both the <i>PCT/CT</i> and the α CGRP transcript is induced during ptOA progression	57
4.1.2. The inactivation of the <i>PCT/CT</i> transcript aggravates ACLT-induced cartilage degeneration	59
4.1.3. Abnormal subchondral bone architecture in <i>CALCA</i> - but not α CGRP-deficient mice	61
4.1.4. Lack of the <i>PCT/CT</i> transcript is associated with indices of increased bone resorption in the subchondral joint compartment	62
4.1.5. Tibial osteophyte formation in ptOA is critically promoted by α CGRP signaling.....	64
4.1.6. Reduced synovitis in <i>CALCA</i> - but not α CGRP-deficient mice.....	65
4.2. Calcitonin receptor signaling is involved in osteophyte formation during the course of ptOA	66
4.2.1. The expression of <i>Calcr</i> is upregulated during ptOA progression	67
4.2.2. Inactivation of CTR does not affect ACLT-induced cartilage degeneration	67
4.2.3. <i>CTR</i> ^{-/-} mice exhibit similar subchondral trabecular bone deterioration to WT animals	69
4.2.4. Deficiency of CTR does not affect bone metabolism parameters in the subchondral joint compartment.....	71
4.2.5. Decreased osteophyte formation in ptOA in <i>CTR</i> ^{-/-} mice	72
4.2.6. Synovitis induced by ptOA is not affected by the deficiency of CTR....	74
4.3. Osteoporosis-induced bone loss is alleviated by pramlintide in a CTR-dependent manner	75
4.3.1. Pramlintide restores OVX-induced trabecular bone loss in the spine of WT mice but not of <i>CTR</i> ^{-/-} mice.....	75
4.3.2. Pramlintide exerts a beneficial effect on OVX-induced bone loss in the distal femur of WT mice but not <i>CTR</i> ^{-/-} mice.	77

4.3.3. Excessive bone resorption is restored by pramlintide treatment in WT but not <i>CTR</i> -deficient mice	79
4.3.4. Pramlintide inhibits osteoclastogenesis in a <i>CTR</i> -dependent manner .	80
5. Discussion.....	84
6. Summary	91
7. Zusammenfassung	93
8. List of abbreviations	95
9. References	99
10. Acknowledgements	114
11. Curriculum Vitae	115
12. Eidesstattliche Erklärung	118

1. Introduction

1.1. Bone

Bone is a highly specialized connective tissue composed of collagen fibers and inorganic mineral crystals. Bone performs multiple physiological functions, including providing mechanical support for load bearing and muscular contraction, forming physical protection for internal organs, maintaining a dynamic reservoir of essential minerals, and offering environmental support for hematopoiesis. Bone is a highly dynamic tissue that undergoes a continuous remodeling process performed by an exquisite duet consisting of osteoblast-mediated bone formation and osteoclast-mediated bone resorption throughout the lifespan. Bone-forming osteoblasts originate from mesenchymal stem cells, depositing calcium and phosphate crystals into osteoid, an organic matrix containing collagens and proteins to form mineralized bone (Ono, Ono, Nagasawa, & Kronenberg, 2014). Whereas osteoclasts, derived from hematopoietic lineage, secrete massive hydrochloric acid to dissolve bone minerals and multiple proteinases to degrade collagen matrix, resulting in a reduction of bone mass and release of calcium and phosphorus ions into circulation (Ponzetti & Rucci, 2021).

The delicate balance between bone resorption and formation maintains bone integrity by replacing old and damaged bone with new bone, contributing to a dynamic bone architecture that accommodates the growing organism's mechanical stress, known as bone modeling and remodeling (Bonewald, 2011). Various systemic and local factors regulate these processes. Under certain pathological conditions, for instance, postmenopausal, aging, or trauma, the precise regulation is disturbed, and the balance between bone anabolism and catabolism is upset, leading to alterations in bone architecture and mineral density, such as osteoporosis or osteopetrosis.

1.1.1. Bone modeling and remodeling

1.1.1.1. Bone modeling

Bone undergoes modeling and remodeling throughout the lifespan. Bone modeling represents the process by which bone reconfigures the structure or reforms the overall shape in response to physiological influences or mechanical loading (Frost, 1994). Alterations in the trabecular arrangement pattern and the mechanical axis occur to adapt to the biomechanical forces by the removal or accretion of bone on the

respective site by independent activation of osteoblasts and osteoclasts. Modeling of bone also occurs during aging, revealed by the diametric growth of long bones caused by periosteum-mediated bone formation and endosteal resorption of old bone. In adults, bone modeling occurs less often than bone remodeling (Kobayashi et al., 2003).

1.1.1.2. Bone remodeling

In adults, the skeleton is completely renewed every 10 years through bone remodeling (Langdahl, Ferrari, & Dempster, 2016). Bone remodeling is a cyclical lifelong process by which bone is renewed to preserve integrity and maintain mineral homeostasis. The bone remodeling unit is a group of osteoclasts and osteoblasts that sequentially resorb old or damaged bone and replace it with a newly formed proteinaceous matrix that is subsequently mineralized to form new bone (Camozzi et al., 2007). Remodeling occurs at random sites as well as at specific locations in need of replacement. The remodeling cycle comprises several overlapping phases: activation, resorption, reversal, formation, and termination (**Figure 1**).

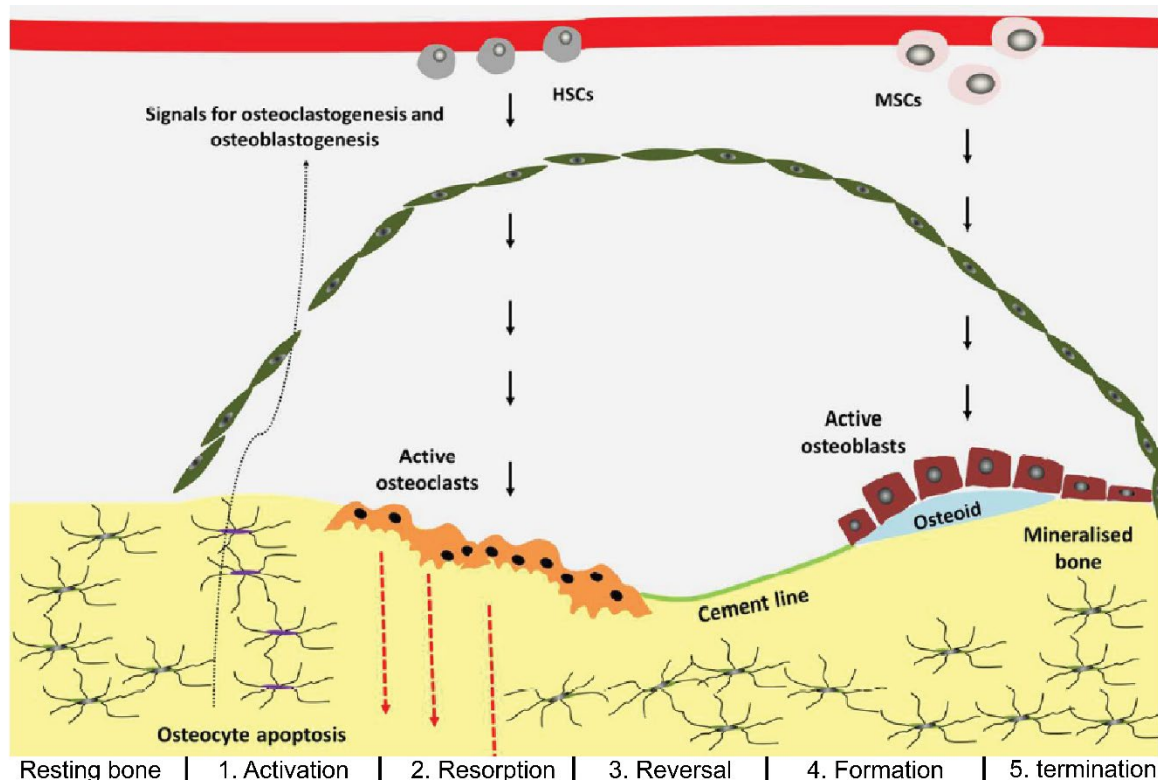


Figure 1. Different phases of bone remodeling cycle. Schematic diagram of the bone remodeling cycle illustrating the phases of activation, resorption, reversal, formation and termination. Osteoclasts and osteoblasts, derived from haemopoietic stem cells (HSCs) and mesenchymal stem cells (MSCs), respectively, are recruited to the bone surface upon initial signaling for bone remodeling. Osteoclasts form a sealing zone with a ruffled border to degrade bone, while osteoblasts synthesize a collagen-rich

matrix known as osteoid, followed by deposition of crystal minerals and thereby the formation of new bone. Figure modified according to (Kenkre & Bassett, 2018).

First, in the activation phase, monocytes from the circulation are recruited to the remodeling sites. Meanwhile, the bone lining cells form a canopy over the remodeling site to expose the underlying bone. Osteoclast precursors are activated and fuse to form multinucleated osteoclasts that attach to the bone surface and form sealing zones around bone-resorbing compartments (Hauge, Qvesel, Eriksen, Mosekilde, & Melsen, 2001). The initiating signal for remodeling at specific sites derives from osteocytes and is transmitted through their extensive network of dendritic processes, whereas hormones that maintain circulating calcium homeostasis, such as parathyroid hormone (PTH) and calcitonin (CT), also contribute to the initiation of bone remodeling (Atkins & Findlay, 2012; Goldring, 2015; Tatsumi et al., 2007).

Following the adherence of osteoclasts to the bone surface, the resorption phase starts with the formation of a ruffled border of osteoclasts to expand the contact surface to bone. Then, hydrogen ions are secreted into the lacunae by osteoclasts via H^+ -ATPase proton pumps, which lowers the pH in the sealing zone to help mobilize minerals, accompanied by the release of various proteinases such as tartrate-resistant acid phosphatase (TRAP), matrix metalloproteinases and cathepsin K to degrade the bone matrix (Silver, Murrills, & Etherington, 1988; Tolar, Teitelbaum, & Orchard, 2004). Afterwards, mature osteoclasts undergo apoptosis, and the resorption process terminates.

In the reversal phase, the bone-forming osteoblasts are recruited at the resorption sites, and bone formation is initiated. To improve subsequent osteoblastic adherence, the unmineralized collagen matrix is removed and a non-collagenous mineralized matrix, known as “cement line”, is formed on the bone surface (Zhou, Chernetky, & Davies, 1994). The exact signaling that mediates the reversal phase remains unclear. A mechanical adaptation theory has been proposed to drive bone formation in the resorption pit (Smit, Burger, & Huyghe, 2002). The resorption of bone generates a strain gradient in lacunae and induces an enhanced extracellular fluid flow. Osteocytes sense such changes and recruit osteoblasts. However, other studies suggested that

osteoclasts and bone-lining cells are involved in transmitting these signals (Delaisse, 2014; Everts et al., 2002; Zhou et al., 1994).

Bone formation is characterized by the synthesis of a new collagen-rich matrix, known as osteoid, and the mineralization of osteoid (Atkins & Findlay, 2012). Osteoid consists of an interwoven network of type I collagen and other matrix proteins and serves as a template for mineral crystal deposition. Osteoblasts regulate the mineralization of osteoid by releasing vesicles containing concentrated calcium and phosphate (Anderson, 2003; Anderson, Garimella, & Tague, 2005). Systemic mineral concentrations also affect the mineralization of bone matrix (Murshed, 2020). At the end of the bone forming phase, some osteoblasts are incorporated as osteocytes in the mineralized bone matrix, and the rest either transform into bone-lining cells, an inactivated form of osteoblasts, or undergo apoptosis (Franz-Odenaal, Hall, & Witten, 2006). The production of a new osteon represents the termination of a bone remodeling cycle.

1.1.2. Osteoblast

Osteoblasts, accounting for 4-6% of total bone resident cells, originate from multipotent mesenchymal stem cells (MSCs), which also give rise to various cells such as chondrocytes, adipocytes, and myoblasts (Phinney & Prockop, 2007). Morphologically, osteoblasts are cuboidal cells with basophilic cytoplasm and are usually found lying on the newly formed bone surface in small groups (Rutkovskiy, Stensl kken, & Vaage, 2016). The differentiation of osteoblasts is initiated when a need for bone modeling or regeneration is detected. The primary commitment of MSCs to the osteoblastic lineage, as well as the subsequent maturation of osteoblasts, is regulated by a number of critical signaling pathways and transcription factors (**Figure 2**).

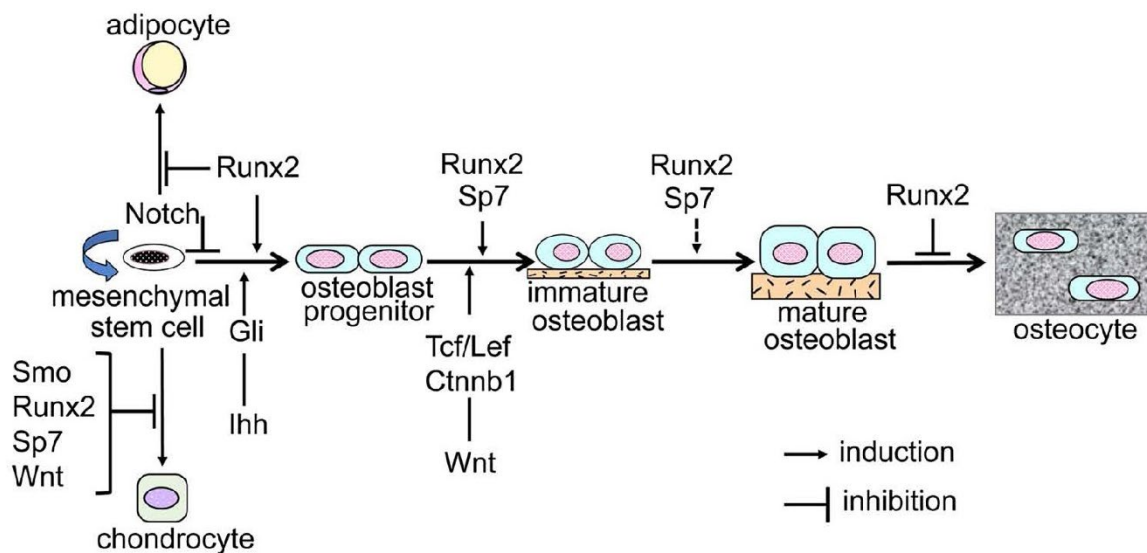


Figure 2. Primary commitment of mesenchymal stem cells to osteoblastic lineage and regulation of osteoblast differentiation. Runt-related transcription factor 2 (Runx2) induces the commitment of mesenchymal stem cells to osteoblasts but inhibits adipocyte and chondrocyte differentiation. Transcription factor Sp7 (SP7) and Wnt-signaling also inhibit chondrocyte differentiation. Runx2 and SP7 are required throughout the whole course of osteoblast differentiation, while Runx2 inhibits mature osteoblasts to transform into osteocytes. Wnt-signaling regulates the early stage of osteoblast differentiation. Figure modified according to (Komori, 2018).

1.1.2.1. Runt-related transcription factor 2 (Runx2)

Runx2 is a key transcription factor in osteoblast differentiation and chondrocyte maturation. Cells expressing Runx2 are defined as preosteoblasts and commit to osteoblastic differentiation (Komori et al., 1997). A modest expression of Runx2 was noticed in uncommitted mesenchymal cells, increasing along the course of differentiation and attaining maximum in immature osteoblasts, and being downregulated in mature osteoblasts. Komori et al. demonstrated the role of Runx2 in osteoblast differentiation using genetically modified mice (Komori et al., 1997). In newborn mice, heterozygous deficiency of Runx2 resulted in impaired ossification in the clavicles and the cranium, while the cartilage development was not affected. Homozygous mutant mice exerted a complete lack of ossification during embryonic development. On a cellular level, osteoblasts from the knockout mice exhibited decreased alkaline phosphatase (ALP) expression and barely detectable osteocalcin and osteopontin. Further studies demonstrated the critical role of Runx2 in late-stage osteoblast differentiation and chondrocyte maturation (Komori, 2019; Maeno et al.,

2011). Using *Runx2* transgenic mice under the control of the paired related homeobox 1 (*Prrx1*) promoter, *Runx2* expression was induced in mesenchymal cells before the onset of bone development. Early onset of *Runx2* expression resulted in calcification of parietal bone, premaxilla, and temporal bone on E13.0, when no calcification was observed in wild type (WT) mice, and an early closure of sutures and fontanelles on E18.5. These observations suggest that *Runx2* is sufficient to commit mesenchymal cells into osteoblastic differentiation and induce intramembranous bone formation, indicating *Runx2* to be the most upstream molecule in osteoblast differentiation.

1.1.2.2. Wnt/ β -catenin signaling pathway

Wnt-signaling is involved in multiple stages of osteoblast differentiation. Several possible patterns of signaling transduction were demonstrated, one of which termed the canonical signaling pathway plays a fundamental role in osteoblast differentiation. Extracellular Wnt ligands interact with Wnt receptors, leading to disruption of β -catenin degradation and thereby accumulation of cytoplasmic β -catenin (Karner & Long, 2017). β -catenin then translocates into the nucleus to bind to transcription factors T-cell factor/lymphoid enhancer factor (Tcf/Lef), resulting in the transcription of downstream genes such as *Runx2* and *Sp7* (Gaur et al., 2005; Glass et al., 2005). Mice lacking low-density lipoprotein receptor-related protein 5 (Lrp5), a vital component of the Wnt receptor, exerted an osteopenic bone phenotype, whereas Lrp5 knock-in either ubiquitously or in osteocytes resulted in an increased bone mass associated with enhanced bone formation rate (Y. Cui et al., 2011; Kato et al., 2002).

1.1.2.3. Osterix

Osterix (*Osx*, also *Sp7*), a zinc finger transcription factor, is required for proper bone formation. *Osx*-deficient mice exhibited no bone formation with unaffected expression of *Runx2*, suggesting *Osx* to be downstream of *Runx2* (Nakashima et al., 2002). Furthermore, the expression of bone formation markers, including sialoprotein, osteonectin, and osteopontin was not detected in mice lacking *Osx*. *Osx* promotes osteogenesis by regulating multiple downstream factors, including alpha-1 type I collagen (*Col1a1*), dickkopf-related protein 1 (*Dkk1*), osteocalcin, and fibromodulin (Niu et al., 2017; Ortuño, Susperregui, Artigas, Rosa, & Ventura, 2013; Y. Yang, Huang, Zhang, & Zhang, 2016). Overexpression of *Osx* in bone marrow stromal cells promotes osteoblastic differentiation evidenced by increased proliferation, elevated alkaline

phosphatase activity, and enhanced formation of bone nodules (Tu, Valverde, & Chen, 2006).

1.1.3. Osteoclast

To date, osteoclasts are the only known cells that specifically resorb bone. They are highly specific multinucleated phagocytic cells derived from hematopoietic stem cells formed by fusion of mononuclear precursors (Jacome-Galarza et al., 2019). Mature osteoclasts form a specialized cell membrane, known as a ruffled border, which maximizes the surface area through which hydrogen ions are released, thereby enhancing the demineralization and degradation of bone matrix (Udagawa et al., 2021). Following the formation of a ruffled border, large quantities of TRAP, a marker enzyme for the osteoclast, and hydrolytic enzymes are released to the sealed microenvironment to degrade the bone matrix.

Appropriate bone resorption is of great importance in maintaining bone integrity and mineral homeostasis, whereas pathologically, excessive bone resorption caused by the dysfunction of osteoclasts occurs in osteoporosis, inflammatory diseases, and bone infection. A number of factors regulate the formation and function of osteoclasts. After noticing that osteoclast formation is greatly promoted in co-culture with osteoblasts, several osteoblast-mediated signaling pathways, namely receptor activator of NF- κ B ligand (RANKL) and subsequently identified RANKL/receptor activator of NF- κ B (RANK)/osteoprotegerin (OPG) signaling, were found to regulate osteoclast formation and activity. In addition, multiple hormones and growth factors play essential roles in the recruitment and maturation of osteoclasts.

1.1.3.1. RANK/RANKL/OPG signaling pathway

RANK, a homotrimeric transmembrane protein member of the tumor necrosis factor receptor superfamily, is expressed in osteoclast precursors and mature osteoclasts (Udagawa et al., 2021). RANKL and its decoy receptor OPG, are two key regulators of osteoclastogenesis with opposing effects secreted by osteoblasts and osteocytes (**Figure 3**). Activation of RANK by binding RANKL facilitates preosteoclast differentiation, osteoclast adherence to the bone surface, and their resorbing activity. In mouse spleen cells, the presence of RANKL induced the formation of osteoclasts, evidenced by an increased number of TRAP-positive multinucleated cells and enhanced ^{125}I -labelled CT binding capacity (Yasuda et al., 1998). Similar observations

were also made in osteoclast progenitors. Soluble RANKL directly induced the formation of mature osteoclasts in a dose-dependent manner in the presence of macrophage colony-stimulating factor (M-CSF) (Motiur Rahman et al., 2015).

On the contrary, OPG suppresses osteoclastogenesis by regulating RANKL/RANK signaling. OPG competitively binds to RANKL with a higher affinity than RANK, thus inhibiting osteoclastogenesis (Motiur Rahman et al., 2015; Simonet et al., 1997). Hepatic expression of OPG in transgenic mice resulted in a remarkable osteopetrosis, accompanied by a decreased osteoclast differentiation. Administration of recombinant OPG increased bone mineral density in WT mice and protected rats against ovariectomy-induced bone loss (Ominsky et al., 2008). Later, Yasuda et al. confirmed that OPG inhibited osteoclast differentiation by directly binding to RANKL and eventually interrupting RANKL/RANK signaling and suppressing osteoclastogenesis (Yasuda et al., 1998). As OPG and RANK competitively bind to RANKL, the ratio of RANKL to OPG has been used as an indicator of bone resorption (Kostenuik, 2005; Ominsky et al., 2008; Yuan et al., 2016). In mice, age-related bone loss is associated with an increased RANKL/OPG ratio. In humans, an increased RANKL/OPG ratio was observed in myeloma, osteolysis, hip fractures, and other non-skeletal diseases such as systemic lupus erythematosus, periodontitis and temporomandibular joint disorders (Abdallah et al., 2005; Ali et al., 2019; Chen et al., 2019; Giuliani, Bataille, Mancini, Lazzaretti, & Barillé, 2001; Grimaud et al., 2003; Teodorescu et al., 2019; Wakita, Mogi, Kurita, Kuzushima, & Togari, 2006).

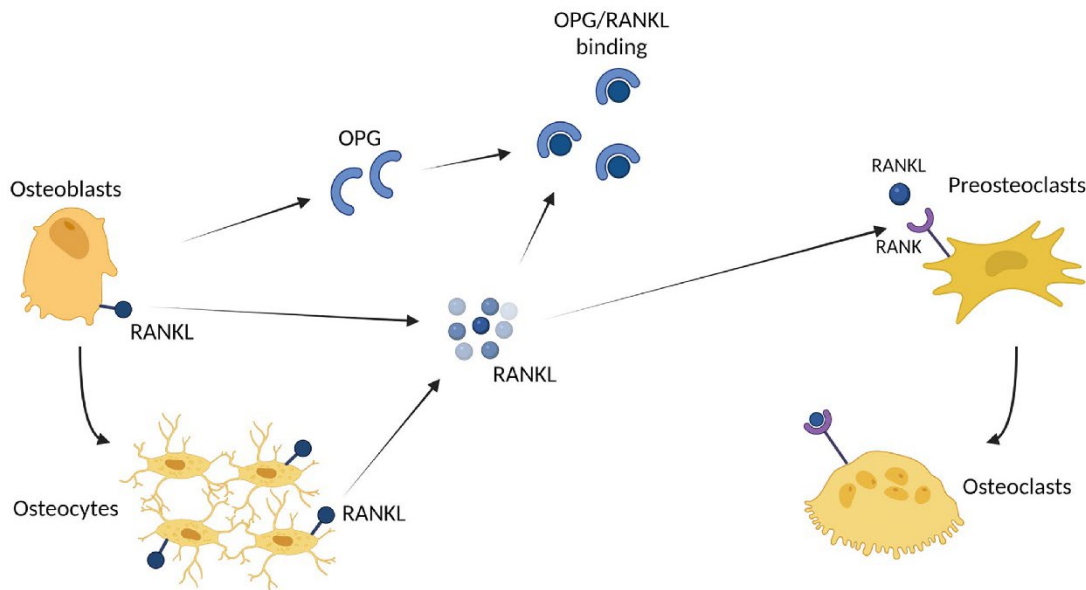


Figure 3. RANK/RANKL/OPG signaling pathway regulates osteoclast differentiation. Osteoblasts and osteocytes secrete receptor activator of NF- κ B ligand (RANKL), which binds to receptor activator of NF- κ B (RANK) expressed on preosteoclasts to promote osteoclast differentiation. Osteoblasts also produce osteoprotegerin (OPG), which competitively binds to RANKL with a higher affinity than RANK and thereby suppresses osteoclastogenesis. Figure modified according to (Kim, Girgis, & McDonald, 2022).

1.1.3.2. Hormonal regulators of osteoclasts

Multiple hormones affect the differentiation and function of osteoclasts directly or indirectly. Estrogen is one of the direct regulators of osteoclasts. The expression of estrogen receptor- α (ER α) was detected in human bone marrow-derived preosteoclasts and along the course of osteoclast formation and maturation (Denger, Reid, & Gannon, 2008; Oreffo et al., 1999). Estrogen induces apoptosis of murine osteoclasts by activating estrogen receptors expressed on osteoclasts (Hughes et al., 1996; Kameda et al., 1997). Loss of estrogen function by either ablation of ER α or surgical ovariectomy in rodents resulted in enhanced bone resorption and decreased bone mass, similar to the osteoporotic bone phenotype observed in postmenopausal patients (Jilka et al., 1992; Nakamura et al., 2007; Wronski, Cintrón, & Dann, 1988). Further evidence showed that estrogen also stimulated the expression of OPG in osteoblasts, suggesting estrogen to govern osteoclastogenesis indirectly (Jia, Zhou, Zeng, & Feng, 2017). Another hormone, CT, suppresses osteoclasts by directly binding calcitonin receptor (CTR). Bone marrow-derived osteoclasts treated with CT exhibited a decreased number of TRAP-positive cells and reduced area of resorbing

pits, suggesting CT inhibits osteoclast formation and activity (Jillian Cornish et al., 2001). On the contrary, other cell types, namely osteoblasts, can also regulate osteoclast formation and function in a paracrine manner. PTH was shown to enhance bone resorption in vivo by interacting with osteoblasts (Mcsheehy & Chambers, 1986). In rodents treated with continuous infusion of PTH, an increased expression of RANKL and decreased OPG was noticed in bone tissue and bone marrow-derived osteoblasts, leading to enhanced osteoclastogenesis and bone resorption (J. C. Huang et al., 2004; Ma et al., 2001). In vitro studies demonstrated that PTH promoted RANKL expression via activation of the Cyclic adenosine monophosphate (cAMP)/protein kinase A (PKA)-cAMP-responsive element binding protein (CREB) pathway and suppressed the expression of OPG (Fu, Jilka, Manolagas, & O'Brien, 2002; John C Huang et al., 2003). Other systemic factors, such as 1,25-dihydroxyvitamin D3, glucocorticoids, and androgens, are of great importance to the development and function of osteoclasts.

1.2. Calcitonin family of peptides in bone

Calcium homeostasis is of critical importance for a series of physiological processes, including coagulation, skeletal mineralization, muscle contraction, and neuronal excitation. CT together with PTH and 1,25-dihydroxyvitamin D3 are the three key hormones that maintain circulating calcium by regulating calcium metabolism in the gut, skeleton and kidneys. CT is a peptide hormone released by the thyroid parafollicular cells to inhibit osteoclast-mediated bone resorption and thereby reducing the calcium influx into the circulation. The calcitonin family of peptides comprises peptides that share a similar structure and act on common receptors, such as procalcitonin (PCT), CT, calcitonin gene-related peptide alpha (α CGRP), and amylin. Their receptors consist of a G protein-coupled receptor, either CTR or calcitonin receptor-like receptor (CRLR), dimerized with one of the three receptor activity-modifying proteins (RAMP1-RAMP3) to form specific receptors for different peptides (**Figure 4**). Despite the similar structure and the homology of their amino acid sequence, the peptides are derived from different tissues and exert diverse biological functions.

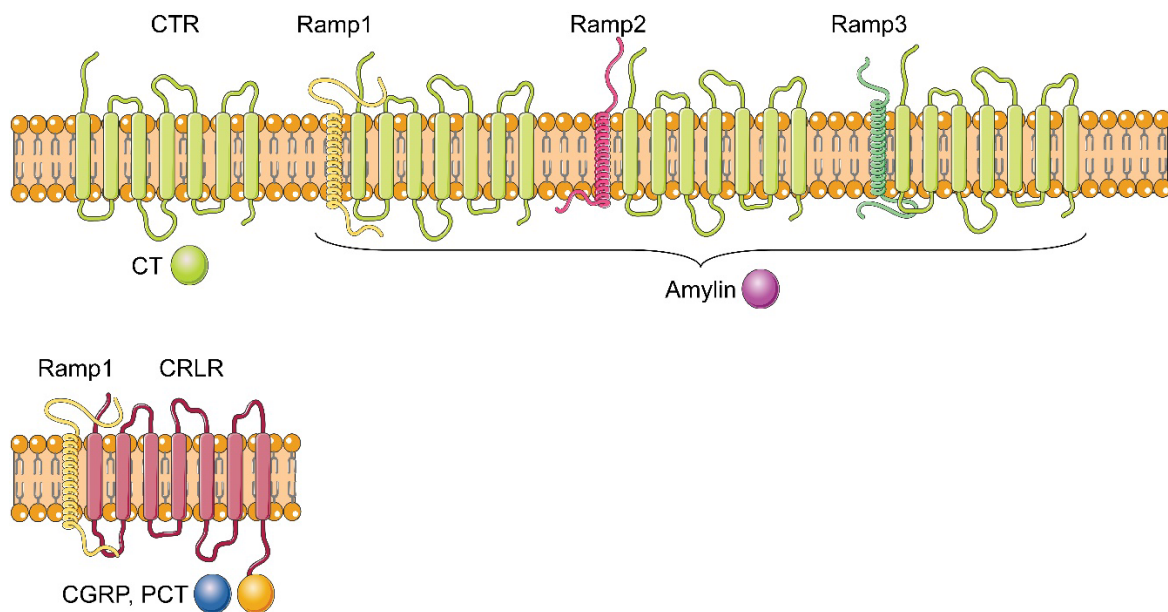


Figure 4. The composition of different receptors and their respective ligands in the calcitonin family of peptides. Calcitonin receptor (CTR) binds calcitonin (CT), and shows high affinity to amylin when dimerized with one of the three receptor activity–modifying proteins (RAMP1–RAMP3). Calcitonin receptor–like receptor (CRLR) combined with RAMP1 represents the receptor for calcitonin gene related peptide (CGRP) and procalcitonin (PCT). This figure was generated using Servier Medical Art, provided by Servier, licensed under a Creative Commons Attribution 3.0 unported license.

1.2.1. Calcitonin and procalcitonin

CT is produced and released by the thyroid gland in response to hypercalcemia. CT and its peptide precursor, PCT, are encoded by the *CALCA* gene (in humans termed *CALC1*), which also gives rise to α CGRP through alternative splicing (Rosenfeld et al., 1983). In the healthy organism, the procalcitonin/calcitonin (*PCT/CT*) transcript is expressed in thyroid C cells, while in neuronal tissue, 95% of the primary RNA transcript is processed to encode α CGRP mRNA (Lou, Gagel, & Berget, 1996). It has been well demonstrated that CT decreases calcium concentrations by inhibiting bone resorption. In mouse bone marrow cultures stimulated by 1,25-dihydroxyvitamin D3 which initiates osteoclast differentiation, CT resulted in a decreased number of TRAP-positive mono-/binuclear cells, suggesting an inhibitory effect of CT in the early stage of osteoclast differentiation (J. Cornish et al., 2001). A decreased number of TRAP-positive multinucleated cells and a reduction in the ratio of multinuclear to mono-/binuclear cells were noticed in cells treated with CT, indicating disturbed cell fusion is associated with CT. Furthermore, CT was found to directly suppress

osteoclastogenesis in cultures of bone marrow macrophages and spleen cells, where a highly purified population of hematopoietic cells was obtained (Granholm, Lundberg, & Lerner, 2007). In the presence of M-CSF and RANKL, CT inhibited the formation of multinucleated osteoclasts and the resorbing activity. In mature osteoclasts, administration of CT caused an immediate decrease in cell motility and cessation of lamellipodial activity, followed by fragmentation of lamellipodia and cell retraction (Chambers & Magnus, 1982). These observations suggest that CT affects the entire course of osteoclast differentiation and the function of mature osteoclasts.

However, the strong inhibitory impact of CT on osteoclasts was confounded by *in vivo* investigations using genetically modified mice. Hoff et al. generated *CALCA*^{-/-} mice lacking both *PCT/CT* and α CGRP transcripts, expecting a bone phenotype with increased bone resorption and decreased bone mass⁷⁴. However, the mice had a greater trabecular bone volume due to enhanced bone formation and unaltered indices of bone resorption compared to WT (**Figure 5**). A follow-up study from the same group demonstrated that mice with exclusive deficiency of α CGRP, with normal levels of circulating CT, had reduced bone mass and exerted an osteopenic bone phenotype, suggesting that α CGRP appears to favor bone formation (Schinke et al., 2004). Therefore, the increased bone mass noticed in mice lacking *CALCA* is most likely explained by the deficiency of CT, suggesting CT inhibits bone formation by targeting osteoblasts, although it has been reported that the expression of CTR is not detected in osteoblasts (Naot et al., 2007; Naot & Cornish, 2008).

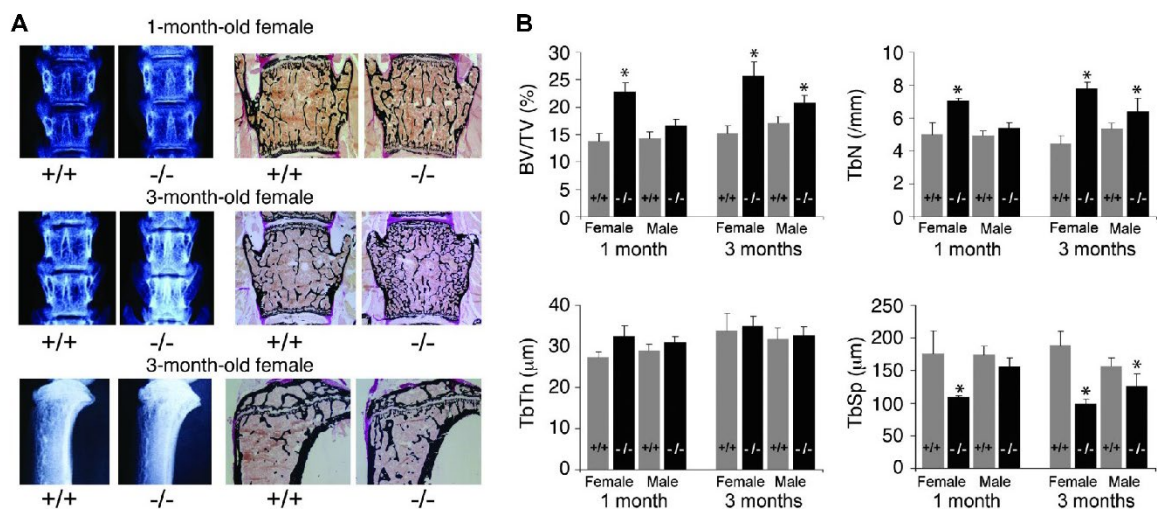


Figure 5. *CALCA*^{-/-} mice exhibit increased bone mass. A Radiographic and histological analysis of vertebrae from 1-month-old and 3-month-old WT (+/+) and *CALCA*^{-/-} (-/-) mice, and of the proximal tibiae

from 3-month-old WT and *CALCA*^{-/-} mice. **B** Static histomorphometric evaluation of bone volume fraction (BV/TV), trabecular numbers (TbN), trabecular thickness (TbTh), and trabecular separation (TbSp) of the vertebral trabecular bone in WT (gray bars) and KO (black bars) mice of both genders at the age of 1 month and 3 months. Figure modified according to (Hoff et al., 2002).

The knowledge of CT-mediated effects was greatly advanced by the generation of mice with CTR ablation. Dacquin et al. first analyzed their skeletal phenotype and noticed that homozygous inactivation of CTR encoding gene, *Calcr*, resulted in embryonic lethality⁷⁸. Therefore, the authors analyzed the bone metabolism in hemizygote *CTR*-deficient mice, in which the expression of *Calcr* was partially downregulated in osteoclasts. *Calcr*^{+/-} mice exhibited an increased bone mass, explained by enhanced bone formation with unaffected bone resorption. Another *CTR*-deficient mouse model was generated by Keller and his colleagues, which was not embryonically lethal (Keller et al., 2014). Similar to the previous reports, *CTR*-deficient mice displayed increased bone formation accompanied by higher circulating alkaline phosphatase levels, while no alterations regarding bone resorption were observed (**Figure 6**). Deficiency of CTR induced upregulation of sphingolipid transporter 2 (SPNS2) followed by increased secretion of sphingosine-1-phosphate (S1P) in osteoclasts, which stimulated osteoblast activity. Therefore, this study suggested that CT-CTR signaling in vivo mediates an osteoclast-osteoblast crosstalk, which inhibits bone formation without affecting bone resorption.

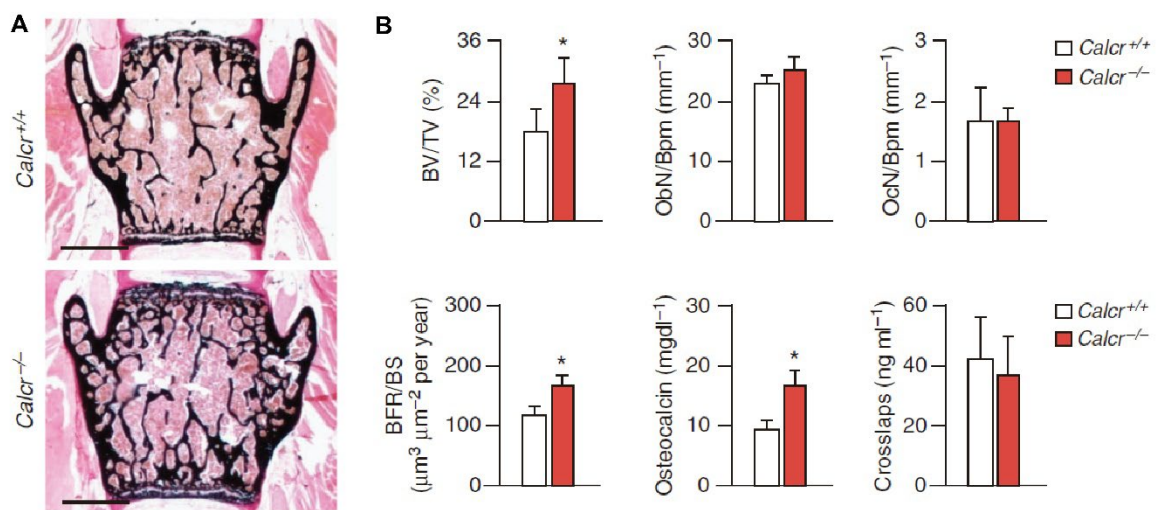


Figure 6. CTR-deficiency increases bone mass and promotes bone formation but not bone resorption. **A** Non-decalcified spine sections from 3-month-old female WT (*Calcr*^{+/+}) and *CTR*-deficient

(*Calcr⁷*) mice. **B** Histomorphometric quantification of the trabecular bone structural parameter, bone volume fraction (BV/TV), and indices of bone formation and bone resorption, including osteoblast and osteoclast number per bone perimeter (ObN/Bpm, OcN/Bpm) and bone formation rate per bone surface (BFR/BS). Osteocalcin and crosslaps were measured in serum. Figure modified according to (Keller et al., 2014).

PCT is an intermediate product during CT synthesis, which, under physiological conditions, is transcribed from the *CALCA* gene in the thyroid gland and undergoes proteolysis mediated by an endopeptidase. In healthy individuals, the concentration of circulating PCT is very low, typically less than 0.1ng/ml. However, in sepsis, systemic infection, and severe inflammation, the secretion of PCT becomes ubiquitous, resulting in a greatly augmented serum level of PCT up to hundreds or thousands of times. The role of PCT as a diagnostic and prognostic marker has been intensively studied in various infectious or inflammatory diseases (Assicot et al., 1993; Wacker, Prkno, Brunkhorst, & Schlattmann, 2013). Furthermore, PCT-guided antibiotic therapy in bacterial sepsis has been widely used to identify patients eligible for early antibiotic de-escalation or discontinuation (Bartoletti et al., 2018; Prkno, Wacker, Brunkhorst, & Schlattmann, 2013; Schuetz et al., 2018).

In comparison to its role as a biomarker, the pathophysiologic function of PCT in health and disease remained less known. Nylén et al. first demonstrated that administration of exogenous PCT was associated with an increased mortality in a septic peritonitis model, established by the intraperitoneal implantation of agar pellets containing a consistent amount of *Escherichia coli* (Nylén et al., 1998). Administration of exogenous human PCT resulted in a significantly increased mortality rate of up to 93% in septic animals compared to 43% in controls, while the lethal effect of sepsis was blunted by prophylactic blockade of PCT associated with a decreased 102h-mortality rate down to 6%.

Furthermore, a pro-inflammatory effect of PCT was suggested in a number of in vitro studies. Application of exogenous PCT increased the expression of surface markers cluster of differentiation 16 (CD16) and cluster of differentiation 14 (CD14) in human neutrophils and lymphocytes, respectively, which is similar to the immune response induced by lipopolysaccharides (LPS) (Wei, Verity, Garle, Mahajan, & Wilson, 2008). In human whole blood and polymorphonuclear leukocytes, recombinant PCT induced

a significant increase of pro-inflammatory cytokines including interleukin-6 (IL-6), tumor necrosis factor alpha (TNF α), and interleukin-1 beta (IL-1 β) in a dose dependent manner (K. L. Becker, Snider, & Nylén, 2010; Liappis et al., 2011). In contrast, Matera et al. reported a neutralizing effect of PCT on LPS-induced cytokine release in human peripheral blood mononuclear cells (Matera et al., 2012). The release of TNF α , interleukin-10 (IL-10), and monocyte Chemoattractant Protein-1 (MCP1) significantly decreased upon stimulation of LPS pre-incubated with PCT compared to that in the LPS group. Other studies took advantages of immunoneutralization of PCT to investigate its effects on sepsis outcome. In a large animal model of a rapidly fatal, porcine polymicrobial sepsis, PCT-reactive rabbit immunoglobulin G (IgG) was administered during the induction of sepsis or 3h after the induction, at which time a very severe physiological dysfunction was observed (Martínez et al., 2001). Neutralization of PCT ameliorated the general condition of the septic animals and significantly decreased the mortality. While none of the control animals survived, a survival rate of 85% with early intervention and 80% with late intervention was noticed (K.L. Becker, Nylén, Snider, Müller, & White, 2003; Martínez et al., 2001). Nevertheless, the physiological effect of PCT remained controversial. In another blinded randomized controlled trial, olcegepant, an antagonist of α CGRP receptor, which was previously reported to be the functional receptor for PCT signaling, was not beneficial in a porcine model of polymicrobial sepsis evidenced by unaltered indices of cardiovascular, hepatic, and renal injuries which affect overall survival rate (Baranowsky et al., 2021; Messerer et al., 2022; Sexton et al., 2008).

Despite the growing knowledge of PCT's effect on the immune system, the role of PCT in the skeletal system remained poorly understood. It has been previously shown that PCT was found to directly inhibit early osteoclast formation both in vitro and in vivo (Baranowsky et al., 2022). Mice lacking PCT exhibited excessive bone resorption upon intermittent PTH treatment, and this effect was further confirmed in vitro, where exogenous PTH reduced the number of osteoclasts and inhibited macrophage migration.

1.2.2. Calcitonin gene-related peptide alpha

In neuronal tissue, instead of *PCT/CT* transcript, *CALCA* gene gives rise to another transcript encoding the precursor of neuropeptide α CGRP (Goodman & Iversen, 1986). There are two isoforms of CGRP, α CGRP and β CGRP, which share over 90%

structural similarity. β CGRP is transcribed from the CALCB gene and is less studied. Therefore, the present introduction and subsequent experiments will primarily focus on α CGRP. Similar to CT, injection of α CGRP decreases the circulating calcium levels (Abdallah et al., 2005). In terms of bone metabolism, α CGRP was found to suppress osteoclast differentiation and bone resorption. In cultures of mouse bone marrow in the presence of 1,25-dihydroxyvitamin D3 or isoproterenol, α CGRP inhibited osteoclast formation, evidenced by decreased TRAP-positive mononuclear cells and subsequent fusion of these cells (J. Cornish et al., 2001; Ishizuka, Hirukawa, Nakamura, & Togari, 2005). A reduced area of resorption pits was noticed in bone marrow-derived osteoclasts treated with α CGRP (Zheng et al., 2010). These observations were further confirmed using ovariectomy (OVX) rodent models, in which osteoporosis is induced by the deficiency of estrogen (K. Valentijn et al., 1997). Although injection of α CGRP inhibited the excessive bone resorption in OVX rats, α CGRP was administered in a concentration around 300 folds higher than CT, suggesting a possible non-specific effect of α CGRP on bone resorption (K. M. Valentijn et al., 1997). No alteration in indices of bone resorption was observed on calvaria treated locally with α CGRP (K. M. Valentijn et al., 1997). In contrast, a number of studies reported a promising role of α CGRP in favoring bone formation. In vitro, α CGRP was found to stimulate the expression of bone morphogenetic protein 2 (BMP2) and promote osteoblast differentiation in primary cultures of human osteoblast-like cells (Tian, Zhang, & Tan, 2013). Recent studies reported that α CGRP promoted the proliferation and osteogenic differentiation of rodent bone marrow stromal cells by upregulating various osteoblast markers, including Runx2, osteocalcin, ALP, and type I collagen (COL1) (Liang, Zhuo, Tang, Wei, & Li, 2015; L. Wang et al., 2010). Systematic ablation of the gene encoding α CGRP in mice resulted in a decreased bone formation rate and reduced bone mass, while mice overexpressing α CGRP in osteoblasts exerted an increased bone mineralized density accompanied by an improved bone formation rate (Ballica et al., 1999; Schinke et al., 2004). Furthermore, it has been previously reported that α CGRP mediated the shift between osteogenic and adipogenic differentiation of aged bone marrow-derived mesenchymal stem cells (Mi et al., 2021). In 12-month-old mice, α CGRP treatment resulted in a significantly increased bone mass associated with a decreased number of adipocytes and increased indices of bone formation (**Figure 7**). In addition, multiple studies demonstrated that α CGRP promotes angiogenesis and endothelial progenitor cell proliferation, which might enhance bone formation indirectly

(Mapp, McWilliams, Turley, Hargin, & Walsh, 2012; Zheng et al., 2010). During the embryonic development of the mandible, the gene expression of α CGRP was detected at E14.5, associated with the gene expression of *vascular endothelial growth factor (VEGF-A)* and the *cluster of differentiation 31 (CD31)* (Maeda, Miwa, & Sato, 2017). Mi et al. reported that local application of α CGRP on a rat distraction osteogenesis model resulted in an increased vessel formation coupled with enhanced bone regeneration (Mi et al., 2021).

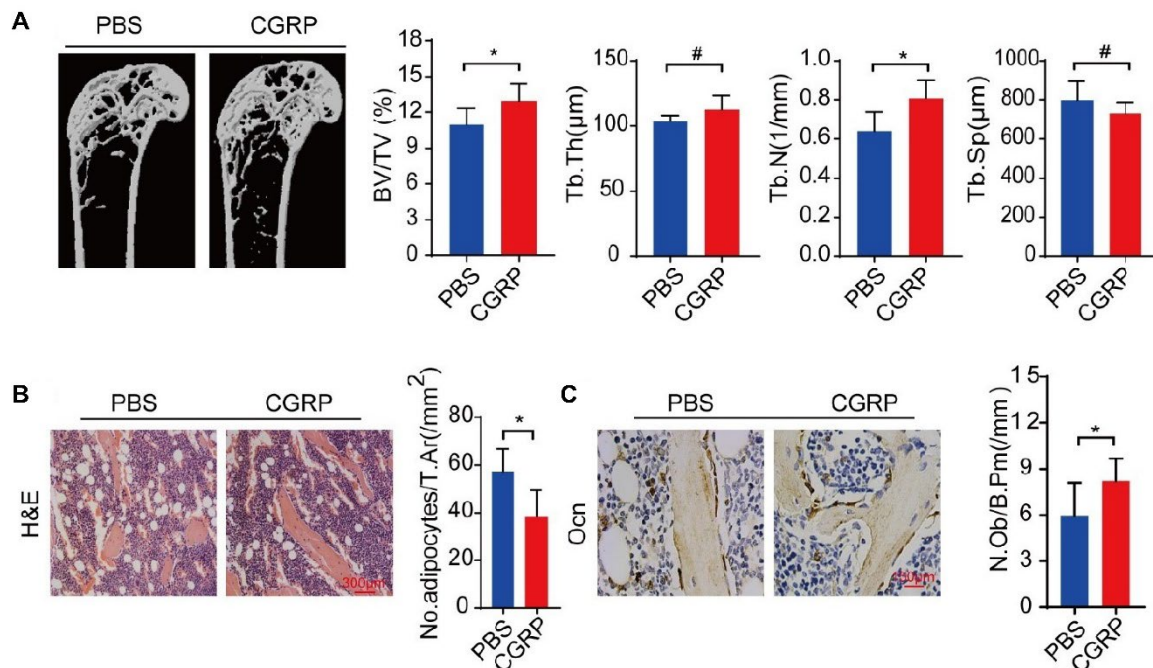


Figure 7. Supplemental CGRP treatment improves bone formation in aged mice. **A** Representative micro-computed tomographs and quantitative analysis of bone volume as a fraction of total bone volume (BV/TV), trabecular thickness (Tb.Th), trabecular number (Tb.N), and trabecular separation (Tb.Sp) of femora from CGRP-treated and control mice. **B** Representative images of hematoxylin and eosin (H&E) staining and quantitative analysis of adipocytes (No.adipocytes/T.Ar) in the bone marrow. **C** Representative images of osteocalcin (Ocn) staining and quantification of osteoblast number per bone perimeter (N.Ob/B.Pm) in the femora of CGRP-treated and control mice. Figure modified according to (Mi et al., 2021).

1.2.3. Amylin

Amylin is a 37-amino acid peptide that shares 50% of its structural identity with α CGRP. Amylin is a pancreatic B-cell hormone co-secreted with insulin in response to hyperglycemia. A number of studies have described the role of amylin as a satiation hormone, regulating glucagon release from the pancreas, food intake, and gastric

emptying (Hay, Chen, Lutz, Parkes, & Roth, 2015; Kanatsuka et al., 1989; Ogawa, Harris, McCorkle, Unger, & Luskey, 1990). In view of bone metabolism, amylin was found to inhibit the formation and maturation of TRAP-positive cells in cultures of bone marrow stimulated with 1,25-dihydroxyvitamin D3 (J. Cornish et al., 2001). Osteoclast activity was also suppressed by amylin, revealed by decreased resorptive pits on bone slices. Furthermore, amylin exerted a stimulatory effect on the proliferation of rat osteoblasts and human osteoblast-like cells, accompanied with increased secretion of osteocalcin (J. Cornish et al., 2004; Tamura, Miyaura, Owan, & Suda, 1992; Villa, Rubinacci, Ravasi, Ferrara, & Guidobono, 1997). In vivo, mice administrated with amylin for 4 weeks exhibited increased trabecular bone volume and cortical thickness in the tibia, associated with increased bone formation and decreased bone resorption (J. Cornish, K. E. Callon, A. R. King, G. J. S. Cooper, & I. R. J. T. A. j. o. p. Reid, 1998). Similar observations were made in mice receiving daily amylin treatment locally over the calvariae for 5 days, where an increase in indices of bone formation and reduced bone resorption were noticed compared to controls (Jillian Cornish, Callon, Cooper, Reid, & communications, 1995).

Using genetically modified mice, Dacquin et al. further investigated the physiological role of amylin in bone metabolism (Dacquin et al., 2004). Interestingly, amylin ablation in mice did not affect the food intake, body weight, and glucose metabolism. *Amylin*^{-/-} mice at the age of 24 weeks exhibited osteoporotic bone phenotype explained by increased osteoclast numbers and elevated urinal elimination of deoxypyridinoline, a degradation product of collagen that was used as an indicator of bone resorption. Conversely, the bone formation was not affected in amylin-deficient mice, evidenced by an unaltered bone formation rate in 12- and 24-week-old WT and amylin-deficient mice (**Figure 8**). Furthermore, similar ALP activity and mineralizing capacity of osteoblast progenitors isolated from amylin-deficient and WT animals was noticed. These findings collectively suggested that amylin inhibits bone resorption but does not affect bone formation.

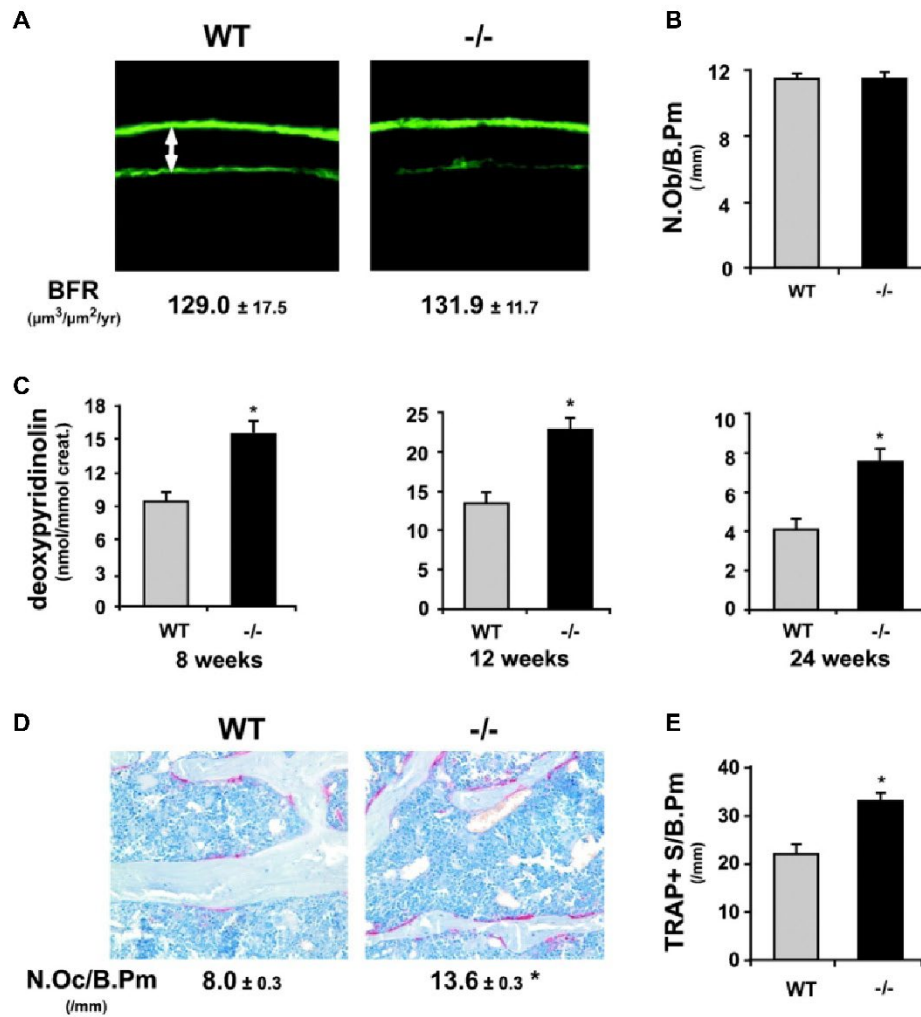


Figure 8. Increased bone resorption but unaltered bone formation in *amylin*^{-/-} mice. **A,B** Representative images of calcein double labeling in 6-mo-old WT and *amylin*-deficient mice. Histomorphometric analysis of bone formation rate (BFR) and osteoblast number per bone perimeter (N.Ob/B.Pm) in 24-week-old WT and *amylin*^{-/-} mice. **C** Urinary deoxyypyridinoline elimination in WT and *amylin*-deficient mice at the age of 8, 12 and 24 weeks. **D, E** Histomorphometric measurements of the number of osteoclasts per bone perimeter (N.Oc/B.Pm) and TRAP-positive surface per bone perimeter (TRAP+ S/B.Pm) in WT and *amylin*-deficient mice. Figure modified according to (Dacquin et al., 2004).

Furthermore, the understanding of amylin's receptors remains controversial. A number of cellular studies demonstrated that amylin receptors are heterodimers of a CTR representing a core receptor protein and one of the three RAMPs, which allows a high-affinity amylin binding (Bailey et al., 2012; Christopoulos et al., 1999; Gingell, Burns, & Hay, 2014; Muff, Bühlmann, Fischer, & Born, 1999). However, this prevailing consensus is confounded by the in vivo study (Dacquin et al., 2004), where mice with *Calcr*-haploinsufficiency inexpertly exhibited a high bone mass phenotype

accompanied by enhanced bone formation but unaffected bone resorption. These observations were opposite to those noticed in amylin^{+/-} mice, where an osteoporotic bone phenotype was found. This inconsistency in bone phenotype suggests that CTR might not be the relevant receptor through which amylin inhibits bone resorption in vivo. Further studies are warranted to uncover the functional receptors of amylin.

In conclusion, peptides of calcitonin family, namely CT, PCT, α CGRP and amylin, appear to be robust modulators of bone metabolism. Degenerative musculoskeletal diseases include a variety of age-related disorders which partially or primarily affect bone metabolism, such as osteoarthritis and osteoporosis, as described below. Therefore, targeting these peptides or related signaling pathways may offer novel insights and promising therapeutic potentials in the management and treatment of these diseases.

1.3. Degenerative musculoskeletal diseases and calcitonin family of peptides

1.3.1. Osteoarthritis

Osteoarthritis (OA) represents one of the most common degenerative diseases of the musculoskeletal system, with a global prevalence of more than 20% in individuals aged 40 and over (A. Cui et al., 2020). Affected patients experience chronic pain, restricted joint function with limited range of motion, and decreased quality of life. The knee is the most commonly affected joint by OA, followed by the hip and hand. OA can occur primarily due to age-related cartilage degeneration, or secondary to a pre-existing joint abnormality, including injury and trauma, inflammation, infection, or joint dysplasia. History of knee injuries represents a major risk factor knee OA. The incidence of post traumatic osteoarthritis (ptOA) in patients sustaining a knee injury, such as an anterior cruciate ligament rupture or a torn meniscus, are 4 times higher than that of primary OA (Muthuri, McWilliams, Doherty, & Zhang, 2011). The pathogenesis of OA has been extensively studied. Although OA has long been considered a disease affecting only cartilage, it has now been well recognized that OA is a disease of the entire joint sparing no tissue. In addition to cartilage degeneration, pathological alterations in subchondral bone and synovial tissues also contribute to the progression of OA (**Figure 9**).

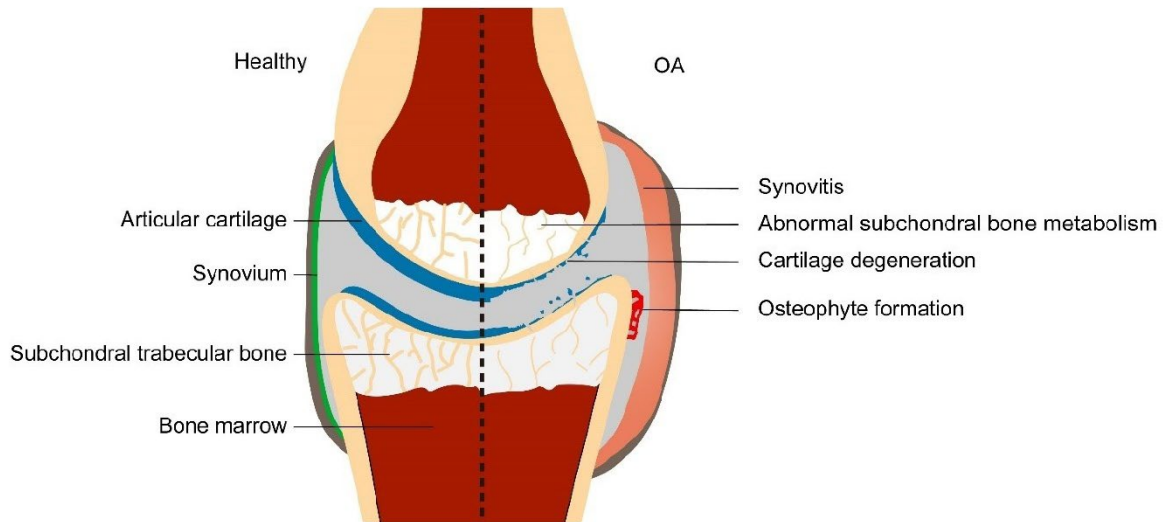


Figure 9. Key pathological changes in osteoarthritis (OA). Cartilage deterioration represents the pathological hallmark of OA. In addition, structural changes of the subchondral bone cause an altered distribution of the mechanical load, and increased cartilage catabolism. The formation of osteophytes and synovitis collectively contribute to the progression of OA.

In joint tissue, articular cartilage functions as a lubricated surface for low-friction articulation of the joint and a buffer transmitter of the mechanical loads to the subchondral bone. Appropriate mechanical loading helps maintain the integrity of the cartilage tissue. However, overuse or altered load distribution leads to cartilage destruction, which represents the pathological hallmark of OA (Logerstedt et al., 2022). The catabolic state of cartilage can be revealed by the upregulation of several markers, including various matrix metalloproteases (MMPs), IL-1 β , IL-6, and TNF α . Moreover, cartilage degeneration can also be initiated by aberrant signaling from the surrounding tissues such as synovium and subchondral bone (Chou et al., 2020; M. Wang et al., 2022; Zhang et al., 2023).

Subchondral bone refers to the bone tissue beneath the articular cartilage, comprising a thin cortical lamella that provides mechanical strength for tissue support, termed subchondral bone plate (SBP), and the underlying subchondral trabecular bone (STB). Subchondral bone undergoes pathological alterations in distinct patterns depending on the stages of the disease (Bettica, Cline, Hart, Meyer, & Spector, 2002; Botter et al., 2011; Klose-Jensen et al., 2015). In early OA, reduced subchondral bone mass is commonly observed, as evidenced by decreased bone volume of the STB and reduced

SBP thickness due to increased osteoclast number and activity in the subchondral bone (Hügler & Geurts, 2017). However, late-stage OA is associated with a sclerotic subchondral bone phenotype characterized by decreased bone resorption and relatively increased bone formation. Although the mechanisms by which alterations in the subchondral bone affect OA development remain insufficiently characterized, a number of studies have demonstrated that early intervention in the abnormal remodeling in the subchondral bone attenuates the progression of OA (Connor et al., 2009; Kadri et al., 2008; Nishii, Tamura, Shiomi, Yoshikawa, & Sugano, 2013; Rodrigues et al., 2018).

Synovium is a specialized type of connective tissue that covers all inner surfaces of the synovial joint capsule except articular cartilage. The synovium can be divided into an intimal lining layer and a sublining layer, both of which are rich in resident immune cells such as macrophages or macrophage-like synoviocytes (Iwanaga et al., 2000; Revell, Al-Saffar, Fish, & Osei, 1995). Synovial inflammation, also known as synovitis, can occur at the onset of early OA and throughout the entire course of the disease. Synovitis is featured by synovial thickening, pannus formation, fluid effusion, and, on a cellular level, infiltration of immune cells, namely macrophages and T cells (Scanzello & Goldring, 2012). Upon stimulation by tissue debris from worn cartilage or factors released from destructed cartilage, synoviocytes are activated and secrete cytokines and chemokines to recruit immune cells, leading to a microenvironment abundant in inflammatory mediators and proteolytic enzymes. This proinflammatory microenvironment is capable of promoting angiogenesis and cartilage degradation, which in turn exacerbates synovitis. Thus, synovitis and cartilage degeneration promote each other, resulting in progressive joint degeneration in OA. Although no clinical study has demonstrated a protective effect of anti-inflammatory treatment on OA progression, synovitis is undoubtedly a potential therapeutic target for OA.

Despite a great number of studies contributing to our growing understanding of molecular mechanisms underlying OA progression, no novel pharmacological approach has shown satisfactory outcomes regarding pOA progression to date. A recent clinical trial showed that participants receiving bone morphogenetic protein 7 (BMP7) for 12 weeks experienced similar pain improvements as placebo treated participants (Hunter et al., 2010). Another 12-month double-blind phase II trial reported that PG-116800, a pharmacological inhibitor of MMPs, is unsuited to treat degenerative

joint disease due to considerable musculoskeletal adverse effects (Krzeski et al., 2007). Therefore, further investigations are warranted to unravel the mechanisms regulating ptOA progression.

1.3.2. Role of *CALCA*-encoded peptides in OA

It has been long suggested that the *CALCA*-encoded peptides play a critical role in OA (Aikawa et al., 2018; Bullock et al., 2014; Morten Asser Karsdal et al., 2006; Wen et al., 2016). A beneficial effect of CT on OA has been demonstrated, including inhibiting subchondral bone metabolism, promoting chondrocyte survival via direct interaction, and relieving pain (Morten Asser Karsdal, Sondergaard, Arnold, & Christiansen, 2007). In chondrocytes, CT stimulated cAMP production and inhibited the degeneration of type 2 collagen (Sondergaard et al., 2006). In experimental rodent models of OA, administration of CT alleviated cartilage damage, evidenced by reduced extracellular matrix degradation and less pronounced subchondral bone changes (Cheng et al., 2013; Mancini et al., 2007). In transgenic mice overexpressing CT, cartilage erosion induced by destabilization of the medial meniscus (DMM) was milder compared to WT controls (Sondergaard et al., 2012). However, two phase III trials showed no statistically significant therapeutic effects of CT on symptomatic OA (Bagger et al., 2005; M. A. Karsdal et al., 2015; Manicourt, Azria, Mindeholm, Thonar, & Devogelaer, 2006). In these studies enrolling 2206 OA patients, long-term administration of oral salmon CT was not associated with improvements in joint space narrowing or higher Western Ontario and McMaster Universities Osteoarthritis (WOMAC) scores. These compelling observations between preclinical studies and clinical trials highlight the need of further understanding the function of CT and its related signaling in OA. In terms of PCT, little is known about its role in the development of ptOA. Previous studies suggested PCT to function as a proinflammatory mediator in the immune system and a direct regulator of bone metabolism. Since excessive synovial inflammation and abnormal subchondral bone remodeling represent the key pathological changes in OA, investigating the potential involvement of PCT in these processes could provide valuable insights into the pathogenesis of ptOA.

Furthermore, α CGRP, as a neuropeptide, was shown to be associated with nociception, vasodilation, and inflammation in the arthritic joints. In human OA, α CGRP expression was found increased in the synovial tissue and fluid from OA patients, and α CGRP-positive nerve fibers were abundant in the joint and meniscus of patients with painful

OA (Minatani et al., 2016; Takano et al., 2017). Animal studies reported that α CGRP exerts a pro-inflammatory and bone-preserving effect in collagen II-antibody-induced arthritis, while administration of α CGRP antagonist BIBN4096 inhibits cartilage degeneration and abnormal subchondral bone remodeling in a murine ptOA model (Tazio Maleitzke et al., 2021; Tazio Maleitzke et al., 2020). Nevertheless, little is known about the function of α CGRP in the onset and development of ptOA.

Taken together, OA represents a significant global health problem that affects the quality of life especially in the elder population. Due to the complex pathogenesis and the involvement of multiple tissue types, no pharmacological treatment to date yields satisfactory therapeutic outcomes. Despite a number of preclinical and clinical studies have been carried out, the roles of *CALCA*-encoded peptides in the pathogenesis of OA remain poorly understood. Further studies are warranted to clarify their specific functions and to investigate a therapeutic potential in this context.

1.3.3. Osteoporosis

In contrast to OA which involves multiple tissue types, osteoporosis is a systematic skeletal disorder that predominantly affects bone. Patients with osteoporosis are characterized by decreased bone mineralized density (BMD), microarchitectural deterioration of bone, compromised bone strength, leading to increased bone fragility and significantly elevated risk of fractures ("Osteoporosis prevention, diagnosis, and therapy," 2001). Osteoporosis and consequent fragility fractures of the hip and spine are considered to be associated with increased mortality. Over 1% of all deaths in patients aged 50 years or older are causally related to hip fracture events, comparable to that due to pancreatic cancer and higher than that caused by stomach cancer (Kanis et al., 2003). Osteoporosis is diagnosed by BMD at the hip or lumbar spine that is less than or equal to 2.5 standard deviations below the mean BMD of a young adult reference population (T-score) (LeBoff et al., 2022). Although osteoporosis can be secondary to a number of medical conditions or medications, cessation of ovarian function in postmenopausal women is the most prevalent cause of osteoporosis. Deficiency of estrogen results in continuous, progressive bone loss caused by uncoupled bone remodeling with excessive bone resorption outweighing bone formation (Manolagas, 2000). The treatment of osteoporosis can be divided into two parts. The anabolic medications such as PTH related peptides stimulate the osteoblastic differentiation and mineral deposition, whereas the anti-resorptive

therapies such as bisphosphonates, RANKL antibody, selective estrogen-receptor modulators, and CT limit the excessive osteoclast function, thereby improve bone mineral density.

Similarly, an increased risk of osteoporotic fracture has long been suggested in patients with diabetes mellitus, despite the BMD remaining unaltered or even increased in type 2 diabetes (T2D) cohort in comparison to controls (Fan, Wei, Lang, & Liu, 2016; Janghorbani, Van Dam, Willett, & Hu, 2007; Schacter & Leslie, 2017; Shah, Shah, & Snell-Bergeon, 2015; Vestergaard, 2007). The adverse impacts of diabetes on the skeleton, also known as diabetes-induced osteoporosis, contribute to an additional fracture burden to conventional osteoporosis (**Figure 10**). Recent meta-analyses demonstrated an increased risk of hip, ankle, and upper arm fractures in the diabetic population compared to controls (Vilaca et al., 2020; H. Wang, Ba, Xing, & Du, 2019). On a pathophysiologic level, reduced bone turnover and relatively decreased bone formation were noticed. In a meta-analysis reviewing 22 studies, the bone turnover markers osteocalcin and C-terminal cross-linked telopeptide were significantly lower in the diabetic cohort (Starup-Linde, Eriksen, Lykkeboe, Handberg, & Vestergaard, 2014). Moreover, it has been suggested that diabetes and hyperglycemia are associated with increased levels of inflammatory cytokines, which promote osteoclast differentiation and function, leading to increased bone resorption (Borst, 2004; Katsuki et al., 1998). Hyperglycemia also promotes bone matrix glycation, which in turn suppresses bone formation and matrix renewal, causing alterations in bone material properties and mechanical failure while loading (Dong, Qin, Xu, & Wang, 2011; Fong, Edelstein, Wang, & Brownlee, 1993; X. Yang, Mostafa, Appleford, Sun, & Wang, 2016).

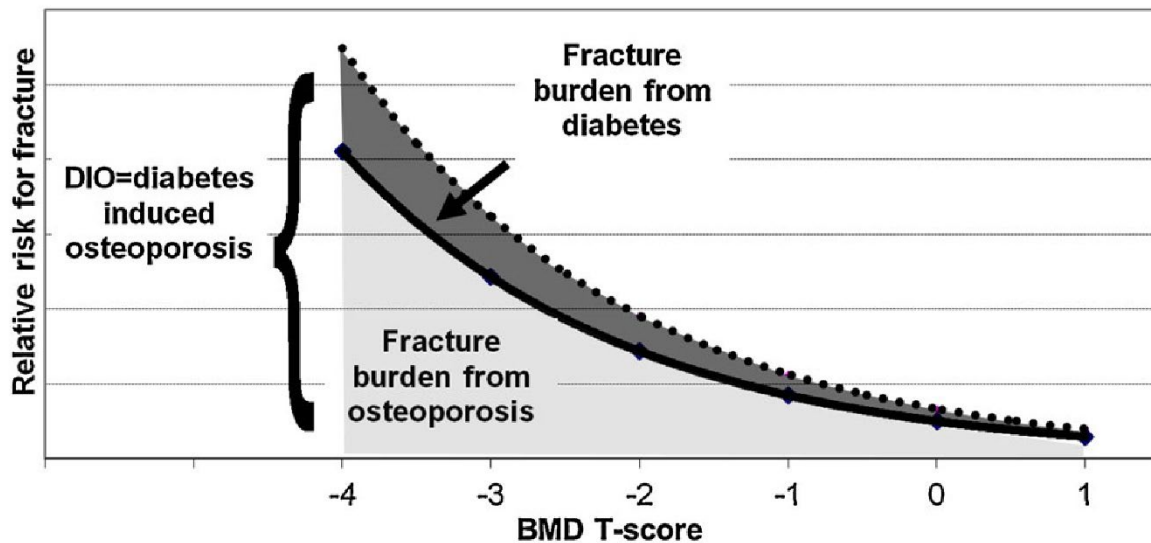


Figure 10. Conceptual framework for diabetes and fractures. The light gray region below the solid line indicates the fracture burden attributable to osteoporosis; the dark gray region between the dotted and solid lines indicates the additional fracture burden attributable to diabetes. Figure modified according to (Schacter & Leslie, 2017).

In addition to the pathophysiological changes caused by hyperglycemia, anti-diabetic medications may also negatively affect bone metabolism, contributing to the increased fracture burden. A meta-analysis showed that insulin, sulphonylureas, and thiazolidinediones were positively associated with an increased risk of fracture, while metformin users were associated with a reduced risk of fracture (Hidayat, Du, Wu, & Shi, 2019). The lower fracture risk is likely due to the general conditions of metformin users, which are usually in the early stage of T2D. Sodium-glucose cotransporter-2 (SGLT2) inhibitors are an emerging class of medication included as a first-line pharmacological therapy for T2D in 2022 ("9. Pharmacologic Approaches to Glycemic Treatment: Standards of Medical Care in Diabetes-2022," 2022). In patients treated with canagliflozin for two years, a decreased BMD was noticed in the total hip but not in other sites (femoral neck, lumbar spine, or distal forearm). In the CANagliflozin cardiovascular Assessment Study (CANVAS), significantly increased fracture incidences were noticed in patients treated with canagliflozin compared to placebo (Watts et al., 2016). These observations suggest that some anti-diabetic medications adversely affect bone metabolism, proposing an urgent need of identifying new potential anti-diabetic therapies that also improve bone quality.

1.3.4. Role of calcitonin family of peptides in osteoporosis

The anti-osteoclastic effect of CT makes it a potential therapeutic for conditions of excessive bone resorption. Therefore, salmon calcitonin (sCT) was developed as an anti-resorptive therapy for postmenopausal osteoporosis and then approved by the United States Food and Drug Administration (FDA). A number of studies showed that sCT reduced the incidence of osteoporotic fractures and increased bone density. In the Prevent Recurrence of Osteoporotic Fractures (PROOF) trial, 5 years of application of sCT at a daily dose of 200IU significantly reduced the risk of new vertebral fractures by 33% in postmenopausal women with osteoporosis (Chesnut et al., 2000). The expected protective effect on vertebral fractures were not observed in patients receiving 400IU sCT. Despite further studies showing that sCT could induce a moderate increase in bone mineral density and maintain trabecular microarchitecture, a randomized, double-blind, placebo-controlled study showed that oral sCT did not affect the proportion of patients with new osteoporotic fractures (Adachi et al., 1997; Henriksen et al., 2016; Mazzuoli et al., 1986; Ringe & Welzel, 2004). As newly developed bisphosphonates and other drugs offer relatively greater efficacy in treating osteoporosis, and as a meta-analysis study reviewing 18 studies suggested an increased cancer incidence associated with sCT use, the European Medicines Agency determined that calcitonin-containing medications should no longer be used in the treatment of osteoporosis (Overman, Borse, & Gourlay, 2013).

In addition to CT, another peptide of calcitonin family, amylin exhibits promising therapeutic potential for osteoporosis due to its osteogenic feature. A previous study reported that the plasma level of amylin was decreased in patients with osteoporosis or T2D, and was negatively associated with the severity of primary osteoporosis (Bronský & Průsa, 2004; X. J. Wang et al., 2023). A number of studies have reported that rodents receiving systemic administration of amylin presented an increased bone mass, explained by promoted osteogenesis and suppressed osteoclast activity and, thereby, decreased bone resorption (Jillian Cornish et al., 2000; J. Cornish, K. E. Callon, A. R. King, G. J. S. Cooper, & I. R. Reid, 1998; J. Cornish et al., 1998). In rats with T2D, administration of exogenous amylin significantly improved bone strength and mineral density, characterized by an increased bone formation rate and decreased osteoclast surface and erosive surface (I. Gutiérrez-Rojas et al., 2013; M.-N. Horcajada-Molteni et al., 2001). Furthermore, ovariectomy-induced bone loss can be

restored by a daily injection of amylin for 30 days (M. N. Horcajada-Molteni et al., 2000). Although it has been well understood that amylin regulates gastric emptying and glucose metabolism, confounding observations were made in mice lacking amylin. Amylin-deficient mice exhibited similar body weight, food intake and serum insulin and glucose levels as WT controls, whereas a pronounced osteoporotic phenotype was observed in the mutant animals. These findings suggest that amylin is dispensable in food intake and glucose metabolism in vivo but plays a crucial role in bone metabolism. Furthermore, the bone-preserving effects demonstrated in experimental animals were not observed in humans. Pramlintide is a synthetic analog of amylin that was approved by the FDA as a treatment for diabetes in conjunction with insulin. In a study recruiting 23 patients with type I diabetes (T1D), pramlintide treatment for 12 months did not affect the levels of various bone metabolism markers and BMD (Borm et al., 1999). As the enrolled patients in this study were not diagnosed with osteopenia or osteoporosis, and as T1D is commonly noticed in young adults without significant alteration in the bone mineral density, further studies are warranted to investigate whether pramlintide is capable of regulating bone metabolism in conditions with deteriorated bone architecture (Shah et al., 2017; Starup-Linde, Hygum, Harsløf, & Langdahl, 2019).

2. Hypothesis and Objectives

OA and osteoporosis are the most prevailing degenerative musculoskeletal diseases in the elderly population, exerting a substantial socioeconomic burden worldwide. In terms of OA, although advances have been made in surgical techniques and the development of prosthetic joints, no novel pharmacological approaches have been demonstrated to efficiently alleviate or halt the progression of OA to date. A number of studies have demonstrated that the calcitonin family of peptides are crucially involved in the development of OA, while two clinical trials reported no significant therapeutic effects of calcitonin on symptomatic OA. Furthermore, the functions of *CALCA*-encoded transcripts and CTR-mediated signaling in the progression of OA remain unclear. As altered subchondral bone metabolism represents one of the key pathological changes in OA, and as *CALCA*-derived peptides and CTR-mediated signaling are potent regulators of bone turnover, it was hypothesized that *PCT/CT* and α *CGRP* transcripts as well as CTR signaling are crucially involved in the progression of ptOA. Regarding osteoporosis, a variety of anti-osteoporosis treatment approaches have been developed and yielded satisfactory outcome in improving BMD and reducing fracture risk. However, osteoporosis also occurs frequently to patients with diabetes. Chronic hyperglycemia and certain anti-diabetic medications can progressively deteriorate bone quality, leading to an increased fracture burden in addition to conventional osteoporosis. Amylin, a member of the calcitonin family of peptides, has been found to not only control glucose metabolism but also improve bone quality in rodents. Therefore, it is of great interest to investigate whether pramlintide, known as the synthetic analog of amylin, is capable of rescuing osteoporotic bone loss in an experimental murine osteoporosis model and to study the mechanism mediating such effect.

Taking these into consideration, in the present work, multiple genetically modified mouse models and experimental disease models were employed to 1) to investigate the functional role of *PCT/CT* and α *CGRP* transcripts in the progression of ptOA; 2) to explore the involvement of CTR-mediated signaling in ptOA development; 3) to study whether osteoporosis induced bone loss can be alleviated by the anti-diabetic medication pramlintide, and whether CTR is the key receptor regulating such effects.

3. Material and Methods

3.1. Material

3.1.1. Chemical and reagents

Name	Art.-Nr /PZN	Manufacturer
0.5M EDTA solution	03690	Sigma-Aldrich
10X DreamTaq Green buffer	EP0713	Thermo Fisher Scientific
1 α ,25-Dihydroxyvitamin D3	D1530	Sigma-Aldrich
2-Methoxyethyl acetate	8060611000	Sigma-Aldrich
Acetic acid	A6283	Sigma-Aldrich
Aceton	179124	Sigma-Aldrich
Agarose	A9539	Sigma-Aldrich
Benzoyl peroxide (with 25% H ₂ O) for synthesis	8016410250	Sigma-Aldrich
Bepanthen Eye and nose ointment	1578681	Bayer Vital
Betaisodona solution, 100 mg/ml	1970433	Mundi pharma
Boric acid	B0394	Sigma-Aldrich
Buprenovet multidose, 0.3 mg/ml	14439053	Richter Pharma
Clindamycin, 150 mg/ml	4468504	Hikma Pharma
DMSO 100%	D2650	Sigma-Aldrich
dNTP Mix	71004	Sigma-Aldrich
DPX new, non-aqueous mounting medium	1.00579	Sigma-Aldrich
Dream Taq	EP0705	Thermo Fisher Scientific
Eosin Y-solution 0.5% alcoholic	1.02439	Sigma-Aldrich
Ethanol, 100%	2212.5	Th. Geyer
Ethanol, 70%	2202.5	Th. Geyer
Ethanol, 80%	2203.5	Th. Geyer
Ethanol, 96%	2209.5	Th. Geyer
Ethylenediaminetetraacetate (EDTA), Titriplex III	1.08418	Merck
Fast green FCF (C.I. 42053)	1.04022	Sigma-Aldrich
Fast Red Violet LB Salt	F3381	Sigma-Aldrich
Formafix 3.5% buffered	70002-3,5-5	Grimm med.
Formaldehyde solution 37%	8.18708	Sigma-Aldrich
Fuchsin acid (C.I. 42685)	1.05231	Sigma-Aldrich
GeneRuler	SM0333	Thermo Scientific

Glycerol	3783.1	Carl Roth
GreenSafe Premium	MB13201	NZYTech
Hematoxylin solution A acc. to Weigert	X906.1	Carl Roth
Hematoxylin solution B acc. to Weigert	X907.1	Carl Roth
Hydrochloric acid (HCl), 25%	1.00312	Merck
Hydrochloric acid (HCl), 37%	1.00314	Merck
Isoflurane	HDG9623	Baxter Deutschland
Isopropanol	1136	Th. Geyer
Kaiser's glycerol gelatine, phenol-free mounting medium	1.08635	Sigma-Aldrich
Korsolex extra instrument disinfectant	973802	Paul Hartmann
Mayer's hemalum solution	1.09249	Sigma-Aldrich
Methanol	1400.25	CHEMSOLUTE
Methyl Methacrylate	8.0059	Sigma-Aldrich
MgCl ₂	7786-30-3	Sigma-Aldrich
N,N-Dimethylformamide	D158550	Sigma-Aldrich
N,N-Dimethyl-p-toluidine	8.2204	Sigma-Aldrich
Naphthol AS-MX phosphate disodium salt	N5000	Sigma-Aldrich
n-Hexan	3907.2	Carl Roth
Nitric acid (HNO ₃), ≥ 65%	X943.1	Carl Roth
Nonylphenyl-polyethyleneglycol acetate	74432	Sigma-Aldrich
Novaminsulfon-ratiopharm, 500mg/ml	3530402	Ratiopharm
O'RangeRuler 20 bp DNA Ladder	SM1323	Thermo Fisher Scientific
Paraffin pellets, M.P. 56-58°C	40-0021-00	MEDITE Medical
Paraformaldehyde 20% solution	15713	Electron Microscopy Sciences
Phosphate buffered saline	P-3818	Sigma-Aldrich
Picric acid solution, saturated	P6744	Sigma-Aldrich
Pramlintide acetate salt	SML2523	Sigma-Aldrich
Recombinant Murine M-CSF	315-02	Peprtech
Recombinant Murine sRANK Ligand (E.coli derived)	315-11	Peprtech
Safranin O (C.I. 50240)	1.15948	Sigma-Aldrich

SCEM medium	SCEM	Section-Lab
Silver nitrate	209139	Sigma-Aldrich
Sodium acetate	1.06268	Merck
Sodium carbonate	223530	Sigma-Aldrich
Sodium hydroxide (NaOH) pallets	402	Avantor Performance Materials
Sodium hydroxide solution	79724	Sigma-Aldrich
Sodium L-tartrate dibasic dihydrate	228729	Sigma-Aldrich
Sodium thiosulfate	1.06512	Sigma-Aldrich
Sterile saline (NaCl 0.9%)	6063042	B. Braun
Sterile water (Aqua)	88992	B. Braun
Sweetener	B006WZZVHE	Goldhand
Sybr Select Master Mix for CFX	4472942	Thermo Fisher Scientific
TaqMan Gene Expression Master Mix	4369016	Thermo Fisher Scientific
Toluidine Blue O	T3260	Sigma-Aldrich
TRIS hydrochloride	PHG0001	Sigma-Aldrich
Tris- (hydroxymethyl)-aminomethan	252859	Sigma-Aldrich
Xylene	360.5	Th. Geyer

3.1.2. Buffers and solutions

Name	Composition	
Acetic acid solution, 1%	10ml	Acetic acid
	990ml	H ₂ O
EDTA solution	0.5M	Titriplex III
	0.45-0.5M	NaOH solution
	Add up to 1000ml	H ₂ O pH7.4
Fast green (FCF) solution, 0.01%	0.1g	Fast green FCF
	1000ml	H ₂ O
HCl-ethanol solution	5ml	25% HCl
	95ml	96% ethanol
Safranin O solution, 0.1%	1g	Safranin O
	1000ml	H ₂ O
TRAP staining solution	140ml	Trap solution A (0.1M Sodium Acetate buffer, pH5)

	60ml	TRAP solution B (0.6% Acetic Acid buffer)
	10mg	Naphthol AS-MX phosphate disodium salt
	1ml	N,N-Dimethylformamide
	60mg	Fast Red Violet LB Salt
Van Gieson's solution	2.5g	Fuchsin acid
	100ml	Glycerol
	5ml	65% Nitric acid
	900ml	Saturated picric acid solution
Weigert's Iron hematoxylin solution	150ml	Hematoxylin solution A acc. to Weigert
	150ml	Hematoxylin solution B acc. to Weigert
10x TBE Buffer	216g	Tris (hydroxyl)aminomethan (Tris Base) (0,9M)
	110g	Boric Acid
	80ml	0.5M EDTA solution (pH8.0)
	Up to 2L	H ₂ O
Lysis buffer A	2.5ml	1M NaOH
	40µl	0.5 M EDTA
	Up to 100ml	H ₂ O
Lysis buffer B	0.63g	Tris-HCl
	Up to 100ml	H ₂ O
Infiltration solution I, II	900ml	Methyl methacrylate (MMA) solution
	3.3g	Benzoyl peroxide (BPO), dried
	100ml	Nonylphenyl-polyethyleneglycol acetate
Embedding solution	900ml	MMA solution
	6.6g	BPO, dried
	100ml	Nonylphenyl-polyethyleneglycol acetate
	2.5ml	N,N-dimethyl-p-toluidine (starter)
Toluidine blue stain solution	1g	Toluidine blue O
	100ml	H ₂ O
		pH4.5
3% Silver Nitrate solution	3g	Silver nitrate
	100ml	H ₂ O

Sodaformol	12.5g	Sodium carbonate
	62.5ml	37% Formaldehyde
	187ml	H ₂ O
5% Sodium thiosulfate solution	5g	Sodium thiosulfate
	100ml	H ₂ O
RANKL stock solution	10ug	RANKL
	1ml	H ₂ O
MCSF stock solution	10ug	M-CSF
	1ml	H ₂ O
VitD stock solution	10ug	1,25-Dihydroxyvitamin D3
	2.4ml	100% ethanol
alpha Minimum Essential Medium	1 vail	Minimum Essential Medium Eagle
	2.2g	sodium bicarbonate
	Up to 1000ml	H ₂ O
Pramlintide solution	5mg	Pramlintide
	25ml	0.9% NaCl

3.1.3. Equipment

Name	Model	Manufacture
μCT scanner	vivaCT 80	Scanco Medical
Acrylate block grinder	ECOMET 30	Buehler
Analytical balance, 220g/0.01mg	BP221S	Sartorius
Anesthesia machine	UniVet Porta	Groppler Medizintechnik
Autoclave	Evo 130/ Evo75	MediTech Service
Cell Counter	TC20	BIO-RAD
Cell Counting Chamber	Neubauer Improved	OPTIK-Labor
Cell Culture Hood	MSC 1.2	Thermo Scientific
Cell Culture Microscope	Axiovert25	Zeiss
Cold light source	KL 1500 LCD	Schott
Cryostat	M630	MEDITE
Cycler	Mastercycler ProS	Eppendorf
Digital Scale, 500g/0.01g	DIPSE TP-500	SSR Produkt
Digital Scale, 600g/0.01g	SCOUT PRO SPU602	OHAUS Corporation

DNA electrophoresis cell	Sub-Sell GT	BIORAD
Dumont forcep	11231-30	Fine Science Tools
Electrophoresis Power Supply	PowerPac 1000	BIO-RAD
Fine scissor-ToughCut	14058-11	Fine Science Tools
Gas evacuation apparatus	R546W	RWD Life Science
Gas filter canister	R510-31	RWD Life Science
Graefe forcep	11054-10	Fine Science Tools
Hair clipper	Hatteker RFC-690	Yiwu Kehan Electrical Appliances
Halsey needle holder	12001-13	Fine Science Tools
Heater	Thermomixer Comfort	Eppendorf
High-speed centrifuge	5430R	Eppendorf
Histomaster Autotechnicon	2065-2-Z-Di	Rowi Elektronik
Imaging System	ChemiDocMP	BIO-RAD
Incubator	VT 6025	Heraeus Holding
Incubator	BBD6620	Thermo Scientific
Induction chamber	UV17006-S	Groppler Medizintechnik
Magnetic stirrer	RCT D S000	IKA-Werke
Micropipette, 0.1-2.5µl	Eppendorf Research plus	Eppendorf
Micropipette, 100-1000µl	Eppendorf Research plus	Eppendorf
Micropipette, 20-200µl	Eppendorf Research plus	Eppendorf
Micropipette, 2-20µl	Eppendorf Research plus	Eppendorf
Microscope	BX50	Olympus optical
Microscope camera	DP72	Olympus optical
NANODROP	2000	Thermo Scientific
Paraffin embedding workstation	HistoStar	Thermo Fisher Scientific
pH Meter	FiveEasy Plus FP20	Mettler-Toledo
Pipette controller	PIPETBOY	INTEGRA Biosciences
Plate reader	VICTOR X5	Perkinelmer
Real-Time qPCR	CFX Connect	BIO-RAD

Roller mixer	RS-TR05	Phoenix Instrument
Rotary microtome	Microm HM 355S	Thermo Fisher Scientific
Safety cabinet	630165/170/2	asecos
ThermoLux thermal pad	464265	Witte + Sutor
Ultrapure water system	PF2XXXXM1	ELGA LabWater
Ultra-Turrax	T18	IKA
Waterbath	1000	pfm Medical

3.1.4. Consumables

Name	Manufacturer
Biosphere plus, filter tips, 0.1-20µl	SARSTEDT
Biosphere plus, filter tips, 1000µl	SARSTEDT
Biosphere plus, filter tips, 200µl	SARSTEDT
Cell Counting Slides	BIO-RAD
Cell culture flask, Filter cap (T-25, T-75)	Sarstedt
Cell strainer 70um	Sarstedt
CELLSTAR Cell Culture Dishes, PS, 14/20mm	Greiner Bio-One
Cover glasses (24×60 mm)	DWK Life Sciences
Cutfix disposable scalpels, # 11	Aesculap
DERMAGRIP nitrile examination gloves	REMESCO
Disposable bags	SARSTEDT
Embedding cassettes	Engelbrecht
Falcon TC-treated Multiwell Cell Culture Plate (6,12,24 well)	Corning
Foliodrape surgical drapes	PAUL HARTMANN
Glass vials with rolled rim, 15ml	Carl Roth
Hard-Shell 96-Well PCR Plates, thin-well	BIO-RAD
Injekt-F syringes, 1ml	B. Braun
Mersilene suture, 4-0	Ethicon
MicroAmp Fast Optical 96-Well Reaction Plate	Applied Biosystems
Microscope slides (76×26×1 mm)	Th. Geyer
Microseal 'B' PCR Plate Sealing Film	BIO-RAD
Microtome Blade - N35HR	FEATHER
Microtome blades, A35	FEATHER Safety Razor
Milllex-GP Filter Unit (Sterile)	Millipore
PCR SingleCap 8er-SoftStrips 0.2ml	Biozym
Safe-Lock tubes, 1.5ml	Eppendorf

SafeSeal reaction tubes, 0.5ml	SARSTEDT
Serological pipettes, 10ml	SARSTEDT
Serological pipettes, 25ml	SARSTEDT
Serological pipettes, 5ml	SARSTEDT
Sterican needles, 26G	B. Braun
Sterican needles, 27G	B. Braun
Sterile gauze swabs	Fink & Walter
Sterile surgical blades	Bayha

3.1.5. Primers

Genotyping primers	
Name	Sequence
Primer 1 (α CGRP ^{-/-} forward)	CAAACCAGGATCCAAACTGCCCCAT CCTGAATATC
Primer 2 (α CGRP ^{-/-} reverse)	GTTCTAGACTTCATTCTGGGGC
Primer 3 (CALCA ^{-/-} WT forward)	GGAGCCTGCCGTCCAGCGAA
Primer 4 (CALCA ^{-/-} KO forward)	GGTGGATGTGGAATGTGTGC
Primer 5 (CALCA ^{-/-} common reverse)	CAGGATCAAGAGTCACCGCT
Primer 6 (CTR ^{-/-} WT forward)	TCCTGGGCTGCTGAGAAAGTATC
Primer 7 (CTR ^{-/-} WT reverse)	ATGTGATTGGCTGGGCACTG
Primer 8 (CTR ^{-/-} KO forward)	ACCATGCATGAGTGTGGAGA
Primer 9 (CTR ^{-/-} KO reverse)	AAGACAGATGGTGAGGGCTGACTG
Sybr green primers	
Name	Sequence
<i>Angptl2</i> forward	TGAGTTGCCATGCCATCAGG
<i>Angptl2</i> reverse	TGGCATTGCAGTCATCTGGT
<i>Angptl4</i> forward	GAGGACCCCTTTTCCGTGTT
<i>Angptl4</i> reverse	CCCAACTTCTCTGGTAGGCG
<i>Socs3</i> forward	GATTCACCCAGGTGGCTACA
<i>Socs3</i> reverse	GAGGCTCTCGGACCTACTGA
<i>Gapdh</i> forward	TGCACCACCAACTGCTTAG
<i>Gapdh</i> reverse	GGATGCAGGGATGATGTTC
<i>Calcr</i> forward	CCTGACAGCAACCGAACCT
<i>Calcr</i> reverse	AGCAGCAATCGACAAGGAGT
Taqman primers	
Name	Assay ID
<i>Calca</i>	Mm00801463_g1
<i>Calcl</i>	Mm00516986_m1

<i>Cre</i>	Mm04336053_g1
<i>CD14</i>	Mm01158466_g1
<i>Sphk1</i>	Mm00448841_g1
<i>αCGRP</i>	Mm00801463_g1

3.1.6. Commercial Kits

Name	Art.-Nr /PZN	Manufacturer
NucleoSpin RNA/Protein	740993.250	MACHEREY-NAGEL
ProtoScript First Strand cDNA Synthesis Kit	E6300s	NEW ENGLAND Biolabs
Kawamoto embedding kit	-	Section-Lab

3.1.7. Softwares

Name	Version	Manufacturer
Adobe Illustrator CC	22.0.0	Adobe Inc.
CellSens Entry	1.6	Olympus Corporation
EndNote	X9	Clarivate Analytics
GraphPad Prism	9.1.1	GraphPad Software Inc.
Microsoft Office 2019	16.22	Microsoft Corporation
OsteoMeasure 7	4.2.0.1	Osteometrics Inc.
μCT Evaluation Program	6.6	Scanco Medical AG
μCT Ray	4.0-4	Scanco Medical AG
ImageJ	V1.5.1	National Institute of Mental Health
BoneJ	V1.4.3	Imperial College London

3.2. Methods

3.2.1. Mice

In the present study, WT, *CALCA*^{-/-}, *αCGRP*^{-/-}, and *CTR*^{-/-} mice were used. The generation of genetically modified mice has been previously described (Hoff et al., 2002; Keller et al., 2014; Lu et al., 1999). All in vivo animal experiments were performed in accordance with the current recommendations of the “Report of the American Veterinary Medicine Association Panel on Euthanasia” and with approval from the “Behörde für Justiz und Verbraucherschutz-Lebensmittelsicherheit und Veterinärwesen”. Mice were housed in a specific pathogen-free animal facility, maintained on standard conditions at a 12-hour light/dark cycle, and fed ad libitum.

3.2.1.1. Genotyping

The genotypes of the mice were confirmed using polymerase chain reaction (PCR) and agarose gel electrophoresis. Tail biopsies were harvested from newborn mice, and DNA was isolated using standard lysis buffer and incubated at 95°C for 2 hours. The composition of PCR and cycler running programs are listed as follows (**Table 1-3**). The sequences of the primers were listed in the section “**3.1.5. Primers**”. The PCR products were loaded on 2-3% agarose gel in Tris-borate buffer with GreenSafe Premium as a nucleic acid stain followed by electrophoresis at 80V for 45 minutes. A gene ruler was used as a reference for the sizes of the PCR products. The gels were visualized with ultraviolet light using the Bio-Rad ChemiDoc Imaging System.

Table 1. PCR protocols for α CGRP^{-/-} mice genotyping

Component	volume (μl)	Program		
10x Dream Green	3	Initialization	95°C	3 min
DMSO 100%	0.6	Denaturation	95°C	30 s
Primer F 10μM	3	Annealing	59.4°C	30 s
Primer R 10μM	3	Elongation	72°C	30 s
MgCl ₂ 25mM	1.8	Last Elongation	72°C	7 min
dNTP Mix 10mM	0.6	Store	4°C	
Dream Taq	0.3	Target band: WT 205 bp Primer 1/Primer 2 KO 220 bp Primer 1/Primer 2		
Genom.DNA	1			
ddH ₂ O	16.7			
3% Agarose gel, O’RangeRuler 20 bp DNA Ladder as gene ruler				

Table 2. PCR protocols for CALCA^{-/-} mice genotyping

Component	volume (μl)	Program		
10x Dream Green	2	Initialization	95°C	3 min
DMSO 100%	0.4	Denaturation	95°C	30 s
Primer F 10μM	1	Annealing	64.3°C	30 s
Primer R 10μM	1	Elongation	72°C	30 s
dNTP Mix 10mM	0.4	Last Elongation	72°C	7 min
Dream Taq	0.2	Store	4°C	
Genom.DNA	1	Target band: WT 300 bp Primer 3/Primer 5 KO 200 bp Primer 4/Primer 5		
ddH ₂ O	14			
2% Agarose gel, DNA Ladder as gene ruler				

Table 3. PCR protocols for *CTR*^{-/-} mice genotyping

Component	volume (μl)	Program		
10x Dream Green	3	Initialization	95°C	3 min
DMSO 100%	0.3	Denaturation	95°C	30 s
Primer F 10μM	0.7	Annealing (first 15 cycles)	63.2°C -0.4°C	30 s
Primer R 10μM	0.7	Annealing (last 20 cycles)	58°C	30 s
dNTP Mix 10mM	0.5	Elongation	72°C	30 s
Dream Taq	0.2	Last Elongation	72°C	7 min
Genom.DNA	1	Store	4°C	
ddH ₂ O	23.6	Target band: WT 250 bp Primer 6/Primer 7 KO 450 bp Primer 8/Primer 9		
2% Agarose gel, DNA Ladder as gene ruler				

3.2.1.2. Perioperative management

In the present study, a minimum acclimation period of 2 weeks after the transportation was provided prior to the operation. Preoperatively, mice were anesthetized by isoflurane inhalation at a concentration of 4% for induction and 1.5% for maintenance. 150 mg/kg clindamycin and 0.1 mg/kg Buprenovet® were administered intraperitoneally to prevent infection and provide analgesia. Ophthalmic ointment was used after anesthesia to maintain ocular hydration. All surgical instruments and materials were sterilized, and the respective surgical sites underwent depilation and disinfection. After the operation, mice were placed in recovery racks overnight and received drinking water with 1 mg/ml metamizole for 3 days.

3.2.1.3. Anterior cruciate ligament transection (ACLT)

The mouse was anesthetized as described previously and placed in the supine position. The right knee joint was exposed via a medial parapatellar incision. The anterior cruciate ligament (ACL) was exposed by lateral dislocation of the patella. The ACLT was made using a microsurgical scalpel, and the transection was confirmed by a positive anterior drawer test. The wound was closed with layered sutures.

3.2.1.4. OVX

Following anesthesia, the mouse was placed in the prone position, and the skin of the flank area was shaved and disinfected. An incision in the center of the dorsal skin was made, and the subcutaneous fascia was bluntly dissected. Following an incision in the posterior abdomen, the left ovary was exposed and excised after ligating the area inferior to the ovary. The identical procedure was performed on the right side. The wound was closed with a layered suturing technique.

3.2.2. Study design

The in vivo experiments utilized two surgical mouse models: the ptOA model induced by ACLT and the postmenopausal osteoporosis model established by OVX. For ptOA, female mice at 12-14 weeks with different genotypes were subjected to ACLT to induce ptOA and sacrificed 4 and 8 weeks postoperatively. In terms of the OVX model, female mice were operated with ovariectomy at the age of 8 weeks. After 4 consecutive weeks, pramlintide treatment was initiated for further 4 weeks. The minimum sample size was calculated using a resource equation approach, yielding a minimum group number of

n = 6 mice (Arifin & Zahiruddin, 2017). Considering the occasional loss of samples during histologic processing, n=8 per group and time point was used. Groups were assigned randomly, and researchers were blinded during sample processing and analyses. All experiments were performed with the involvement of appropriate replicates.

3.2.3. Sample preparation

Mice were sacrificed at indicated time points, and tissues were harvested for further processing. For sacrifice, all the mice were deeply anesthetized with isoflurane inhalation, followed by terminative blood collection via cardiac puncture. The blood samples were placed at room temperature for 30 minutes and centrifuged at 3000rcf, 4 °C for 15 minutes, and the supernatant serum was obtained and stored for further analysis. For mice with ptOA, the operated knee and the contralateral healthy knee were dissected and fixed in Formafix for 48 hours. For mice operated with OVX, the skeleton was dissected with the removal of skin and organs in thoracic and abdominal cavities and then fixed in Formafix for 48 hours. After fixation, the lumbar spine (L2-L5), right femur, and right tibia were isolated for subsequent radiological and histological analysis. The rest of the skeleton was transferred into 70% ethanol for long-term storage.

3.2.4. X-ray microtomography (μ CT) evaluation

Scanco vivaCT, 80 with a voxel size of 15.6 μ m at 70kVp, 113 μ A, and 400ms integration time, was used for μ CT analysis. μ CT Ray V4.0-4 and ImageJ were used to generate the three-dimensional models and the representative images. The bilateral knees, lumbar spine, and femora were scanned after fixation. For subchondral trabecular bone and osteophyte evaluation, the volume of interest (VOI) was defined by manual contouring, while the analysis for spinal trabecular bone, femoral trabecular bone, and femoral midshaft cortex was carried out using automatic evaluation scripts. The femoral trabecular bone was evaluated using the volume from 500 μ m to 2500 μ m proximal to the distal growth plate, while a volume within 1000 μ m in the middle of the diaphysis was used for cortical bone evaluation. Regarding spinal trabecular bone, a 500 μ m volume from the distal growth plate of the L4 vertebra body was defined as VOI. The respective volumes were evaluated using μ CT Evaluation Program V6.6. The assessed parameters include osteophyte volume (mm^3), bone volume fraction (BV/TV; %), trabecular number (Tb.N; mm^{-1}), trabecular thickness (Tb.Th; mm), and trabecular

separation (Tb.Sp; mm), cortical thickness (Ct.Th; mm) and cortical porosity (Ct.Po; %). Data were reported according to the guidelines for tissue imaging by the American Society of Bone and Mineral Research (Dempster et al., 2013).

3.2.5. Histology

3.2.5.1. Paraffin Histology

Following μ CT analysis, the knee samples were further processed for paraffin embedding and histological analysis. In brief, the knee samples were decalcified in 0.5M EDTA (pH7.4) solution for 7 days at 4°C in a roller mixture, with a solution change on the third day. Afterward, the samples were dehydrated in an autotechnicon with ascending concentrations of ethanol and xylene baths (**Table 4**) and subsequently embedded in paraffin. Coronal sections with a thickness of 4 μ m were prepared. Bone-inflammation-cartilage (BIC) stain, TRAP stain, and hematoxylin and eosin (H&E) stain were carried out (**Table 5-7**).

Table 4. Paraffin Program of Autotechnicon

Reagent	Time (hour)	Times
70% ethanol	1	2
80% ethanol	1	1
96% ethanol	1	1
100% ethanol	1	2
Xylene	1	2
Paraffin (58-60°C)	1	3

Table 5 Steps of the BIC stain

Reagent/ Equipment	Time (min)	Times/Endpoint
62°C incubator	60	1
Xylene	5	3
100% ethanol	2	2
96% ethanol	2	2
Weigert's iron hematoxylin	10	1
Running tap water	30	Blueing
Van Gieson's solution	15	1
Distilled water	Gently rinsing	Removing excess stain

Reagent/ Equipment	Time (min)	Times/Endpoint
0.01% Fast green	3	1
1% Acetic acid	10-15 sec	1
0.1% Safranin O	5	1
96% ethanol	2	2
100% ethanol	2	2
Xylene	2	3
DPX new mounting medium	Mounting	/

Table 6 Steps of the TRAP stain

Reagent/ Equipment	Time (min)	Times/Endpoint
60°C incubator	15-30	1
Xylene	5	3
100% ethanol	2	2
96% ethanol	2	1
80% ethanol	2	1
70% ethanol	2	1
Distilled water	2	1
TRAP substrate solution at 37°C with shaking	30-60	1
Distilled water	Dipping	1
Mayer's hemalum solution, 1:10 diluted	1	1
Running tap water	10	Blueing
Kaiser's glycerol gelatin mounting medium	Mounting	/

Table 7 Steps of the H&E stain

Reagent/ Equipment	Time (min)	Times/Endpoint
60°C incubator	15-30	1
Xylene	5	3
100% ethanol	2	2
96% ethanol	2	1
80% ethanol	2	1
70% ethanol	2	1
Distilled water	2	1
Mayer's hemalum solution	6	1
Tap water	2	1

HCl-ethanol solution	Dipping	2-3
Running tap water	10	Blueing
Eosin Y-solution 0.5% alcoholic	3	1
80% ethanol	Differentiation/clearing	/
96% ethanol	1	1
100% ethanol	2	2
Xylene	2	3
DPX new mounting medium	Mounting	/

3.2.5.2. Non-decalcified acrylate histology

The spine and tibia samples were further processed according to acrylate embedding protocol. Followed by dehydration in an autotechnicon with ascending concentrations of ethanol, the samples were infiltrated with destabilized MMA solution twice for 48 hours and then embedded with fresh-made MMA embedding solution. The polymerization was carried out at 4°C overnight. After grinding the plastic blocks, 3-5 µm thick sections were prepared for subsequent TRAP, toluidine blue, and Von Kossa/ Van Gieson stain. The acrylate program of the autotechnicon and staining protocol are detailed as follows (**Table 8-10**).

Table 8. Acrylate Program of Autotechnicon

Reagent	Time (hour)	Times
70% ethanol	2	2
80% ethanol	2	2
96% ethanol	2	2
100% ethanol	2	2

Table 9. Steps of the toluidine blue staining

Reagent/ Equipment	Time (min)	Times/Endpoint
Deplasting	5	3
100% ethanol	2	2
96% ethanol	2	1
80% ethanol	2	1
70% ethanol	2	1
Distilled water	2	1
1% Toluidine-blue solution	30	1
Distilled water	Dipping	1

70% ethanol	Differentiation	/
80% ethanol	Differentiation/Clearing	/
96% ethanol	2	1
100% ethanol	1	2
Xylene	5	3
DPX new mounting medium	Mounting	/

Table 10. Steps of the Von Kossa staining

Reagent/ Equipment	Time (min)	Times/Endpoint
Deplasting	5	3
100% ethanol	2	2
96% ethanol	2	1
80% ethanol	2	1
70% ethanol	2	1
Distilled water	2	1
3% silver nitrate solution	5	1
Distilled water	10	1
Sodaformol	5	1
Running Tap water	10	1
5% sodium thiosulfate solution	5	1
Tap water	10	1
Van Gieson stain solution	20	1
Tap water	Rinsing briefly	/
80% ethanol	Rinsing briefly	/
96% ethanol	Rinsing briefly	1
100% ethanol	1	2
Xylene	2	3
DPX new mounting medium	Mounting	/

3.2.5.3. Non-decalcified frozen histology

An independent group of WT animals was employed for frozen sections. The operated knees were dissected 4 weeks after ACLT and processed according to a modified Kawamoto frozen section protocol (Kawamoto & Kawamoto, 2014). In brief, the knee joints were dissected and fixed with 4% PFA at 4°C overnight. Following washing in PBS 3 times, the samples were infiltrated with ascending sugar solution with a concentration of up to 30% and embedded with SCEM medium. 5-7µm thick

cryosections were prepared and stored at -80°C for subsequent immunofluorescence staining.

3.2.5.4. Immunofluorescence staining

The frozen sections were air dried at room temperature for 30 minutes and washed with PBS 3 times, followed by blocking in 3% BSA/5% donkey serum/PBS. Then, the sections were incubated with anti-PCT (1:150, LSBio, LS-C296040), anti-CT (1:200, Invitrogen, PA5-16464), anti-CGRP (1:300, Abcam, ab47027), anti-CTR (1:300, Bioss Antibodies, bs-0124R-TR), and anti-CRLR (1:200, Bioss Antibodies, bs-1860R-TR) at 4°C overnight. Following subsequent washing, a secondary antibody (1:500, Life technologies, A21098) was applied, and Fluomount-G with DAPI (Thermo Fisher Scientific, 00-4959-52) was used as the mounting medium. Images were acquired using a spinning disk fluorescent microscope and processed using ImageJ.

3.2.5.5. Histomorphometry

Histomorphometric analysis was carried out to evaluate the pathological changes in the knee joints and spine. The structural and cellular parameters of the trabecular bone were measured in the tibial subchondral bone and spinal vertebra body. The analysis was performed using an OsteoMeasure system connected to a BX50 microscope equipped with a DP72 camera. For trabecular bone evaluation, the indices of osteoblasts were quantified on H&E-stained sections, while the osteoclast parameter measurement was carried out on TRAP-stained sections. The assessed parameters included osteoblast surface per bone surface (Ob.S/BS; %), number of osteoblasts per bone perimeter (Ob.N/B.Pm; mm^{-1}), osteoclast surface per bone surface (Oc.S/BS; %) and number of osteoclasts per bone perimeter (Oc.N/B.Pm; mm^{-1}).

3.2.5.6. Histological scoring

To further describe the pathological changes in the diseased knees, semi-quantitative Osteoarthritis Research Society International (OARSI) score, osteophyte score, and synovitis score were graded using knee sections stained with BIC. For each sample, four joint quadrants were scored separately, and the total scores of tibial and femoral compartments as well as the total joints were plotted and presented.

3.2.5.6.1. OARSI score

The OARSI scoring system was used to grade the cartilage degeneration (Gerwin, Bendele, Glasson, & Carlson, 2010). The details of the scoring are listed as follow (Table 11).

Table 11. Description of the OARSI score

Grade	Changes
0	Normal
0.5	Loss of Safranin-O without structural changes
1	Small fibrillations without loss of cartilage
2	Vertical clefts down to the layer immediately below the superficial layer and some loss of surface lamina
3	Vertical clefts/erosion to the calcified cartilage extending to < 25% of the articular surface
4	Vertical clefts/erosion to the calcified cartilage extending to 25-50% of the articular surface
5	Vertical clefts/erosion to the calcified cartilage extending to 50-75% of the articular surface
6	Vertical clefts/erosion to the calcified cartilage extending > 75% of the articular surface

3.2.5.6.2. Osteophyte score

The maturity and size of the osteophyte were scored to assess the osteophyte formation (Range 0-6) (Little et al., 2009). The scoring method is presented (Table 12).

Table 12. Description of the osteophyte score

Grade	Changes	
	Size	Maturity
0	None	None
1	< 1 × the thickness as the adjacent cartilage	Predominantly cartilaginous
2	1-3 × the thickness as the adjacent cartilage	Mixed cartilage and bone with active vascular invasion and endochondral ossification
3	> 3 × the thickness as the adjacent cartilage	Predominantly bone

3.2.5.6.3. Synovitis score

The synovitis was scored by measuring the thickness of the synovial lining cell layer and the cellular density of the synovial stroma (Lewis et al., 2011). The grading details

are listed as follow (**Table 13**).

Table 13. Description of the synovitis score

Grade	Changes	
	Enlargement of synovial lining cell layer	Density of cells in synovial stroma
0	1-2 cell layers	Normal
1	3-4 cell layers	Slightly increased
2	5-9 cell layers	Moderately increased
3	≥ 10 cell layers	Greatly increased

3.2.6. Gene expression analysis

For the gene expression in OA progression, an independent set of WT animals (C57BL/6) was employed for gene expression analysis. The mice were subjected to ACLT, and the right knee joints were harvested at 2, 4 and 8 weeks postoperatively. Sham-operated WT mice were employed as controls, and the knee joints were collected 2 weeks after the induction. Regarding the gene expression of osteoclasts, bone marrow-derived osteoclasts were cultured and harvested at the indicated time points. All samples were processed using a standardized RNA isolation protocol. RNA was purified using a NucleoSpin RNA kit and quantified using Nanodrop 2000. Complementary DNA (cDNA) was then synthesized using the ProtoScript First Strand cDNA Synthesis Kit. Real-time quantitative reverse transcription polymerase chain reaction (qRT-PCR) was performed using TaqMan Assay-on-Demand primer sets or Sybr green reaction system. Glyceraldehyde-3-phosphate dehydrogenase (*Gapdh*) was used as a housekeeping gene, and the expression of target genes was presented in arbitrary units (A.U.) relative to the expression of *Gapdh* mRNA. Primer sequences are listed in “**3.1.5. Primers**” section.

3.2.7. ELISA

The serum samples for ELISA analysis were isolated from the WT mice used in gene expression analysis. Commercial ELISA kits were applied to measure the concentration of CT (LS-F23047, LSBio, Seattle, USA), PCT (CSB-E10371m, CUSABio, Houston, USA), and CGRP (LS-F37469, CUSABio, Houston, USA) according to manufacturer’s instructions.

3.2.8. Primary osteoclast isolation and differentiation

Separate sets of WT and *CTR*^{-/-} mice of mixed genders and ages were used for primary osteoclast isolation. In brief, the bilateral femora, tibiae, and hip bones were dissected, and the surrounding soft tissue was removed. Then, the bones were transferred to the cell culture hood, and the bone marrow cavities were cut open on the proximal femora and distal tibia. The hip bones were cut on the distal end of the ilia. Each of the two opened bones was loaded with the open sides downwards into a PCR tube mounted in an Eppendorf tube. The bottom of the PCR tube was cut open. The loaded tubes were centrifuged at 8000rpm, room temperature for 30 seconds, and the bone marrow was collected in the Eppendorf tube. The bone marrow pellets were resuspended in 500µl medium and filtered through a 70µm cell strainer. The cell counting was performed using a Neubauer cell counting chamber according to the manufacturer's protocol. The cell solution was diluted to a density of 7 million cells per ml according to the counting results, and the cells were seeded into cell culture plates depending on the experimental design.

3.2.9. Cell culture

In the present study, all cells were cultured in complete Minimum Essential Medium Alpha modification (α -MEM), supplemented with 10% fetal bovine serum, and 1% Penicillin/Streptomycin. Cells were kept at 37°C, 95 % relative humidity, and 5% CO₂ in an incubator. For osteoclast differentiation, osteoclast precursors were isolated and differentiated for 3 days in α -MEM containing 10nM 1,25-dihydroxyvitamin D₃. For the following 6 days, the cells were treated with M-CSF (20ng/ml) and RANKL (40ng/ml) to allow terminal differentiation. To investigate the effects of pramlintide on osteoclast differentiation, osteoclast precursors were treated with pramlintide (100nM) for 3 days. For short-term treatment, the cells were treated with pramlintide for 6 hours.

3.2.10. RNA sequencing and transcriptome analysis

Osteoclast total RNA samples were sent to BGI Genomics for mRNA sequencing. In brief, the transcriptome library was generated according to a standard mRNA library construction procedure with sequencing carried out on the DNBSEQ platform. Following quality control on the raw reads, the sequencing data was filtered using SOAPnuke (version v1.5.2, developed by BGI) to remove low-quality reads or adaptor-containing reads. Subsequently, the filtered clean data was aligned to the reference genome (GRCm39) using Hierarchical Indexing for Spliced Alignment of Transcripts

(HISAT) software. The statistics of the mapping rate and the distribution of reads on the reference sequence were evaluated to validate the quality of alignment. For gene expression analysis, clean reads were mapped to reference transcripts using Bowtie2 (ver 2.2.5), and expression levels were calculated using RSEM (v1.2.8). Volcano plot, Cluster heatmap and differentially expressed gene (DEG) analysis were carried out using Dr. Tom system and Galaxy web platform.

3.2.11. Statistics

Statistical analyses were performed using GraphPad Prism version 9.1.1 (GraphPad Software Inc., La Jolla, USA). Outliers are determined via Grubbs' test with a p value > 0.05 and excluded for further analysis. Unpaired two-tailed students t-test, one-way ANOVA, and two-way ANOVA followed by Tukey's post-hoc test were used as indicated to determine differences. Differences were considered statistically significant at $p < 0.05$.

4. Results

4.1. *PCT/CT* transcripts protect from cartilage deterioration and subchondral bone loss, while α CGRP is a potent driver of osteophyte formation

OA represents one of the primary causes of chronic pain, impaired mobility and decreased quality of life in the aged population. A number of studies have suggested that the calcitonin family of peptides is crucially involved in the pathogenesis of OA, including ptOA. Nevertheless, it still remains poorly understood how *CALCA*-encoded peptides are involved in the progression of ptOA. In this first part, *CALCA*^{-/-} mice lacking both *PCT/CT* transcript and α CGRP transcript, and α CGRP^{-/-} mice with deficiency of solely α CGRP transcript, were employed and subjected to ACLT to delineate their roles in ptOA.

4.1.1. The expression of both the *PCT/CT* and the α CGRP transcript is induced during ptOA progression

To assess the involvement of the *CALCA*-encoded peptides in ptOA progression, expression of the *PCT/CT* and α CGRP transcripts were first monitored in ACLT- and sham-operated knees of WT mice. The expression of *PCT/CT* transcript was upregulated 4 weeks after the surgery, while no differences were detected 2 or 8 weeks postoperatively compared to the sham group. α CGRP expression was increased 4 and 8 weeks after ACLT (**Figure 11A**). CRLR represents the receptor that mediates the biological effects of both PCT and α CGRP. CRLR-encoding gene, *Calcr1*, was overexpressed throughout ptOA progression. Then, the expression of *CALCA*-encoded peptides and CRLR during ptOA was further analyzed on protein level using immunofluorescent staining (**Figure 11B**). Fluorescent microscopy showed that signals of PCT, CRLR and α CGRP were observed in the subchondral bone compartment, while only PCT and CRLR were detected in the articular cartilage of the ptOA knees 4 weeks after the induction. Of note, the expression of CT protein was not noticed, suggesting that the upregulated *PCT/CT* transcript gives rise to the PCT protein, instead of CT, during ptOA. Finally, using ELISA, the circulating levels of PCT, CT, and CGRP were measured in WT mice during ptOA progression (**Figure 11C**). No significant differences were observed in the levels of all three *CALCA*-derived peptides, indicating a local impact of *CALCA* expression in ptOA progression.

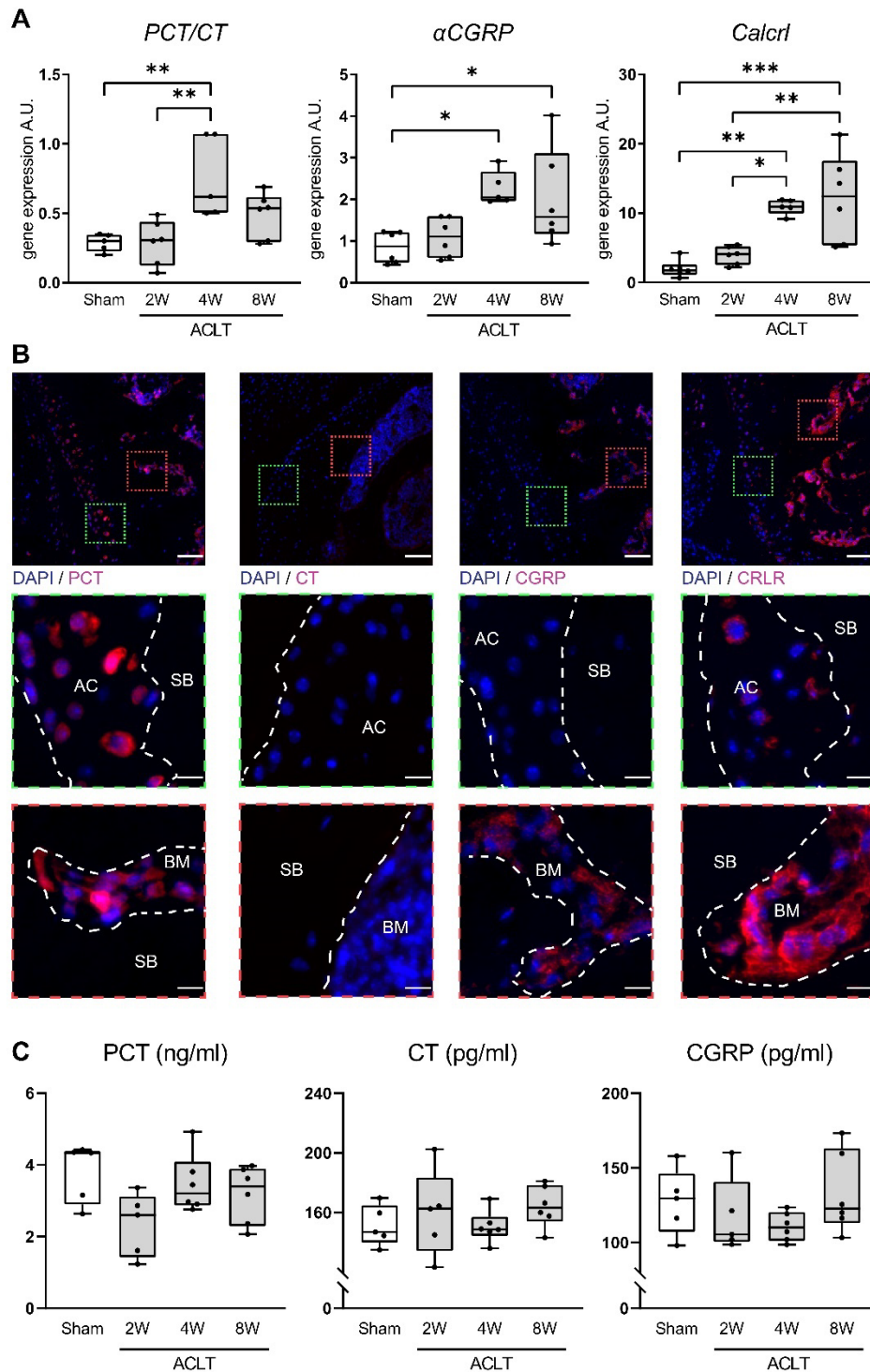


Figure 11. The *PCT/CT* and α *CGRP* transcripts are overexpressed during pOA progression. A Gene expression analysis of the *PCT/CT* and α *CGRP* transcript in addition to the CRLR (encoded by *Calcr1*) in WT knees subjected to sham or ACLT surgery and harvested at the indicated time points. n = 5-6 biologically independent animals per group, presented in arbitrary units (A.U.) relative to expression of *Gapdh* mRNA. **B** Representative overview images of immunofluorescent stainings specific for PCT, CT, CGRP, and CRLR in the proximal tibia of the knee joint 4 weeks after ACLT. Site-matched images with higher magnification are presented in red and green boxes below. Subchondral bone (SB), articular

cartilage (AC) and subchondral bone marrow (BM) are indicated. Scale bar = 1st row 100 μm ; 2nd and 3rd rows 25 μm . **C** Serum concentrations of the indicated proteins in WT mice at the indicated time points after sham or ACLT surgery as measured by ELISA. n = 5-6 biologically independent animals per group as indicated per time point. Ordinary one-way ANOVA, box plots represent median with minimum and maximum whiskers. *P < 0.05, **P < 0.01, ***P < 0.001. Figure modified according to (Jiang et al., 2024).

4.1.2. The inactivation of the *PCT/CT* transcript aggravates ACLT-induced cartilage degeneration

To delineate the functions of *CALCA*-derived transcripts in ptOA, *CALCA*- and αCGRP -deficient mice were subjected to ACLT and compared to WT controls. Deficiency of *CALCA* results in the absence of PCT, CT and αCGRP , while $\alpha\text{CGRP}^{-/-}$ mice exclusively lack αCGRP . As cartilage degeneration represents the hallmark of ptOA progression, ACLT-induced articular cartilage deterioration was first investigated in the employed mouse lines. At 4 weeks after the surgery, WT joints displayed remarkably reduced proteoglycans, accompanied by cartilage fibrillations and erosion (**Figure 12A**). Semiquantitative grading using OARSI scores revealed that scores of the total joint in *CALCA*-deficient mice were significantly higher than WT controls, while αCGRP -deficient mice displayed lower total joint scores compared to either WT or *CALCA*^{-/-} mice at the 4-week time point (**Figure 12B**). Similar observations were made in the OARSI scores of the femur and tibia compartments. *CALCA*^{-/-} mice showed a significantly higher score in the femur compared to either WT or αCGRP -deficient mice, while a reduced tibial OARSI score was detected in αCGRP -deficient mice. At 8 weeks after surgery, no significant changes were detected in either *CALCA*-deficient or αCGRP -deficient mice compared to WT controls, however, the OARSI scores in mice lacking αCGRP were significantly lower than that in *CALCA*-deficient mice. To further characterize cartilage degeneration, histomorphometric analysis were carried out to measure the thickness of subchondral bone plate and the ratio of hyaline cartilage to calcified cartilage in the diseased joints. In WT mice, ACLT resulted in a thinner layer of subchondral bone plate and a reduced hyaline cartilage proportion at both 4 and 8 weeks postoperatively (**Figure 12C**). For comparison of mouse lines, the data of operated knees were then normalized to those of the contralateral healthy knees and fold changes were plotted. *CALCA*^{-/-} mice displayed a significantly more pronounced reduction in the thickness of the subchondral bone plate 4 and 8 weeks after ACLT,

while no significant differences in the hyaline cartilage proportion were noticed between the three employed mouse lines at both time points studied (**Figure 12D**).

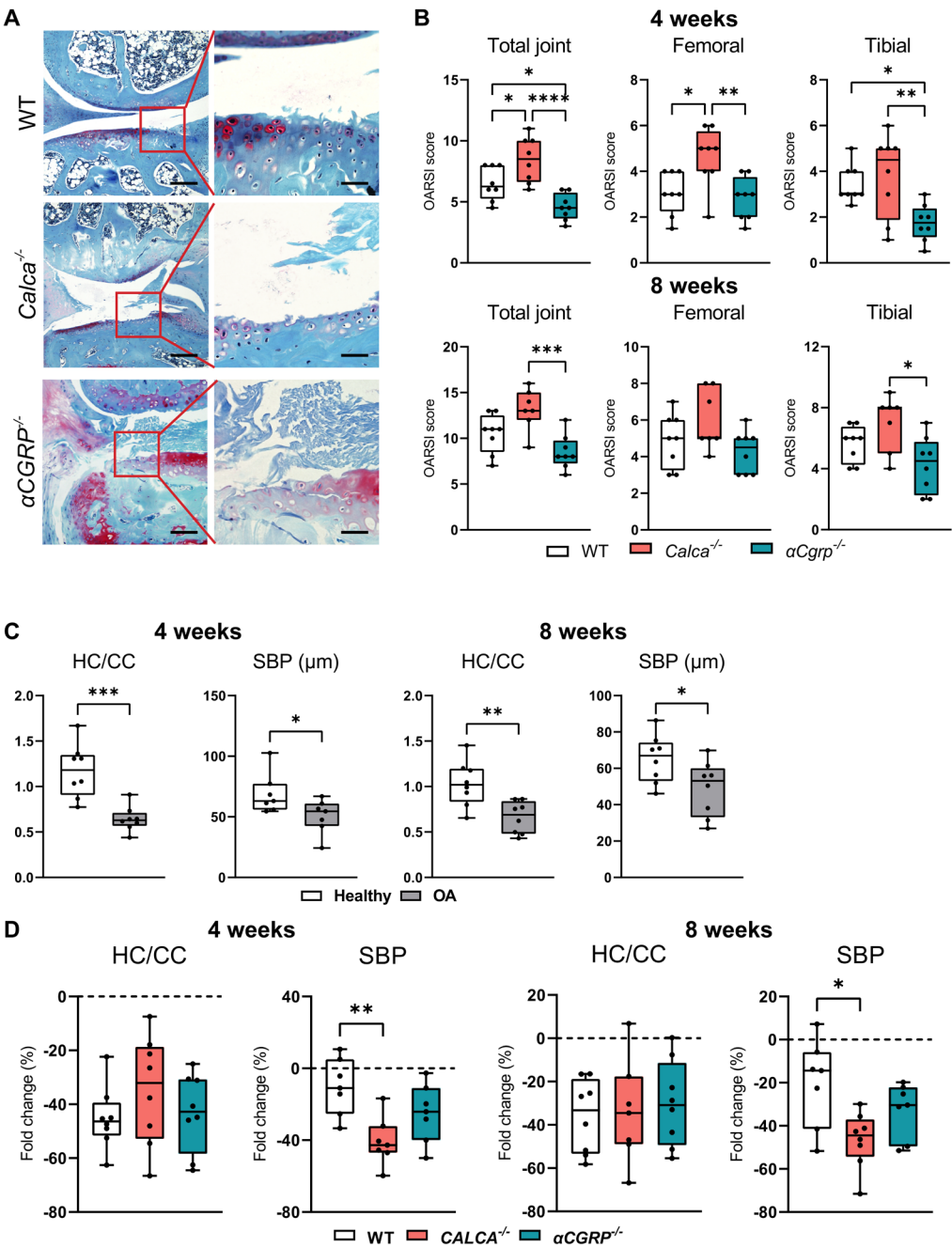


Figure 12. PCT/CT-deficiency aggravates cartilage degeneration after ACLT. A Representative images of medial knee joints stained with BIC 4 weeks after ACLT (scale bar = left column 200 μm; right column 50 μm). The articular cartilage stains red and the bone stains blue. **B** Osteoarthritis Research Society International (OARSI) scoring of total joints as well as of femoral and tibial compartments at the indicated time points. **C** Quantitative analysis of the ratio of hyaline cartilage thickness to calcified cartilage thickness (HC/CC) and the subchondral bone plate thickness (SBP) in healthy and diseased knees from WT mice 4 and 8 weeks after ACLT. **D** Relative alterations at the indicated timepoints (ACLT

vs. contralateral healthy controls) in the SBP and HC/CC. n = 7-8 biologically independent animals as indicated per group and time point. For **B** and **D** ordinary one-way ANOVA was used and for **C** unpaired two-tailed students t-test was used to determine differences. Box plots represent median with minimum and maximum whiskers. *P < 0.05, **P < 0.01, ***P < 0.001, ****P < 0.0001. Figure modified according to (Jiang et al., 2024).

4.1.3. Abnormal subchondral bone architecture in *CALCA*- but not α CGRP-deficient mice

Next, to assess changes in subchondral bone microstructure induced by ACLT, radiological analysis was carried out in injured and contralateral healthy joints. In WT mice, decreased bone volume per tissue volume of the subchondral trabecular bone was noticed in ptOA knees compared to contralateral controls at 4 and 8 weeks postoperatively (**Figure 13A**). Similarly, the trabecular numbers were decreased 4 weeks after ACLT, while trabecular thickness and separation remained unaltered in WT ptOA knees at both time points studied. To compare alterations in genetically modified mice, fold changes of operated joints to contralateral controls were presented. *CALCA*-deficient mice exhibited a significantly more pronounced subchondral bone deterioration. At 4 weeks postoperatively, the reduction in bone volume per tissue volume, trabecular numbers and thickness were significantly more pronounced in *CALCA*^{-/-} mice compared to either WT or α CGRP^{-/-} mice (**Figure 13B, C**). At 8 weeks after ACLT, the structural parameters did not differ between the three employed mouse lines, except a more pronounced reduction in trabecular numbers in α CGRP-deficient mice. A potential explanation is that the severe joint deformity at this late stage of ptOA may mask phenotypical changes.

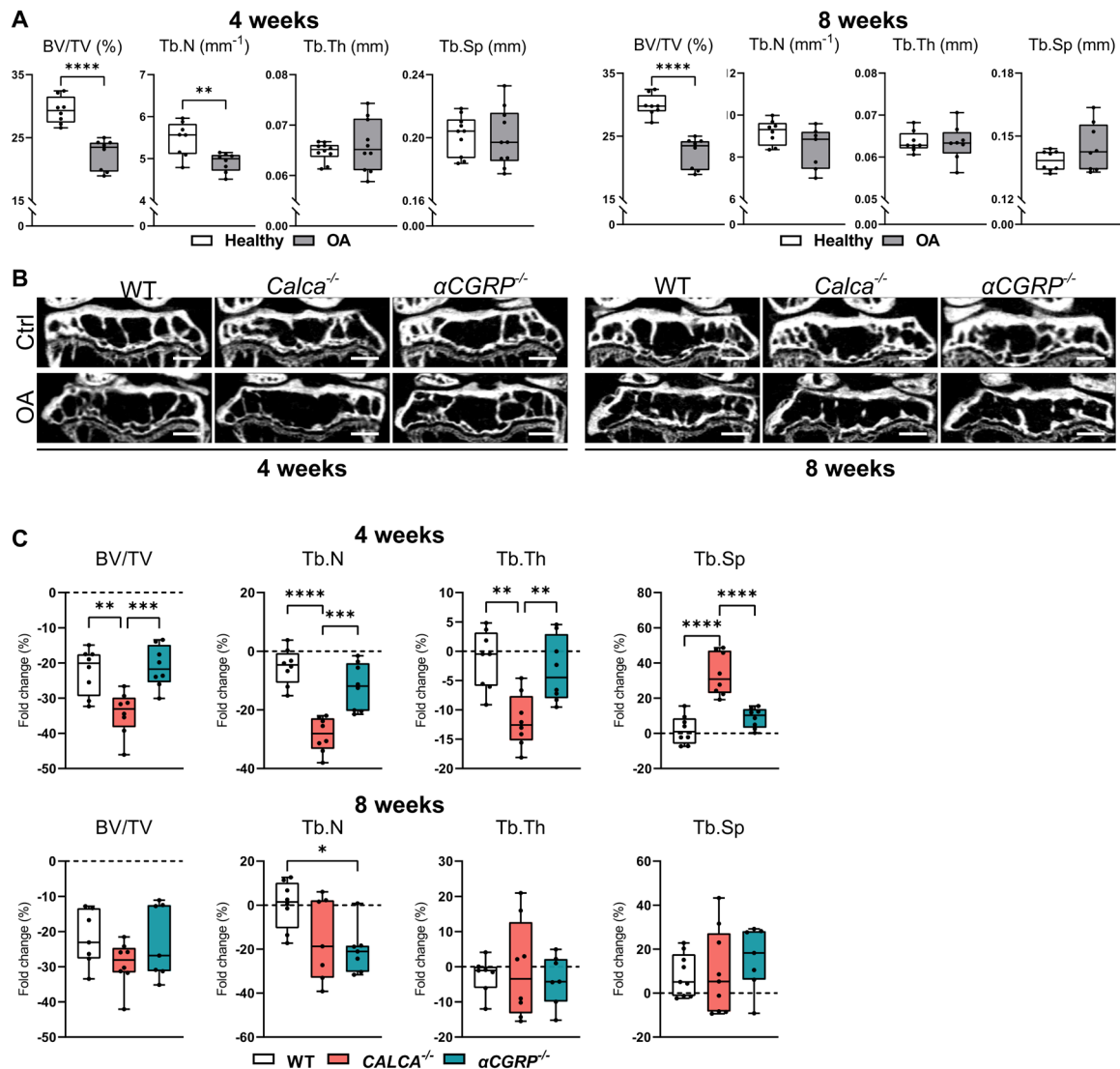


Figure 13. Lack of the *PCT/CT* transcript exacerbates loss of subchondral trabecular bone. A μ CT-based, quantitative analysis of tibial subchondral trabecular bone of the bone volume fraction (BV/TV), trabecular numbers (Tb.N), trabecular thickness (Tb.Th), and trabecular separation (Tb.Sp) at the indicated time points in WT mice. **B** Representative micro-CT coronal views of tibial subchondral trabecular bone of diseased (OA) and contralateral control (Ctrl) knees from the indicated groups 4 and 8 weeks after ACLT (scale bar = 500 μ m). **C** Relative alterations at the indicated time points (ACLT vs. contralateral healthy controls) in BV/TV, Tb.N, Tb.Th and Tb.Sp, expressed as fold differences. n = 7-8 biologically independent animals as indicated per group and time point. For **A** unpaired two-tailed students t-test and for **C** ordinary one-way ANOVA was used to calculate differences. Box plots represent median with minimum and maximum whiskers. *P < 0.05, **P < 0.01, ***P < 0.001, ****P < 0.0001. Figure modified according to (Jiang et al., 2024).

4.1.4. Lack of the *PCT/CT* transcript is associated with indices of increased bone resorption in the subchondral joint compartment

Next, cellular histomorphometric analysis were performed to delineate the pathomechanism underlying the differences observed in the subchondral bone structure. Knee sections were stained for the osteoclast marker TRAP, and the number and surface of TRAP-positive multinuclear cells were measured. In WT mice, a remarkable increase in osteoclast parameters were noticed in the subchondral bone compartment at 4 and 8 weeks after ACLT (**Figure 14A**). Comparing to WT mice, *CALCA*^{-/-} mice displayed elevated osteoclast surface per bone surface and osteoclast number per bone perimeter at 4 weeks postoperatively, while α *CGRP*-deficient mice exhibited decreased osteoclast indices (**Figure 14B, C**). Likewise, at 8 weeks after ACLT, higher osteoclast numbers were noticed in *CALCA*^{-/-} mice compared to those in WT and α *CGRP*-deficient mice, while no significant differences were noticed in osteoclast parameters between α *CGRP*-deficient mice and WT controls.

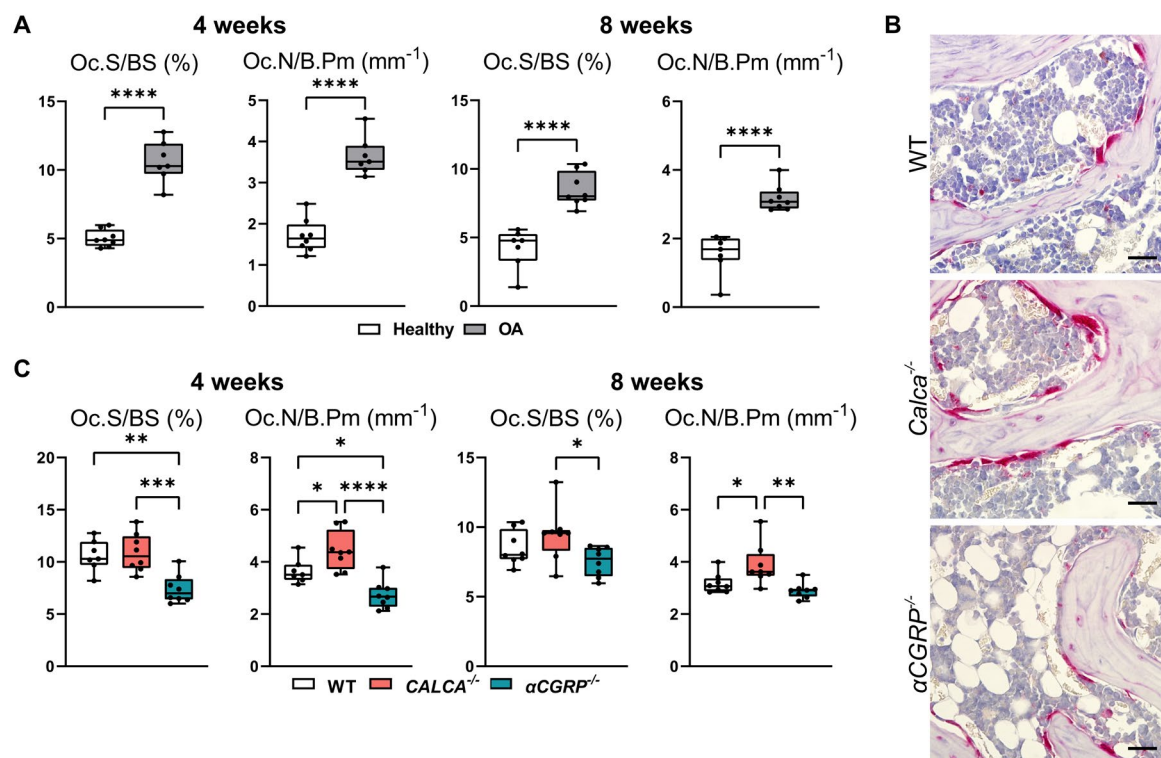


Figure 14. Mice lacking the *PCT/CT* transcript display indices of increased bone resorption in subchondral bone after ACLT. A Histomorphometric analysis of osteoclast surface per bone surface (Oc.S/BS) and numbers of osteoclasts per bone perimeter (Oc.N/B.Pm) at the indicated time points. **B** Representative TRAP-stained images of tibial subchondral bone of ptOA knees 4 weeks after ACLT (scale bar = 50 μ m). **C** Quantification of Oc.S/BS and Oc.N/B.Pm in mutant and WT mice at the indicated timepoints. n = 7-8 biologically independent animals as indicated per group and time point. For **A** unpaired two-tailed students t-test and for **C** ordinary one-way ANOVA was used to determine

differences. Box plots represent median with minimum and maximum whiskers. *P < 0.05, **P < 0.01, ***P < 0.001, ****P < 0.0001. Figure modified according to (Jiang et al., 2024).

4.1.5. Tibial osteophyte formation in ptOA is critically promoted by α CGRP signaling

For the next step, the formation of osteophyte was evaluated using radiological measurements and histological grading to further characterize the ptOA progression in the employed mouse lines. First, the volume of osteophytes of the total joint as well as the femoral and tibial compartments was quantified (**Figure 15A**). In both *CALCA*- and *α CGRP*-deficient mice, decreased osteophyte volume was noticed in the total joint and tibia at 4 and 8 weeks postoperatively, whereas the femoral osteophyte volume remained unaffected (**Figure 15B**). Furthermore, the composition and size of the osteophytes were measured using a semi-quantitative scoring on knee sections stained with BIC (**Figure 15C**). In line with the observations made in μ CT analysis, *CALCA*- and *α CGRP*-deficient mice showed significantly reduced osteophyte scores to a similar extent in the total joint and tibial compartment compared to WT controls at both time points studied (**Figure 15D**). No significant differences were noticed in the scores of femoral osteophytes in all employed mouse lines.

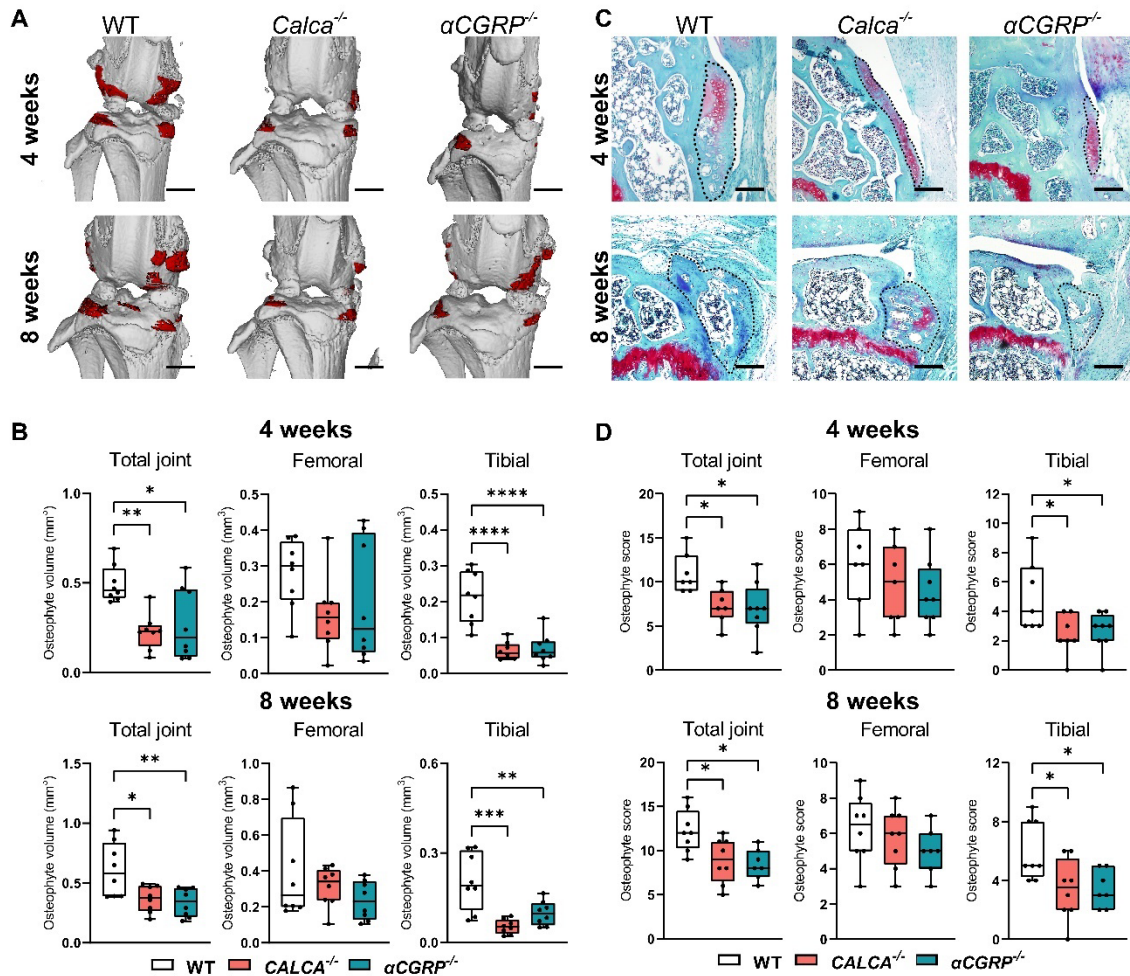


Figure 15. Inactivation of the α CGRP transcript results in reduced osteophyte formation. **A** Representative three-dimensional μ CT reconstruction of the osteophytes (red) in ptOA knees from the indicated groups 4 and 8 weeks after surgery (scale bar = 1 mm). **B** Quantitative evaluation of osteophyte volume in the total joint as well as femoral and tibial compartments at the indicated time points. **C** Representative histological images of osteophytes from the indicated groups stained with BIC at indicated time points (scale bar = 200 μ m). **D** Semi-quantitative grading of the maturity and size of osteophytes in the total joint, femoral and tibial compartments at the indicated time points. n = 7-8 biologically independent animals as indicated per group and time point. Ordinary one-way ANOVA was used to determine statistical differences. Box plots represent median with minimum and maximum whiskers. *P < 0.05, **P < 0.01, ***P < 0.001, ****P < 0.0001. Figure modified according to (Jiang et al., 2024).

4.1.6. Reduced synovitis in CALCA- but not α CGRP-deficient mice

Synovitis represents an independent driver of ptOA and exacerbates cartilage destruction. To understand the role of the CALCA-derived transcripts on synovial inflammation, synovial hyperplasia was assessed using the synovitis scoring system

(Figure 16A). The synovitis scores in the total joint of *CALCA*^{-/-} mice were significantly lower compared to those of WT mice 4 and 8 weeks after ACLT, while no significant differences were detected between *αCGRP*^{-/-} mice and WT controls **(Figure 16B)**. Likewise, *CALCA*-deficient mice displayed a reduced tibial synovitis score 8 weeks after ACLT compared to WT mice, which was not the case in mice lacking *αCGRP*. The femoral synovial inflammation remained unaffected in the employed mutant mouse lines at both 4 and 8 weeks postoperatively.

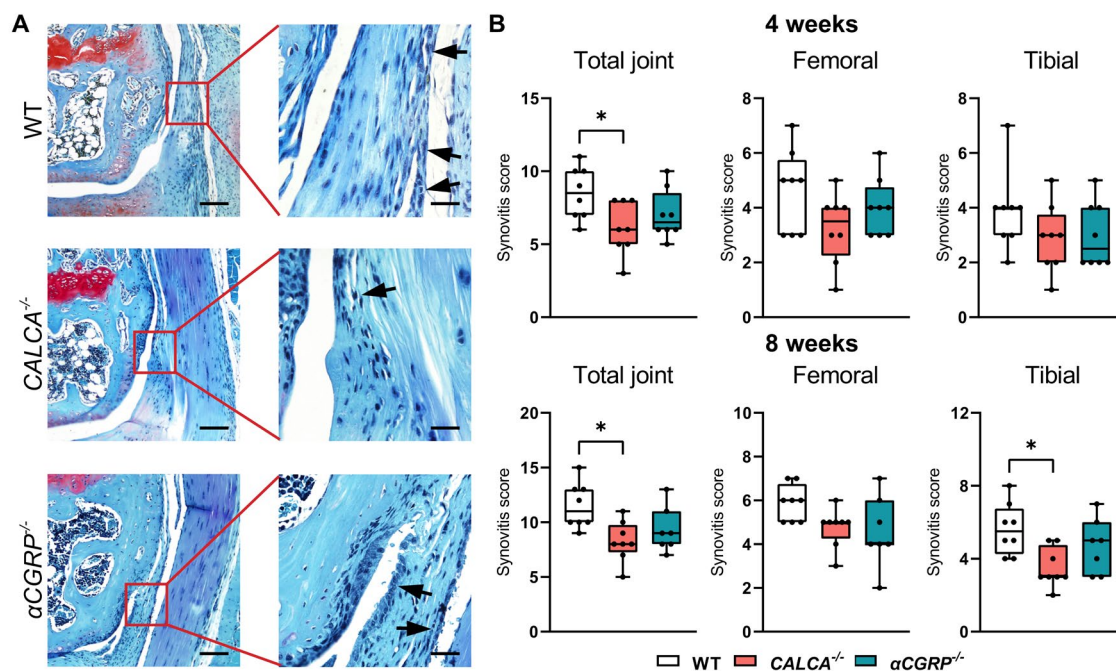


Figure 16. The absence of the *PCT/CT* transcript of the *CALCA* gene alleviates ACLT-induced synovitis. **A** Representative images of femoral synovitis at 4 weeks postoperatively, evidenced by synovial hypertrophy and hyperplasia (black arrows) in the indicated groups stained with BIC (scale bar = left column 200 μ m; right column 50 μ m). **B** Synovitis scoring of the total joint, femoral and tibia compartments at the indicated time points. $n = 7-8$ biologically independent animals as indicated per group and time point. Ordinary one-way ANOVA was used to determine statistical differences. Box plots represent median with minimum and maximum whiskers. * $P < 0.05$. Figure modified according to (Jiang et al., 2024).

4.2. Calcitonin receptor signaling is involved in osteophyte formation during the course of ptOA

In the previous subproject, it has been shown that *PCT/CT* transcript is crucially involved in several key pathological changes of ptOA development, including cartilage

degradation, abnormal subchondral bone turnover and synovitis. However, due to the lack of mouse model with specific deficiency of CT, it remained unclear whether such effects are resulted from PCT or CT. To this end, taking advantage of *CTR*^{-/-} mice, the objective of the following work was to investigate the impact of CTR-mediated signaling in the progression of ptOA, and therefore, to delineate the distinct functions of PCT and CT in ptOA.

4.2.1. The expression of *Calcr* is upregulated during ptOA progression

To investigate the involvement of CTR signaling in the progression of OA, first, the expression of the CTR encoding gene, *Calcr*, was evaluated in ACLT- and sham-operated knees of WT mice. The expression of *Calcr* at 2 weeks postoperatively was not altered compared to that of the sham group, while a significant upregulation was observed 4 and 8 weeks after ACLT (**Figure 17A**). Next, the expression of CTR was analyzed on protein level during ptOA in WT mice. Fluorescent microscopy showed that CTR was expressed in both articular cartilage and subchondral bone marrow (**Figure 17B**).

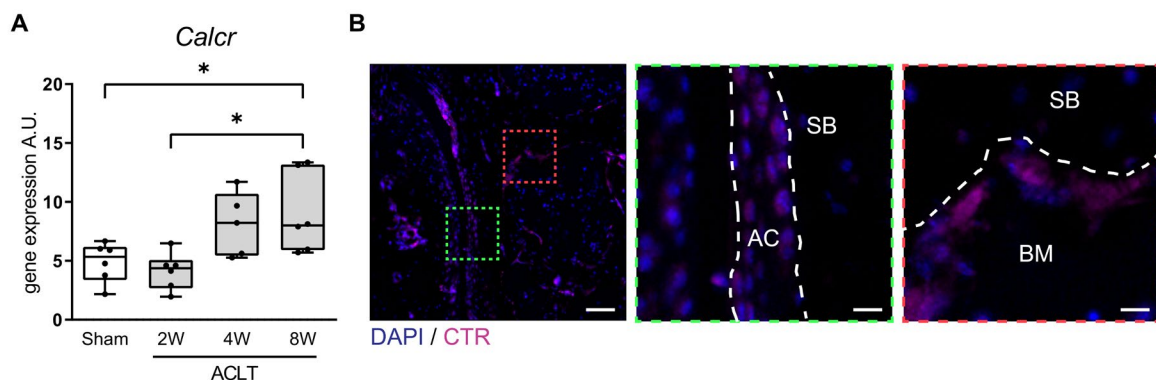


Figure 17. The expression of CTR is induced during ptOA progression. **A** Gene expression analysis of CTR encoding gene *Calcr* in WT knees subjected to sham or ACLT surgery and harvested at the indicated time points. n = 5-6 biologically independent animals per group, presented in arbitrary units (A.U.) relative to expression of *Gapdh* mRNA. **B** Representative overview images of immunofluorescent stainings specific for CTR in the proximal tibia of the knee joint 4 weeks after ACLT. Site-matched images with higher magnification are presented in red and green boxes on the right side. Subchondral bone (SB), articular cartilage (AC) and subchondral bone marrow (BM) are indicated. Scale bar = left 100 μ m; middle and right 25 μ m. Ordinary one-way ANOVA was used to determine statistical differences. Box plots represent median with minimum and maximum whiskers. *P < 0.05.

4.2.2. Inactivation of CTR does not affect ACLT-induced cartilage degeneration

To assess the effect of CTR-dependent signaling in ptOA, WT and *CTR*-deficient mice were employed and operated with ACLT. The articular cartilage degeneration in ptOA joints were first evaluated using OARSI scores. At 4 weeks after the operation, the total OARSI scores of *CTR*^{-/-} knees did not differ from that of WT joints, with no significant changes in tibial or femoral scores, respectively. Similar observations were made in the diseased knees at 8 weeks postoperatively, where no significant differences were noticed between WT and *CTR*-deficient mice in the OARSI scores of the total joints, tibial or femoral compartments (**Figure 18A, B**). To further characterize cartilage degeneration, histomorphometric measurements were carried out on the thickness of subchondral bone plate and the ratio of hyaline cartilage to calcified cartilage. To compare relative alterations in WT and *CTR*^{-/-} mice, the values of ptOA knees were normalized to those of the contralateral healthy knees, and the fold changes were plotted and presented. Here, the thickness of subchondral bone plate and hyaline cartilage proportion was reduced to a similar extent in *CTR*-deficient and WT animals at 4 and 8 weeks postoperatively (**Figure 18C**).

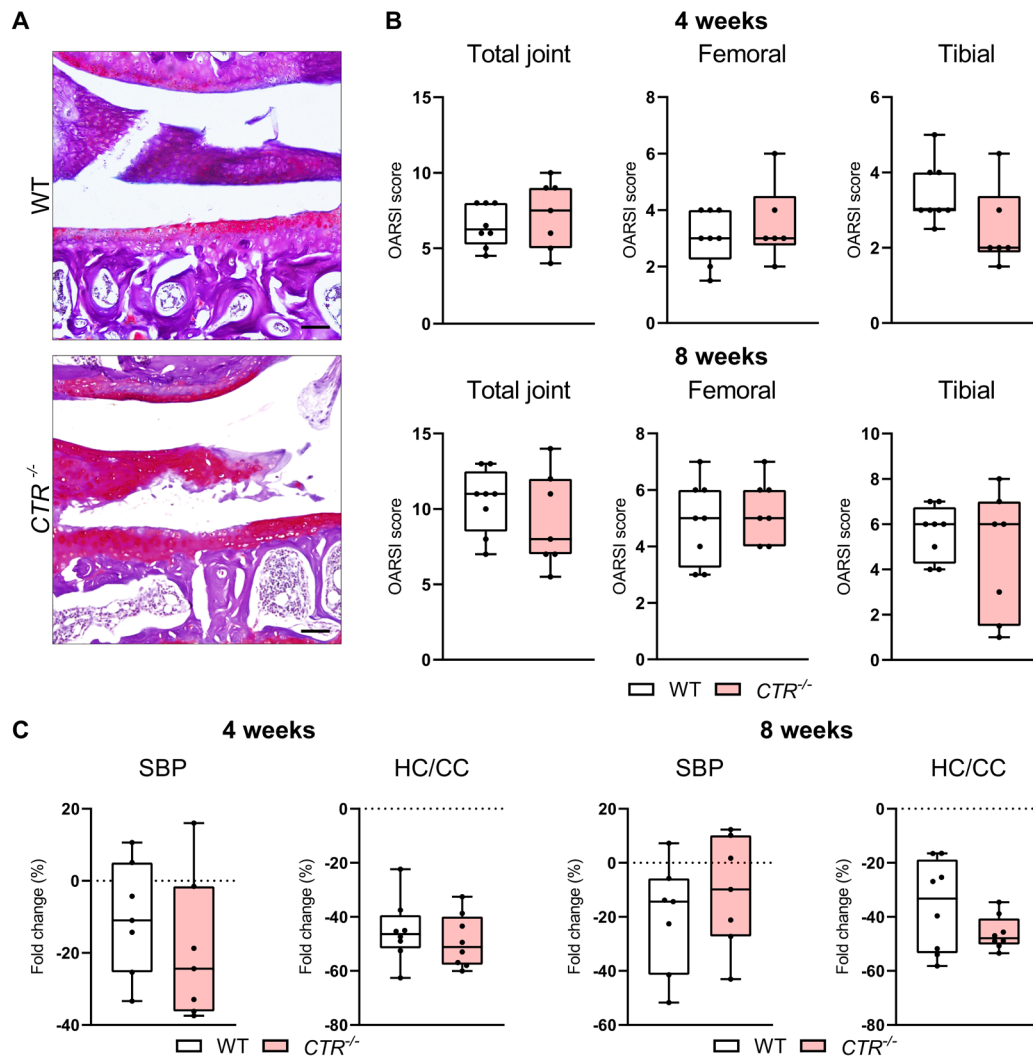


Figure 18. *CTR*-deficiency does not affect cartilage degeneration after ACLT. A Representative images of medial knee joints stained with BIC 4 weeks after ACLT (scale bar = 100 μ m). **B** Osteoarthritis Research Society International (OARSI) scoring of total joints as well as of femoral and tibial compartments at the indicated time points. **C** Quantitative analysis of the subchondral bone plate thickness (SBP) and the ratio of hyaline cartilage thickness to calcified cartilage thickness (HC/CC) in healthy and diseased knees from WT and *CTR*-deficient mice 4 and 8 weeks after ACLT. Relative alterations (ACLT vs. contralateral healthy controls) were calculated and presented. $n = 7$ -8 biologically independent animals as indicated per group and time point. Unpaired two-tailed students t-test was used and to calculate differences. Box plots represent median with minimum and maximum whiskers.

4.2.3. *CTR*^{-/-} mice exhibit similar subchondral trabecular bone deterioration to WT animals

For the next step, using μ CT, the effects of the deficiency of *CTR* in the subchondral bone changes induced by ptOA were investigated. As previously described, ACLT

resulted in a significantly decreased bone mass in the operated knees compared to contralateral healthy controls 4 and 8 weeks after the induction. *CTR*-deficient mice exhibited a decreased bone volume per tissue volume and trabecular number to the same extent as WT mice, while a more pronounced reduction in trabecular thickness and an increase in trabecular separation were noticed in the joints of genetically modified animals at 4 weeks postoperatively (**Figure 19A, B**). No differences were observed in the subchondral bone structural parameters between *CTR*^{-/-} and WT mice 8 weeks after ACLT (**Figure 19B**).

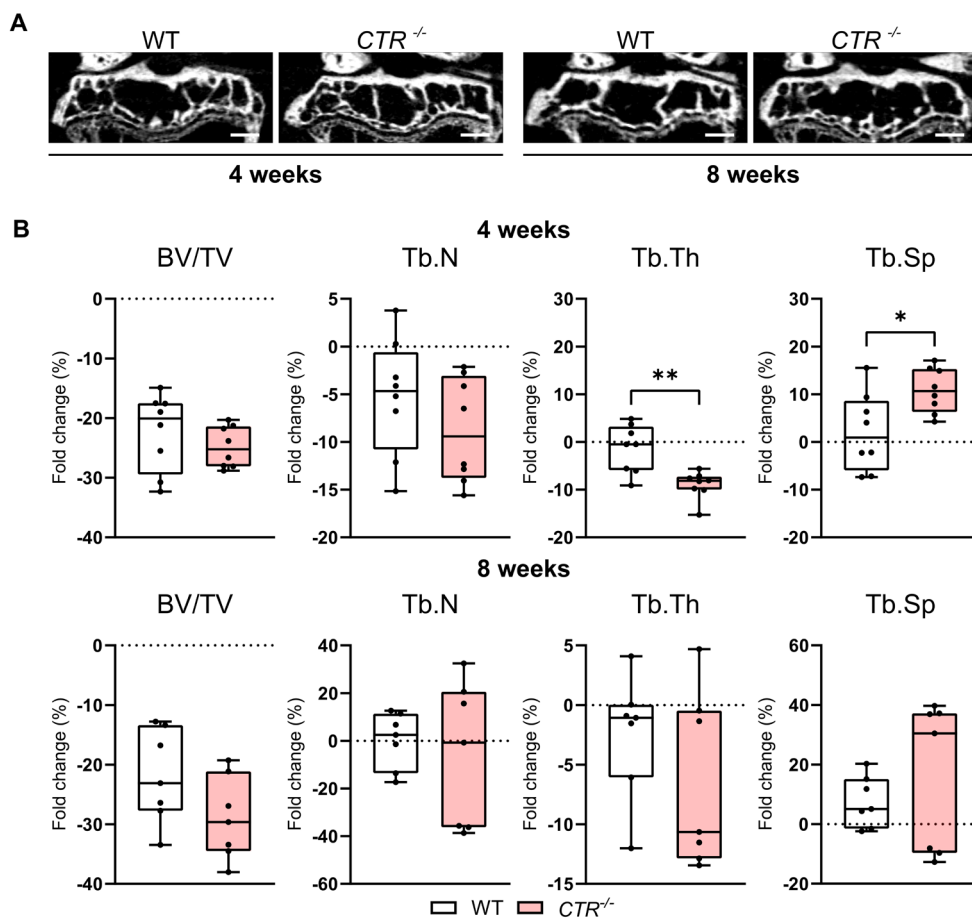


Figure 19. Inactivation of CTR-mediated signaling is not associated with more pronounced subchondral bone deterioration. **A** Representative μ CT coronal views of tibial subchondral trabecular bone of diseased knees from the indicated groups at the indicated time points (scale bar = 500 μ m). **B** Quantitative analysis of tibial subchondral trabecular bone of the bone volume fraction (BV/TV), trabecular numbers (Tb.N), trabecular thickness (Tb.Th), and trabecular separation (Tb.Sp) at the indicated time points in WT and *CTR*-deficient mice. Relative alterations were expressed as fold differences. n = 7-8 biologically independent animals as indicated per group and time point. Unpaired two-tailed students t-test was used and to calculate differences. Box plots represent median with minimum and maximum whiskers. *P < 0.05, **P < 0.01.

4.2.4. Deficiency of CTR does not affect bone metabolism parameters in the subchondral joint compartment

To delineate the alterations in the structural parameters observed in the subchondral trabecular bone, histomorphometric analysis was performed on knee sections stained for TRAP to evaluate osteoclast parameters, and sections stained with H&E for osteoblast measurements. As mentioned previously, ACLT induced significantly increased osteoclast indices in the subchondral bone of WT mice. Likewise, in *CTR*^{-/-} mice, an increase in osteoclast parameters was observed in the operated knees relative to healthy controls, which was less pronounced at 4 weeks postoperatively but to a similar extent 8 weeks after the operation (**Figure 20A, B**). In terms of bone formation, no alterations in osteoblast indices were noticed in the diseased knees of both mouse strains 4 and 8 weeks after operation (**Figure 20C**).

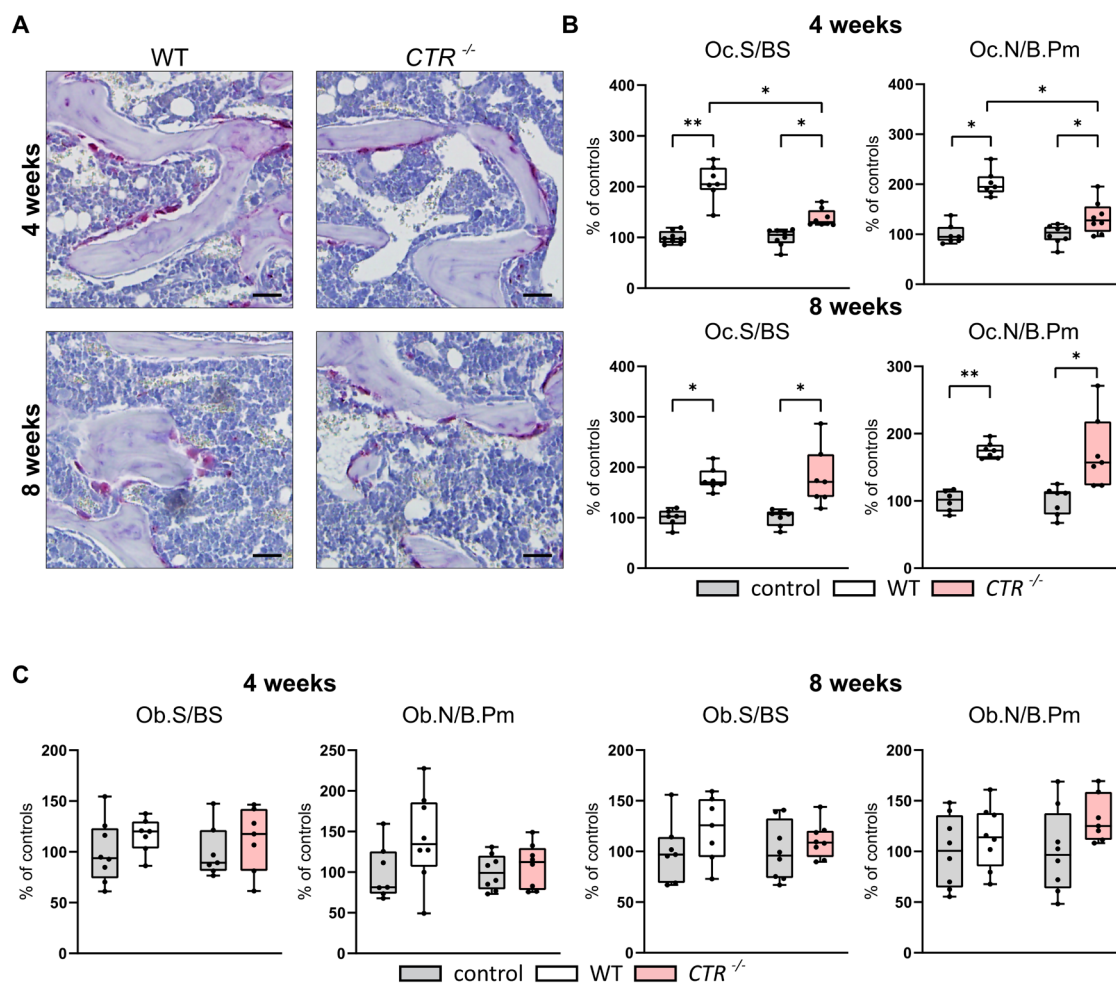


Figure 20. Mice lacking CTR display increased bone resorption in subchondral bone to a same extent as WT mice after ACLT. A Representative TRAP-stained images of tibial subchondral bone of ptOA knees from indicated mouse lines 4 and 8 weeks after ACLT (scale bar = 50 μ m). **B**

Histomorphometric analysis of osteoclast surface per bone surface (Oc.S/BS) and numbers of osteoclasts per bone perimeter (Oc.N/B.Pm) at the indicated time points in TRAP-stained ptOA sections. Relative alterations were expressed as fold differences. **C** Histomorphometric analysis of osteoblast surface per bone surface (Ob.S/BS) and numbers of osteoblasts per bone perimeter (Ob.N/B.Pm) at the indicated time points. Relative alterations were expressed as fold differences. n = 7-8 biologically independent animals as indicated per group and time point. Two-way ANOVA followed by Tukey's post-hoc test was used to determine differences. Box plots represent median with minimum and maximum whiskers. *P < 0.05, **P < 0.01.

4.2.5. Decreased osteophyte formation in ptOA in *CTR*^{-/-} mice

To further characterize the progression of OA in *CTR*^{-/-} mice, radiological and histological evaluations of osteophytes were carried out in the diseased joints. Osteophyte volume was measured using μ CT analysis, whereas the size and maturity of osteophytes were scored on knee sections stained with BIC. μ CT evaluation showed that the total osteophyte volume was significantly reduced in the operated joints of *CTR*^{-/-} mice compared to WT controls 8 weeks after surgery (**Figure 21A, B**). The femoral osteophyte volume at 8 weeks and the tibial osteophyte volume at both time points were reduced in the operated joints of mice lacking CTR. Likewise, semi-quantitative scoring of osteophyte composition and size showed that *CTR*-deficient mice had lower osteophyte scores in the total joint at 4 and 8 weeks postoperatively and in the tibial compartment 8 weeks after ACLT (**Figure 21C, D**).

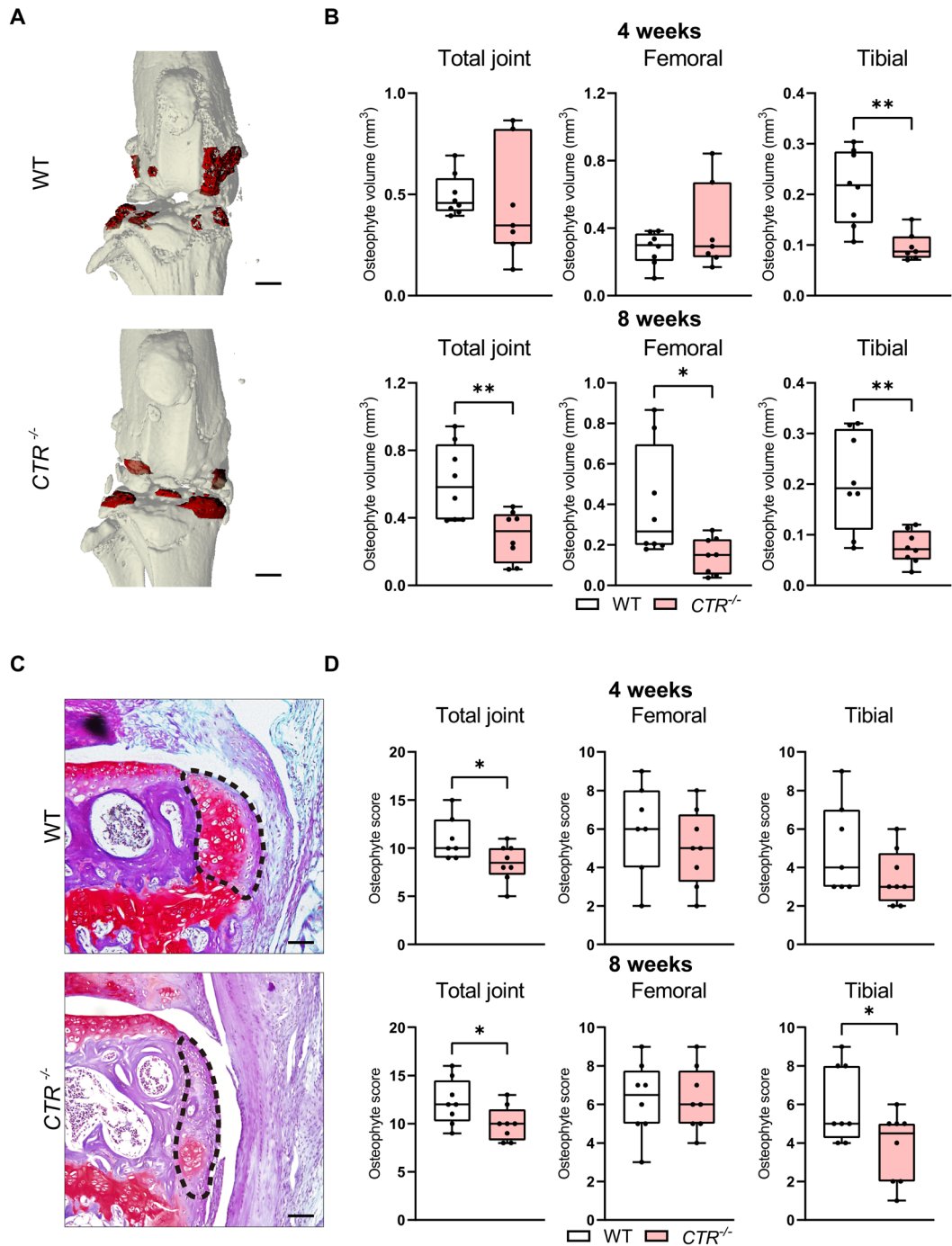


Figure 21. Ablation of CT-CTR signaling results in reduced osteophyte formation. **A** Representative three-dimensional micro-CT reconstruction of the osteophytes (red) in ptOA knees from the indicated groups 4 weeks after surgery (scale bar = 1 mm). **B** Quantitative evaluation of osteophyte volume in the total joint as well as femoral and tibial compartments at the indicated time points. **C** Representative histological images of tibial osteophytes from indicated groups stained with BIC at 4 weeks postoperatively (scale bar = 200 μ m). **D** Semi-quantitative grading of the maturity and size of osteophytes in the total joint, femoral and tibial compartments at the indicated time points. n = 7-8 biologically independent animals as indicated per group and time point. Unpaired two-tailed students t-

test was used and to calculate differences. Box plots represent median with minimum and maximum whiskers. *P < 0.05, **P < 0.01.

4.2.6. Synovitis induced by ptOA is not affected by the deficiency of CTR

Synovitis indicates the inflammatory status of the diseased joints, representing an independent driver of OA onset and progressive cartilage destruction. To study the role of CTR-mediated signaling in synovitis, synovial hyperplasia was evaluated using a semi-quantitative synovitis score (**Figure 22A**). No significant differences were noticed in the synovitis scores of total joints, femoral and tibial compartments of mice of both genotypes at all time points (**Figure 22B**).

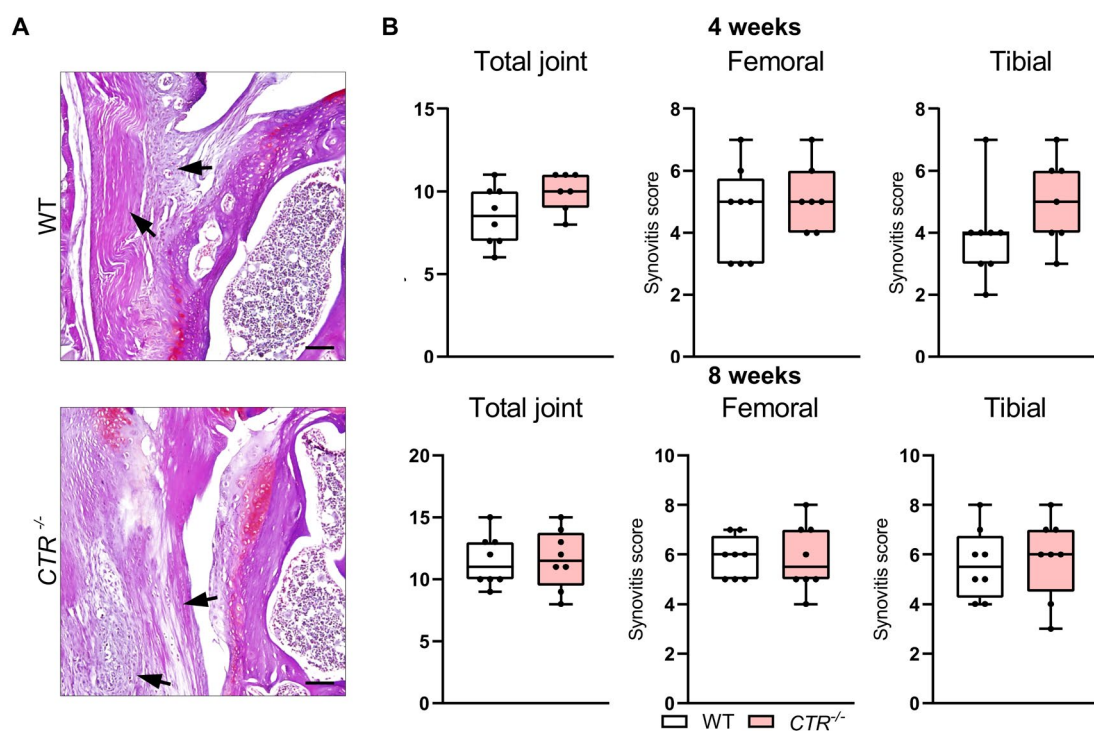


Figure 22. ACLT-induced synovitis in mice lacking CTR does not differ from that in WT mice. A Representative images of femoral synovitis, evidenced by synovial hypertrophy and hyperplasia (black arrows) in the indicated groups stained with BIC (scale bar = 200 μ m). **B** Synovitis scoring of the total joint, femoral and tibia compartments at the indicated time points. n = 7-8 biologically independent animals as indicated per group and time point. Unpaired two-tailed students t-test was used and to calculate differences. Box plots represent median with minimum and maximum whiskers.

Collectively, these observations demonstrated that the expression of *CALCA*-derived peptides and their relative receptors are induced along the course of ptOA progression

in WT mice. Regarding the ACLT-induced alterations in genetically modified mice, *CALCA*^{-/-} mice displayed more pronounced cartilage degeneration and subchondral bone loss but alleviated synovial inflammation. In contrast, deficiency of αCGRP and inactivation of CT-CTR signaling were associated with decreased osteophyte formation. Together, these findings provide a detailed understanding of the roles of *CALCA*-encoded peptides in OA.

To further understand the role of calcitonin family of peptides in degenerative musculoskeletal disorders, OVX mouse model was employed in the following work, to mimic postmenopausal osteoporosis, which represents another leading cause of mortality and morbidity in the aged population. The objective of the following part of work was therefore to investigate a potential function of an amylin analog, pramlintide in osteoporosis and the underlying mechanisms mediating such effects.

4.3. Osteoporosis-induced bone loss is alleviated by pramlintide in a CTR-dependent manner

Besides OA, osteoporosis is another prevalent degenerative musculoskeletal disorder characterized by bone resorption outweighing bone formation, followed by decreased BMD and an increased risk of fractures. Furthermore, an additional fracture burden has long been suggested in patients with diabetes due to chronic hyperglycemic conditions and certain anti-diabetic medications. Amylin, a pancreatic B-cell hormone co-secreted with insulin, has been shown not only to regulate glucose metabolism, but also to preserve bone mass. Taking these into consideration, the following investigation aimed to assess the functional role of pramlintide in bone metabolism using an experimental osteoporosis model, and to identify whether the amylin analog pramlintide exerts its biological function by interacting with CTR.

4.3.1. Pramlintide restores OVX-induced trabecular bone loss in the spine of WT mice but not of *CTR*^{-/-} mice.

In this subproject, WT and *CTR*^{-/-} mice were employed and subjected to OVX at the age of 8 weeks. After 4 consecutive weeks, pramlintide treatment was initiated for further 4 weeks. First, the trabecular bone architecture in the lumbar spine was analyzed using μCT (**Figure 23A**). Morphological evaluation showed that OVX caused a significant decrease in bone volume fraction and trabecular thickness in WT mice

compared to sham controls. Administration of pramlintide reversed OVX-induced bone loss, accompanied by increased trabecular number and decreased trabecular separation in the spinal trabecular bone (**Figure 23B**). Whereas in *CTR*-deficient mice, although OVX induced reduction in the bone mass and the trabecular thickness, no alterations in the trabecular structural parameters were detected in mice treated with pramlintide.

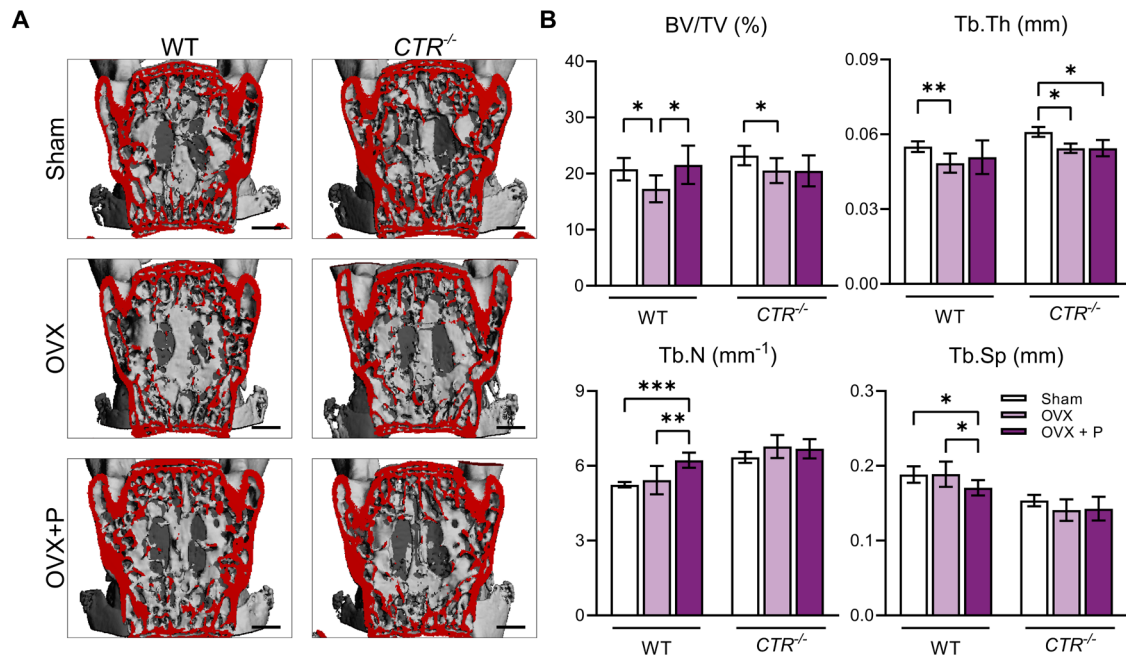


Figure 23. Pramlintide exerts a preservative effect on OVX induced bone loss in the spinal trabecular bone in WT mice, but not in *CTR*-deficient mice. **A** Representative μ CT reconstructions of the coronal views of the spinal trabecular bone (scale bar = 500 μ m). **B** Quantitative analysis of the structural parameters, including bone volume fraction (BV/TV), trabecular thickness (Tb.Th), trabecular separation (Tb.Sp), and trabecular numbers (Tb.N) of the lumbar trabecular bone from the indicated groups. $n = 7-8$ biologically independent animals as indicated per group. Two-way ANOVA followed by Tukey's post-hoc test was used to determine differences. Bar graph represents the means \pm standard deviation. * $P < 0.05$, ** $P < 0.01$, *** $P < 0.001$.

To further confirm the observations made in μ CT evaluation, non-decalcified histology of the lumbar spine was performed (**Figure 24A**). Here, evaluation of the 2-dimensional bone structure revealed that OVX led to significantly decreased bone volume fraction and trabecular thickness in the spine of WT mice. Administration of pramlintide prevented OVX-induced bone loss, evidenced by restored bone volume, decreased trabecular separation and increased trabecular number (**Figure 24B**). In *CTR*^{-/-} mice,

OVX resulted in a trend of decreased bone volume fraction and trabecular thickness, while no alterations in the structural parameters were noticed in the pramlintide treated group compared to the OVX group. Briefly, these observations suggest that OVX-induced morphological alterations in the spinal trabecular bone are restored by pramlintide in WT but not *CTR*-deficient mice.

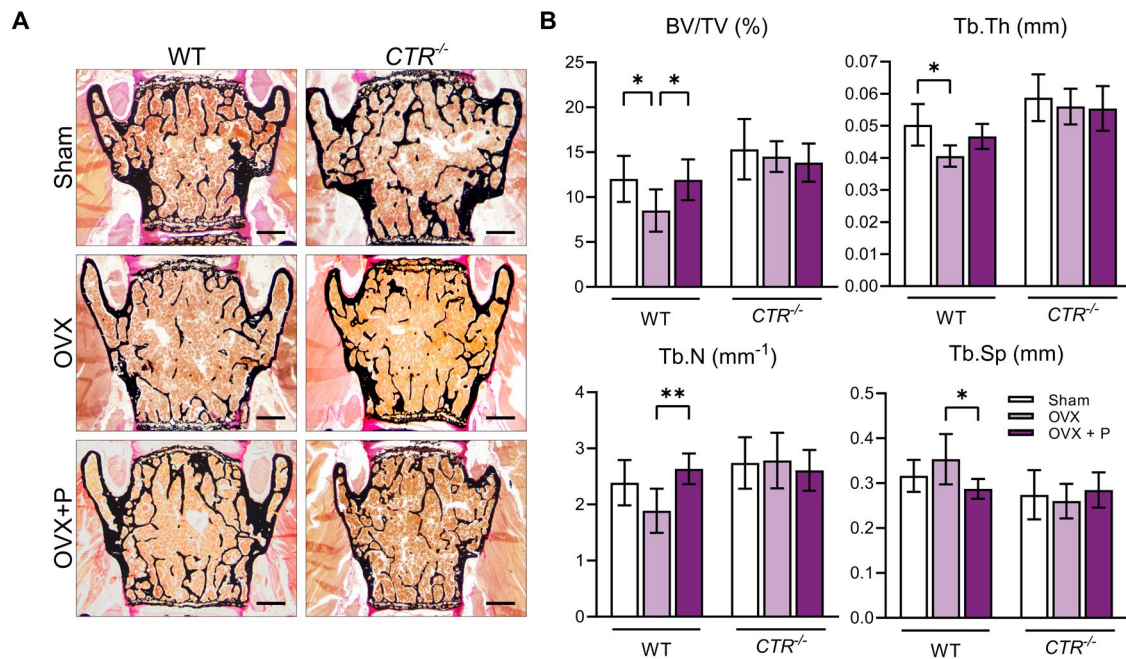


Figure 24. Pramlintide protects from OVX induced bone loss in WT but not *CTR*-deficient mice. **A** Representative images of non-decalcified sections stained with Von Kossa/ Van Gieson of the lumbar spine from the indicated groups (scale bar = 500 μ m). **B** Histochemical evaluations of the bone volume fraction (BV/TV), trabecular thickness (Tb.Th), trabecular separation (Tb.Sp), and trabecular numbers (Tb.N) of the lumbar spine sections. $n = 7-8$ biologically independent animals as indicated per group. Two-way ANOVA followed by Tukey's post-hoc test was used to determine differences. Bar graph represents the means \pm standard deviation. * $P < 0.05$, ** $P < 0.01$.

4.3.2. Pramlintide exerts a beneficial effect on OVX-induced bone loss in the distal femur of WT mice but not *CTR*^{-/-} mice.

To investigate the effects of pramlintide on osteoporotic bone alterations in the appendicular skeleton, radiographic analysis of the distal femoral trabecular bone (**Figure 25A**) and the femoral midshaft cortical bone (**Figure 25D**) was conducted. In the trabecular bone of distal femur, μ CT evaluation revealed that OVX caused a decrease in bone volume fraction and trabecular number and an increase in trabecular separation in both WT and *CTR*-deficient mice. Pramlintide exerted a protective effect

on OVX-induced bone loss only in WT mice, evidenced by decreased trabecular separation and increased trabecular number compared to the OVX group (**Figure 25B, C**). No alterations in the trabecular bone morphology were observed in *CTR*^{-/-} mice treated with pramlintide. In terms of cortical bone, the femoral midshaft was evaluated and the thickness and porosity of the cortical bone remained unchanged in all groups in both employed mouse lines (**Figure 25E, F**). Collectively, these data suggest that pramlintide restores OVX-induced trabecular bone deterioration in the appendicular skeleton of WT mice, which is not the case in *CTR*-deficient mice.

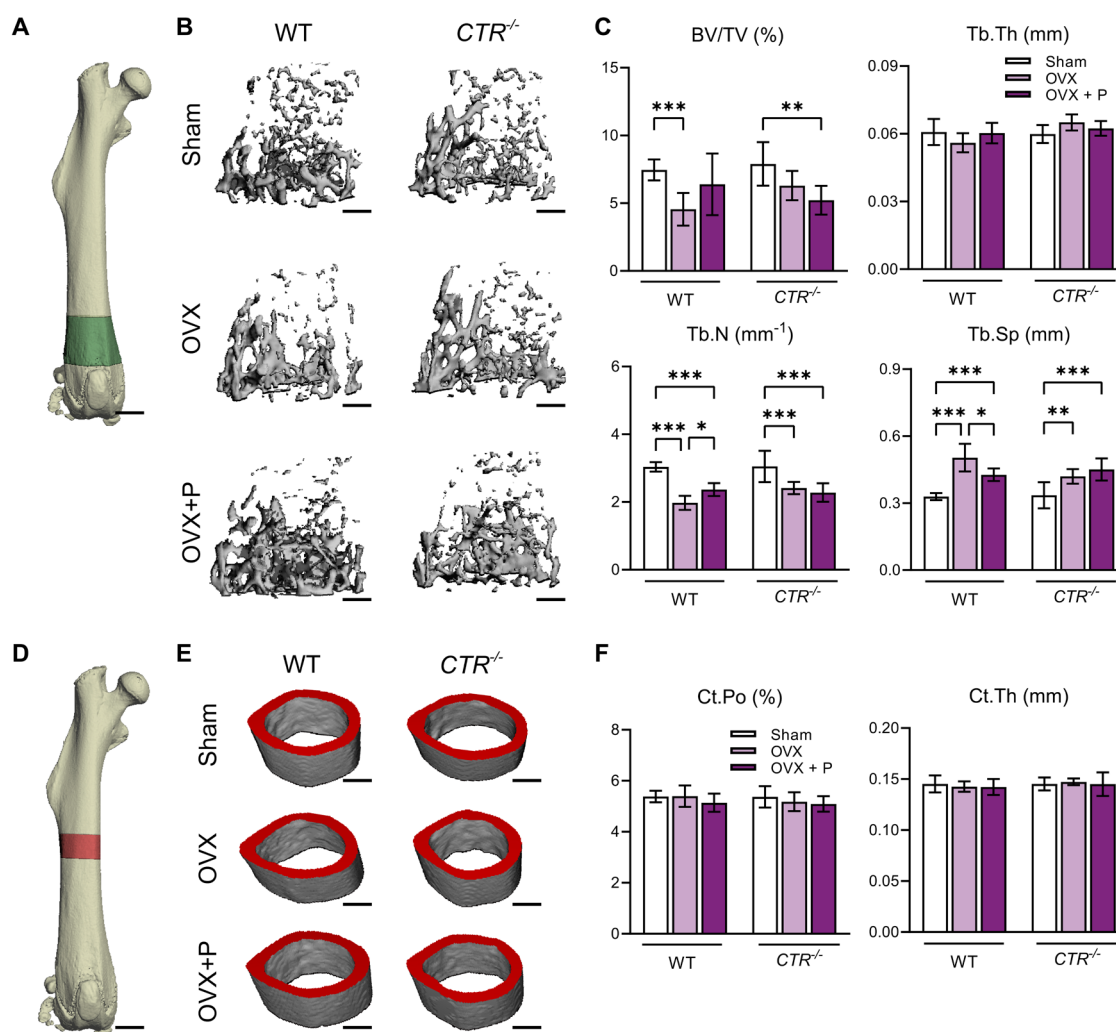


Figure 25. Pramlintide restores structural alterations in appendicular trabecular bone of WT osteoporotic mice. **A** Representative three-dimensional view of the region of interest for the evaluation of appendicular trabecular bone (green) (scale bar = 2 mm). **B** Representative three-dimensional reconstructions of the trabecular bone of the distal femur from the indicated groups (scale bar = 300 μ m). **C** μ CT based quantification of bone volume fraction (BV/TV), trabecular numbers (Tb.N), trabecular thickness (Tb.Th), and trabecular separation (Tb.Sp) of the femoral trabecular bone from the indicated groups. **D** Representative three-dimensional view of the region of interest for the evaluation of the

cortical bone in the femoral midshaft (red) (scale bar = 2 mm). **E** μ CT reconstructions of the femoral midshaft in the indicated groups (scale bar = 200 μ m). **F** Quantitative analysis of cortical bone thickness (Ct.Th) and cortical bone porosity (Ct.Po) in the indicated groups. n = 7-8 biologically independent animals as indicated per group. Two-way ANOVA followed by Tukey's post-hoc test was used to determine differences. Bar graph represents the means \pm standard deviation. *P < 0.05, **P < 0.01, ***P < 0.001.

4.3.3. Excessive bone resorption is restored by pramlintide treatment in WT but not *CTR*-deficient mice

To understand the pathomechanism underlying the effect of pramlintide on bone metabolism, bone formation and bone resorption parameters were measured on non-decalcified spine sections. All mice were labeled with calcein 9 and 2 days before the sampling. Dynamic bone histomorphometry revealed that the bone formation rate was not affected by OVX or pramlintide treatment in mice of both genotypes (**Figure 26A, B**). At the cellular level, OVX decreased osteoblast numbers and surface in both WT and mutant animals, whereas no alterations were observed upon pramlintide treatment (**Figure 26C**). In sharp contrast, osteoclast indices were dramatically increased in WT OVX mice compared to sham controls, which were then normalized upon administration of pramlintide. In mice lacking *CTR*, osteoclast parameters remained unaltered after the induction of OVX and the pramlintide treatment (**Figure 26D, E**). These findings suggest that pramlintide appears to limit excessive bone resorption caused by OVX in WT mice, but not *CTR*^{-/-} mice.

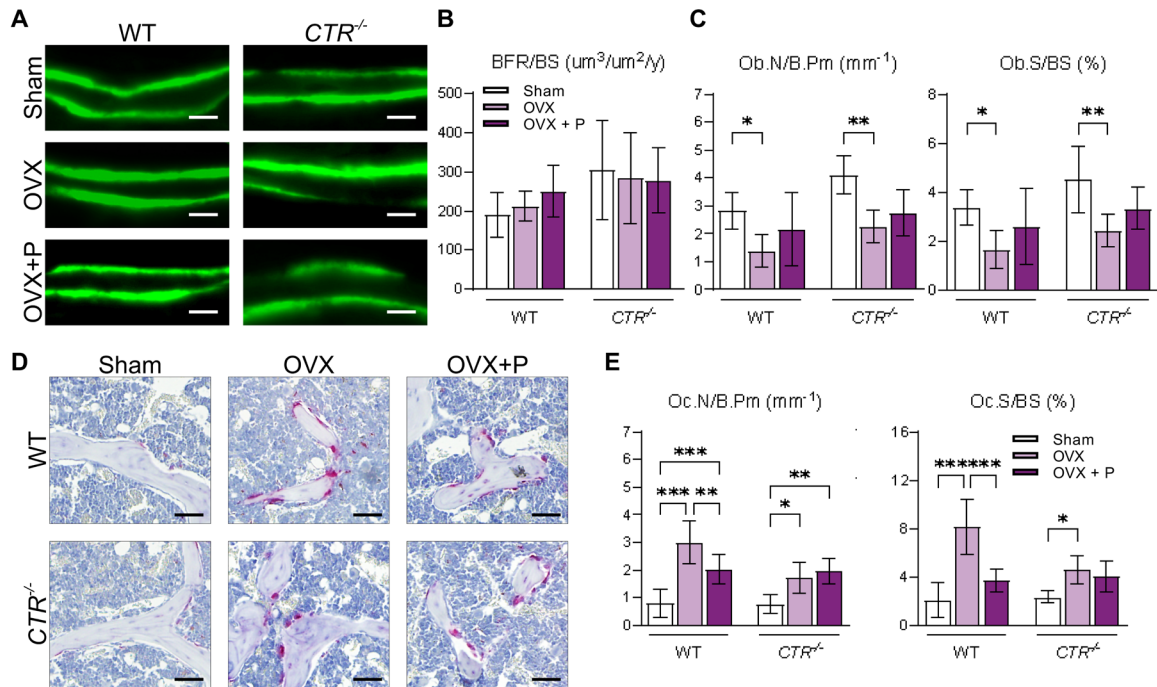


Figure 26. Pramlintide limits excessive bone resorption in WT OVX mice. **A** Representative fluorescence images of double calcein labeling in trabecular bone of spine sections (scale bar = 40 μ m) and **B** quantification of the bone formation rate per bone surface (BFR/BS). **C** Histomorphometric analysis of osteoblast surface per bone surface (Ob.S/BS) and numbers of osteoblasts per bone perimeter (Ob.N/B.Pm) on spine sections from the indicated groups. **D** Representative images of TRAP-stained spine sections of the indicated group (scale bar = 100 μ m) s. **E** Histomorphometric analysis of osteoclast surface per bone surface (Oc.S/BS) and numbers of osteoclasts per bone perimeter (Oc.N/B.Pm) spine sections from the indicated groups. n = 7-8 biologically independent animals as indicated per group. Two-way ANOVA followed by Tukey's post-hoc test was used to determine differences. Bar graph represents the means \pm standard deviation. *P < 0.05, **P < 0.01, ***P < 0.001.

4.3.4. Pramlintide inhibits osteoclastogenesis in a CTR-dependent manner

As it is well established that in the musculoskeletal system, CTR is predominantly expressed in osteoclasts (Ikegame et al., 1995), and as excessive bone resorption represents the primary pathophysiological change in postmenopausal osteoporosis, the functional role of pramlintide in osteoclast differentiation was investigated in vitro. Bone marrow-derived mesenchymal cells from WT and CTR^{-/-} mice were isolated and cultured in an osteoclastogenic medium supplemented with vehicle or pramlintide (**Figure 27A**). In WT osteoclasts, pramlintide resulted in a significant decrease in the number of osteoclasts, which was not the case in CTR-deficient osteoclasts (**Figure 27 B**).

To further identify the downstream targets regulated by pramlintide, genome-wide transcriptome analysis using RNA-seq was performed using osteoclasts from WT and *CTR*^{-/-} mice treated with pramlintide for 6 hours on the third day of differentiation. Analysis of the transcriptome data revealed 149 differentially expressed genes in WT osteoclasts treated with pramlintide and 483 in *CTR*^{-/-} osteoclasts (**Figure 27C**). Since the inhibitory effect of pramlintide was only observed in WT osteoclasts, following analysis was carried out on the genes that were exclusively regulated in WT osteoclasts (**Figure 27D**). A number of osteoclastogenesis-related genes were identified (**Figure 27E**). Following qRT-CTR validation, it has been found that sphingosine kinase 1 (*Sphk1*) and suppressor of cytokine signaling 3 (*Socs3*) were upregulated, while angiopoietin-like 4 (*Angptl4*) was downregulated in WT osteoclasts in the presence of pramlintide but not in *CTR*^{-/-} osteoclasts. The expression of cAMP responsive element modulator (*Crem*) was upregulated to a similar extent in *CTR*^{-/-} osteoclasts compared to WT osteoclasts upon stimulation with pramlintide. Furthermore, the expression of cluster of differentiation 14 (*CD14*) was stimulated in WT osteoclasts but downregulated in *CTR*-deficient osteoclasts (**Figure 27F**). Taken together, these data suggest that pramlintide exerted a protective effect on OVX-induced bone loss by suppressing osteoclastogenesis in a CTR-dependent manner.

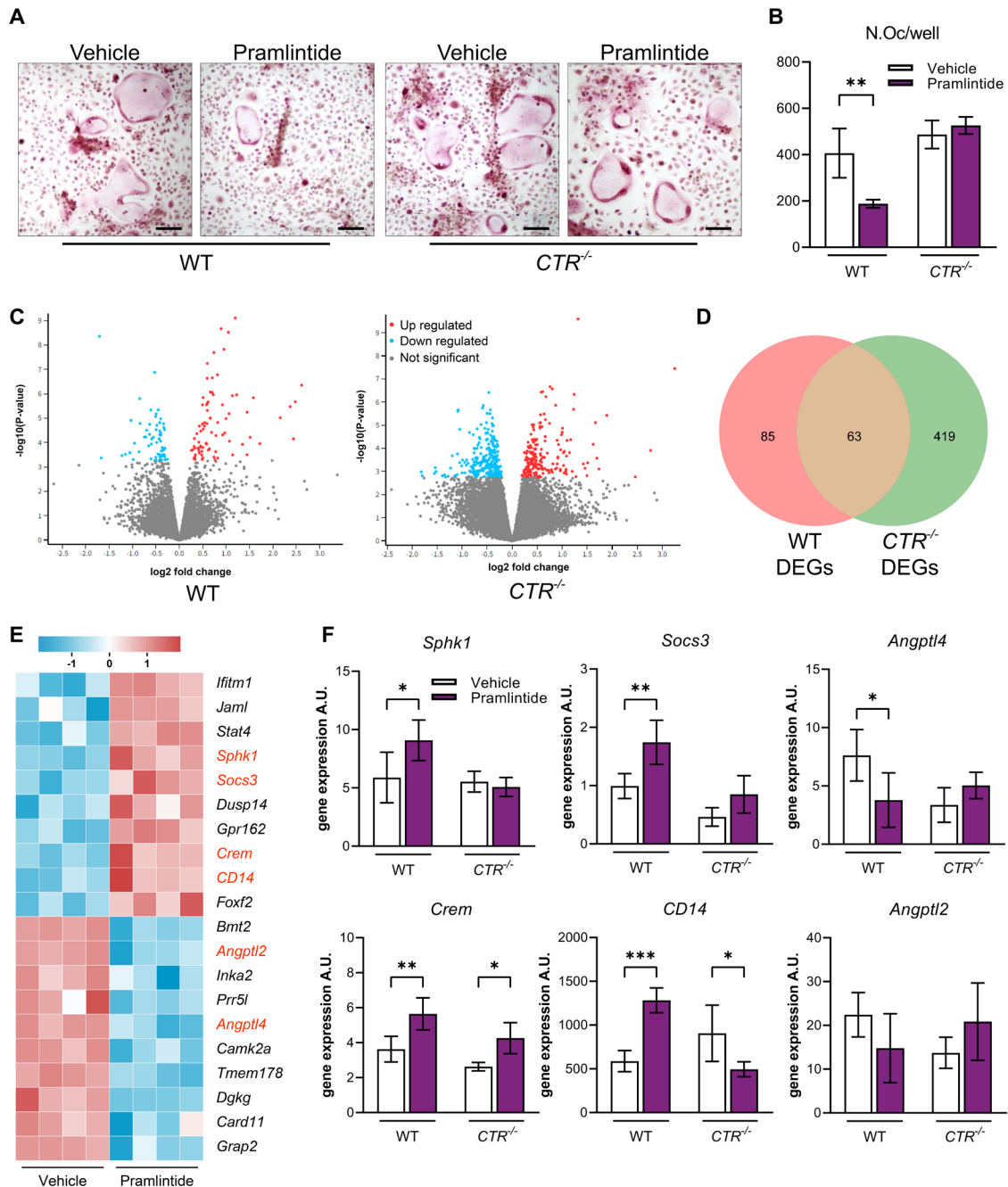


Figure 27. Pramlintide inhibits osteoclast differentiation in vitro in a CTR-dependent manner. A Representative images of TRAP-stained osteoclast culture in the indicated mouse lines (scale bar = 100 μ m). **B** Quantification of the number of osteoclasts (Oc.N) in cultures of bone marrow derived cells from WT or CTR -deficient mice treated with pramlintide or vehicle for 3 days. **C** Volcano plot of regulated genes in the osteoclasts of the indicated genotypes treated with pramlintide for 6 hours on the third day of differentiation ($P < 0.05$, fold change > 1.2). Up- (red dots) and down- (blue dots) regulated genes as well as genes without significant differences (gray dots) were plotted. **D** Venn diagram presenting the differentially expressed genes (DEGs) in either WT and/or $CTR^{-/-}$ osteoclasts upon treatment of pramlintide. **E** Heatmap of 20 DEGs with highest fold changes exclusively in WT osteoclasts. Each

column represents one sample and each row represents one gene. Z-scores were calculated based on the expression level of each gene and visualized in a color scale (blue = downregulated, red = upregulated). Genes associated with osteoclastogenesis were highlighted in red. **F** Gene expression analysis of the indicated genes using qRT-PCR. n = 4 biologically independent replicants per group, presented in arbitrary units (A.U.) relative to expression of *Gapdh* mRNA. For **A** and **F**, two-way ANOVA followed by Tukey's post-hoc test was used to determine differences. Bar graph represents the means \pm standard deviation. Box plots represent median with minimum and maximum whiskers. *P < 0.05, **P < 0.01, ***P < 0.001.

5. Discussion

Degenerative musculoskeletal diseases, namely OA and osteoporosis, are the leading cause of decreased quality of life in the elderly. It has been widely accepted that calcitonin family of peptides, especially CT, PCT, α CGRP and amylin are potent regulators of bone metabolism. Nevertheless, the roles of *CALCA*-derived transcripts and CT-CTR signaling in ptOA, and the effects of pramlintide, an amylin analog, on osteoporotic bone deterioration remained to be addressed. Therefore, the present study aimed to investigate 1) the functional relevance of both the *CALCA*-derived *PCT/CT* and *α CGRP* transcript in a mouse model of ptOA, 2) the role of CTR-mediated signaling in the development of ptOA and 3) the effect of amylin analog, pramlintide, on osteoporosis and the mechanisms by which pramlintide functions. The present work shows that in ptOA, the *PCT/CT* transcript is crucially involved in cartilage degeneration, abnormal subchondral bone remodeling, and synovitis, whereas the *α CGRP* transcript, together with CTR-mediated signaling pathways, are of great importance to the formation of osteophytes. Regarding osteoporosis, pramlintide protects from OVX-induced bone loss by inhibiting osteoclastogenesis in a CTR-dependent manner.

PtOA is a chronic degenerative joint disease that primarily affects the knees, affecting over 50% of individuals who have experienced an anterior cruciate ligament injury (Whittaker, Woodhouse, Nettel-Aguirre, & Emery, 2015). Despite considerable research input, no novel therapeutic targets to date showed promising potential in preventing the ultimate surgical intervention (Bannuru et al., 2019). As cartilage deterioration and abnormal subchondral bone turnover represent the hallmarks of OA development, a role of *CALCA*-encoded peptides in OA has long been suggested due to its remarkable anti-resorptive and chondroprotective properties (T. Maleitzke et al., 2023; Tazio Maleitzke et al., 2021; Tazio Maleitzke et al., 2020). For example, pharmacological inactivation of α CGRP signaling has been reported to attenuate cartilage degeneration and pain perception in experimental ptOA, which however could not be confirmed in a prospective clinical trial (Jin et al., 2018; Walsh, Mapp, & Kelly, 2015). Moreover, in cultures of human osteoarthritic articular chondrocytes, CT has been found to stimulate the synthesis of type II collagen, and to inhibit collagenase activities (Hellio, Peschard, Cohen, Richard, & Vignon, 1997). Similarly, studies using experimental models of rodent OA have shown that CT alleviates cartilage damage by

suppressing extracellular matrix degradation and promoting type II collagen expression and protects from subchondral bone destruction (Cheng et al., 2013; Mancini et al., 2007). Of note, the function of CT precursor, PCT, in ptOA remained to be addressed. A role of PCT in degenerative joint disease is conceivable, as, similar to rheumatoid arthritis, synovial inflammation represents an independent driver and a key exacerbator of ptOA, and as it has been previously shown that PCT augments pro-inflammatory signaling in multiple pathological conditions (Baranowsky et al., 2021; Baranowsky et al., 2022; K.L. Becker et al., 2003; K. L. Becker et al., 2010; T. Maleitzke et al., 2023).

In this study, the disease progression in *CALCA*- and *αCGRP*-deficient mice was compared to that in WT mice to test a potential, pathophysiologic involvement of *PCT/CT* and *αCGRP* transcript in ptOA. By comparing *CTR*^{-/-} mice to WT mice, the functional role of CT-CTR signaling was further investigated in ptOA. As *CALCA*^{-/-} animals lack all three *CALCA*-encoded peptides (PCT, CT, and *αCGRP*), the comparison to *αCGRP*-deficient mice allowed to delineate the function of the *PCT/CT* transcripts. Since it has been previously reported that PCT exerts its biological functions by binding to CRLR, utilizing *CTR*^{-/-} mice in comparison with *CALCA*^{-/-} and WT mice enabled to assess the pathophysiologic role of PCT and CT in ptOA, respectively. Firstly, the expression of *PCT/CT* and *αCGRP* transcripts was significantly induced in the ptOA knees of WT mice. On a protein level, immunofluorescence showed strong signal intensities in ptOA knees stained with either a PCT- or an *αCGRP*-specific antibody. A potential impact of PCT and *αCGRP* was further supported by the finding of a robust induction of CRLR on mRNA and protein levels during ptOA, which mediates the biological actions of both ligands. In contrast, no expression of the CT protein was detected, indicating that mRNA expression of the *PCT/CT* transcript primarily results in PCT protein production during ptOA. This may be explained by the fact that bone and cartilage cells, unlike thyroid C-cells, are unlikely to have the enzymatic machinery to convert PCT to CT (Russell, King, Smillie, Kodji, & Brain, 2014). Furthermore, CTR encoding gene, *Calcr* was upregulated during ptOA, and a CTR immunofluorescence was noticed in the subchondral bone and articular cartilage, suggesting the involvement of CTR-mediated signaling in ptOA.

The articular cartilage degeneration was assessed using OARSI histopathological grading and histomorphometric measurements of the subchondral bone plate thickness and the ratio of hyaline cartilage to calcified cartilage. It was observed that *CALCA*-deficient mice displayed enhanced cartilage deterioration and a decreased subchondral bone plate thickness, which was not the case in α *CGRP*- or *CTR*-deficient animals. Furthermore, the ACLT-induced subchondral bone deterioration was more pronounced in *CALCA*^{-/-} mice at 4 weeks postoperatively, associated with increased indices of osteoclastogenesis. In contrast, α *CGRP*^{-/-} and *CTR*^{-/-} mice did not exhibit enhanced subchondral bone loss. Compared to WT mice, mice lacking α CGRP displayed reduced osteoclast parameters in the diseased joint, while deficiency of CTR did not affect subchondral bone resorption. These observations suggest that PCT exerts a protective effect on cartilage degeneration and limits subchondral bone loss by suppressing elevated osteoclastogenesis. This is in line with previous studies, where a local effect of PCT on bone resorption was demonstrated (Baranowsky et al., 2022; Keller et al., 2014).

The formation of osteophytes represents one of the most common radiographic features of late-stage degenerative joint disease (Takahashi, Takeda, Matsuzaki, Kuroki, & Hosono, 2021). In the present work, all mutant mice displayed a significantly decreased osteophyte volume in the diseased joint compared to WT controls. Similarly, semi-quantitative scoring of histological knee sections showed a reduced osteophyte size and maturity in *CALCA*^{-/-}, α *CGRP*^{-/-}, and *CTR*^{-/-} mice. Thus, it can be concluded that the α *CGRP* transcript and CTR-mediated signaling are of great importance to osteophyte formation. Osteophytes represent a type of ectopic mineralized tissue that allows the joint to adapt to the altered biomechanical loading and limit abnormal joint micromotion. The osteophytosis process closely mimics bone regeneration in fracture healing (Hsia et al., 2018). Previous studies have shown that α CGRP is crucially involved in proper bone regeneration in murine osteotomy models and is capable of promoting callus mineralization (Appelt et al., 2020; Wee et al., 2023). Furthermore, mice lacking α CGRP displayed an osteopenic phenotype due to a decreased bone formation (Schinke et al., 2004). Although a clinical study has shown that blockade of α CGRP did not demonstrate clinical meaningful improvement in the pain relief or the joint function (Jin et al., 2018), results from the present work indicate that pharmacological targeting α CGRP or its receptor may inhibit osteophyte formation and

maturation. In terms of CT-CTR signaling, although it has been previously reported that *CTR*-deficient mice exhibited an increased bone mass and enhanced bone formation (Dacquin et al., 2004; Keller et al., 2014), the present work suggest that CTR-mediated signaling is a potent driver of osteophyte formation.

Synovitis is another key pathophysiological change which is present at the onset of ptOA and persists throughout the whole course of the disease (Felson et al., 2016; Roemer et al., 2011). Evaluating synovitis, mice lacking *CALCA* transcript exhibited significantly decreased synovitis scores, compared to WT controls. Of note, no alterations were observed in the synovitis scores in *CTR*- or α *CGRP*-deficient animals, suggesting that the reduced synovitis in *CALCA*^{-/-} mice is most likely due to the lack of pro-inflammatory PCT signaling. These observations are in line with a previous study, in which a pro-inflammatory effect of PCT was demonstrated. Using experimental mouse models of septic shock, PCT was found to exert a harmful effect on sepsis progression and to enhance the expression of pro-inflammatory cytokines (Baranowsky et al., 2021). Thus, a similar mechanism of action is conceivable in the setting of ptOA, where activated synoviocytes and immune cells in the inflamed synovium secrete a variety of cytokines, chemokines and proteolytic enzymes, ultimately promoting cartilage degeneration, and pathological subchondral bone remodeling (Mathiessen & Conaghan, 2017). However, the reduced synovitis appears to be irrelevant to the observations made in terms of cartilage deterioration and abnormal subchondral bone remodeling.

Collectively, these findings suggest that the PCT exerts diverse site-specific effects in ptOA, characterized by i) protection from cartilage degeneration, ii) alleviation in subchondral bone loss, and iii) exacerbation of synovitis, whereas α CGRP and CTR-mediated signaling are indispensable for the formation of osteophytes.

Osteoporosis is characterized by decreased bone mass and excessive bone resorption, leading to compromised bone mechanical properties and increased risks of osteoporotic fractures. Amylin is another peptide of the calcitonin family with a potential therapeutic benefit for osteoporosis. Pramlintide, a synthetic analog of amylin, is an FDA-approved medication for patients with diabetes who fail to lower blood glucose by solely using insulin. Although the bone-preserving property of amylin has long been suggested, a clinical study has shown that pramlintide treatment for 12 months did not

affect the bone mineral density in patients with T1D (Borm et al., 1999). As a potential explanation, T1D is commonly noticed in young adults without significant alteration in the bone mineral density, and is associated with a state of low bone turnover (Shah et al., 2017). In contrast, osteoporosis primarily affects the elderly, and is characterized by decreased bone mineral density due to excessive bone resorption. As CTR is predominantly expressed on osteoclasts in the musculoskeletal system and represents a core component of the amylin receptor, it was assumed that the amylin analog pramlintide may play a role in the pathological bone metabolism in osteoporosis. The present work demonstrated a protective effect of pramlintide on OVX-induced bone loss in WT mice. Administration of pramlintide for 4 weeks significantly restored the OVX-induced bone loss, evidenced by significantly reduced osteoclast activity with unaltered bone formation parameters, suggesting pramlintide to preserve bone mass by suppressing osteoclastogenesis. In vitro cultures of bone marrow-derived osteoclasts further confirmed that pramlintide exerted a pronounced inhibitory effect on the formation of osteoclasts. These observations were in line with a previous study, in which normal and diabetic animals receiving systemic treatment of amylin exhibit increased bone mass and improved bone strength associated with decreased erosion on the bone surface (Irene Gutiérrez-Rojas et al., 2013).

The receptor that regulates the biological function of pramlintide or amylin remained controversial. A number of in vitro studies suggested that CTR represents the core protein component of amylin receptor (Bailey et al., 2012; Christopoulos et al., 1999; Gingell et al., 2014; Muff et al., 1999). However, confounding observations were made in the in vivo study using genetically modified mouse models. Dacquin et al. reported that *amylin*^{+/-} mice exhibited a decreased bone mass due to an increase in bone resorption, whereas mice with haplo-deficiency of CTR displayed a high bone mass phenotype and increased bone formation (Dacquin et al., 2004). Furthermore, compound heterozygote mice for CTR and amylin inactivation displayed both increased bone resorption and bone formation, similar to the bone phenotypes observed in *amylin*^{+/-} and *CTR*^{+/-} mice. These findings collectively suggested that CTR is not the functional receptor through which amylin inhibits bone resorption in vivo. In the present work, mice lacking CTR failed to respond to the beneficial impact of pramlintide on OVX-induced bone deterioration. In *CTR*^{-/-} mice, OVX resulted in a decreased bone volume accompanied by altered trabecular microarchitecture. Unlike

WT mice, pramlintide did not restore the OVX-induced bone loss in the trabecular bone of either the lumbar spine or the distal femur in *CTR*-deficient mice. Cellular histomorphometry showed that indices of osteoclastogenesis were not affected by pramlintide, suggesting that *CTR* is the predominant receptor that regulates the suppressing impact of pramlintide on bone resorption.

Mechanistically, these observations were further confirmed on a gene expression level. In addition to the inhibitory impact of pramlintide on the osteoclastogenesis of bone marrow-derived stromal cells, genome-wide expression analysis followed by qRT-PCR confirmation revealed that pramlintide suppressed the expression of *Angptl4* while stimulated *Sphk1*, *Socs3*, *Crem*, and *CD14* expression. *Angptl4* is a regulator of lipid metabolism that has been reported to enhance the resorptive activity in human osteoclasts but not to affect the differentiation and viability, suggesting a positive relation of *Angptl4* with osteoclast function (Knowles, Cleton-Jansen, Korsching, & Athanasou, 2010). *Sphk1*, a sphingosine kinase that phosphorylates sphingosine to generate bioactive S1P, was upregulated in osteoclasts treated with pramlintide. It has been previously reported that *Sphk1* expression and activity were induced during RANKL-induced osteoclastogenesis, and silencing *Sphk1* enhanced osteoclast differentiation by regulating nuclear factor of activated T cells, cytoplasmic, calcineurin dependent 1 (NFATc1) and c-Fos levels (Ryu et al., 2006). *Socs3* has been shown to suppress bone resorption. Mice lacking *Socs3* specifically in hematopoietic and endothelial cells exhibited a remarkably increased osteoclastogenesis and prominent bone destruction, causing a 50% reduction in trabecular bone volume (Wong et al., 2006). Furthermore, it has been reported that *Crem* is negatively associated with osteoclastogenesis. *Crem*-deficient mice, compared to WT controls, exhibited increased osteoclast parameters and calvarial porosity to a greater extent in response to intermittent PTH treatment (Liu, Lee, Adams, Gronowicz, & Kream, 2007). These findings further confirmed that pramlintide suppresses osteoclast formation and activity. Of note, the alterations in *Sphk1*, *Socs3*, and *Angptl4* were only observed in WT but not *CTR*-deficient osteoclasts, suggesting that the inhibitory effects of pramlintide are mediated predominantly by the *CTR* signaling pathway. However, the observation that pramlintide alters the expression of *Crem* and *CD14* in *CTR*-deficient osteoclasts suggests the existence of another, as yet unidentified, pramlintide receptor that is however not involved in the regulation of bone resorption.

This study has several limitations. First, the applied experimental ptOA model or osteoporosis model is not capable of fully mimicking the complex disease progression in patients (Zaki, Blaker, & Little, 2022). Also, different results may be obtained in alternative models, such as destabilization of the medial meniscus, which usually yields a less progressive form of ptOA (Glasson, Blanchet, & Morris, 2007). Second, the bone-preserving effects of pramlintide against osteoporosis were investigated using non-diabetic animals, while it remains unclear whether the same effects apply to mice under the influence of hyperglycemia. Third, since CTR not only represents the exclusive receptor for CT but also constitutes amylin-specific receptors by dimerizing with RAMPs, the effects of deactivating amylin signaling and CT-CTR signaling in *CTR*-deficient mice cannot be delineated. Finally, it will also be crucial to study the role of *CALCA*-encoded peptides and CTR in primary, non-traumatic OA, as it represents the most common cause of degenerative joint disease and exhibits significant pathophysiological and biomechanical differences from ptOA.

In conclusion, the current work shows that the *PCT/CT* transcript protects from cartilage degeneration and subchondral bone loss in ptOA, while *α CGRP* transcript and CTR-mediated signaling function as a potent driver of osteophyte formation in ptOA, at least in mice. Furthermore, pramlintide exhibits a protective effect against OVX-induced bone loss in a CTR-dependent manner by suppressing osteoclastogenesis. These findings offer new insights to current understanding of bone biology, suggesting that targeting the calcitonin family of peptides and receptors may hold significant therapeutic potential in musculoskeletal degenerative diseases.

6. Summary

OA and osteoporosis are highly frequent degenerative diseases in the aged population, contributing to a decreased quality of life and increased mortality. The calcitonin peptide family consists of peptides with a similar structure to CT, although with different origins and diverse biological functions, all of which are potent systemic and local regulators of bone metabolism. However, the following knowledge gaps remained to be addressed. First, the role of the *CALCA*-encoded peptides, including PCT, CT and α CGRP, in the development of ptOA remained unclear. Furthermore, little was known about the effect of the amylin analog pramlintide, an anti-diabetic medication adjuvant to insulin, on the osteoporotic bone loss, and it remained controversial through which receptor potential biological effects were mediated.

To investigate the role of the calcitonin family of peptides in the development of ptOA, female *CALCA*^{-/-} mice lacking both *PCT/CT* and *α CGRP* transcripts and *α CGRP*^{-/-} mice with exclusive ablation of α CGRP were subjected to ACLT. As a control, *CTR*^{-/-} mice with specific dysfunction of CT-CTR signaling and WT mice were employed. Histologic, histomorphometric and radiologic measurements were carried out to evaluate changes in cartilage degeneration, subchondral bone structure, synovitis, and osteophyte formation. The data showed that the expression of *PCT/CT*, *α CGRP* and CTR was induced after ACLT. Compared to WT controls, *CALCA*^{-/-} mice exhibited increased cartilage degeneration, more pronounced subchondral bone loss, and reduced osteophyte formation and synovitis, whereas no alterations but decreased osteophyte formation were observed in *α CGRP*^{-/-} and *CTR*-deficient mice.

To study the effect of pramlintide on osteoporosis-induced bone loss, OVX was performed in WT and *CTR*-deficient mice, followed by histologic and radiographic evaluations to measure alterations in bone morphometry and bone metabolism. In vitro experiments using bone marrow-derived osteoclast cultures followed by genome-wide transcriptome profiling were carried out to investigate a potential mechanism underlying the effect of pramlintide on osteoclastogenesis. It was noticed that pramlintide restored the OVX-induced bone loss in the spinal and distal femoral trabecular bone of WT mice, but not of *CTR*^{-/-} mice. Furthermore, pramlintide was found to inhibit osteoclastogenesis in a CTR-dependent manner, as demonstrated by both in vivo and in vitro observations.

In conclusion, the present study demonstrates that *PCT/CT* transcript protects against the progression of ptOA, whereas *αCGRP* transcript and CTR-mediated signaling exacerbate osteophyte formation in ptOA. Furthermore, the amylin analog, pramlintide interacts with CTR to restore OVX-induced bone loss by inhibiting bone resorption. These findings provide new insights into the calcitonin peptide family as potential therapeutic targets for ptOA and offer a new possible application for pramlintide in the treatment of osteoporosis.

7. Zusammenfassung

OA und Osteoporose sind sehr häufige degenerative Erkrankungen in der älteren Bevölkerung, die zu einer erheblich verminderten Lebensqualität und einer erhöhten Sterblichkeit beitragen. Die Familie der Calcitonin-Peptide besteht aus Peptiden, die eine ähnliche Struktur wie CT aufweisen, wenn auch mit unterschiedlichem Ursprung und vielfältigen biologischen Funktionen, die alle starke systemische und lokale Regulatoren des Knochenstoffwechsels sind. Die folgenden Wissenslücken müssen jedoch noch geschlossen werden. Erstens ist die Rolle der *CALCA*-kodierte Peptide, einschließlich PCT, CT und α CGRP, bei der Entwicklung von ptOA noch unklar. Darüber hinaus war nur wenig über die Wirkung des Amylin-Analogons Pramlintid, eines Antidiabetikums, auf den osteoporotischen Knochenverlust bekannt, und es blieb unklar, über welchen Rezeptor potentielle biologische Funktion vermittelt werden.

Um die Rolle der Calcitonin-Peptidfamilie bei der Entwicklung von ptOA zu untersuchen, wurden weibliche *CALCA*^{-/-} Mäuse, denen sowohl *PCT/CT*- als auch α *CGRP*-Transkripte fehlen, sowie α *CGRP*^{-/-} Mäuse mit ausschließlicher Ablation von α CGRP einer ACLT unterzogen. Als Kontrolle wurden *CTR*^{-/-} Mäuse mit spezifischer Dysfunktion der CT-CTR Signalübertragung und WT Mäuse verwendet. Es wurden histologische, histomorphometrische und radiologische Messungen durchgeführt, um pathologische Veränderungen der Knorpeldegeneration, der subchondralen Knochenstruktur, der Synovitis und der Osteophytenbildung zu bewerten. Die Daten zeigten, dass die Expression von PCT/CT, α CGRP und CTR nach ACLT induziert wurde. Im Vergleich zu WT-Kontrollen wiesen *CALCA*^{-/-} Mäuse eine verstärkte Knorpeldegeneration, einen ausgeprägteren subchondralen Knochenverlust und eine geringere Osteophytenbildung und Synovitis auf, während bei α *CGRP*- und *CTR*-defizienten Mäusen keine Veränderungen, aber eine geringere Osteophytenbildung beobachtet wurden.

Um die Wirkung von Pramlintid auf den Osteoporose-induzierten Knochenverlust zu untersuchen, wurde bei WT- und *CTR*-defizienten Mäusen eine Ovariectomie durchgeführt, gefolgt von röntgenologischen und histologischen Untersuchungen, um Veränderungen der Knochenmorphometrie und des Knochenstoffwechsels zu messen. In vitro-Experimente mit aus Knochenmark gewonnenen Osteoklastenkulturen und anschließende genomweite Transkriptom-Profilierung wurden durchgeführt, um einen

möglichen Mechanismus zu untersuchen, der der Wirkung von Pramlintid auf die Osteoklastenbildung zugrunde liegt. Es wurde festgestellt, dass Pramlintid den OVX-induzierten Knochenverlust im spinalen und distalen femoralen trabekulären Knochen von WT-Mäusen wiederherstellte, nicht jedoch von *CTR*^{-/-} Mäusen. Darüber hinaus konnten wir nachweisen, dass Pramlintid die Osteoklastogenese in einer *CTR*-abhängigen Weise hemmt, wie sowohl in vivo als auch in vitro beobachtet wurde.

Zusammenfassend zeigt die vorliegende Studie, dass das *PCT/CT* Transkript vor dem Fortschreiten der ptOA schützt, während das *αCGRP*-Transkript und die *CTR*-vermittelte Signalgebung die Osteophytenbildung bei ptOA verschlimmern. Darüber hinaus interagiert das Amylin-Analogon Pramlintid mit *CTR*, um den OVX-induzierten Knochenverlust durch Hemmung der Knochenresorption wiederherzustellen. Diese Ergebnisse geben neue Einblicke in die Calcitonin Peptid Familie als potenzielle therapeutische Ziele für ptOA und bieten eine neue mögliche Anwendung für Pramlintid bei der Behandlung von Osteoporose.

8. List of abbreviations

μCT	X-ray microtomography
A.U.	Arbitrary units
AC	Articular cartilage
ACL	Anterior cruciate ligament
ACLT	Anterior cruciate ligament transection
ALP	Alkaline phosphatase
α-MEM	Minimum essential medium alpha
Angptl2	Angiopoietin-like 2
Angptl4	Angiopoietin-like 4
BFR	Bone formation rate
BFR/BS	Bone formation rate per bone surface
BIC	Bone-inflammation-cartilage
BM	Subchondral bone marrow
BMD	Bone mineralized density
BMP2	Bone morphogenetic protein 2
BMP7	Bone morphogenetic protein 7
BPO	Benzoyl peroxide
BV/TV	Bone volume per tissue volume
CANVAS	Canagliflozin cardiovascular Assessment Study
CD14	Cluster of differentiation 14
CD16	Cluster of differentiation 16
CD31	Cluster of differentiation 31
cDNA	Complementary DNA
COL1	Type I collagen
Col1a1	Alpha-1 type I collagen
Crem	Camp responsive element modulator
CRLR	Calcitonin receptor-like receptor
CT	Calcitonin
Ct.Po	Cortical porosity
Ct.Th	Cortical thickness
CTR	Calcitonin receptor
DEG	Differentially expressed gene

Dkk1	Dickkopf-related protein 1
DMM	Destabilization of the medial meniscus
EDTA	Ethylenediaminetetraacetate
ER α	Estrogen receptor- α
FCF	Fast green
FDA	United States Food and Drug Administration
Gapdh	Glyceraldehyde-3-phosphate dehydrogenase
H&E	Hematoxylin and eosin
HC/CC	Hyaline cartilage to calcified cartilage
HCl	Hydrochloric acid
HISAT	Hierarchical Indexing for Spliced Alignment of Transcripts
HNO ₃	Nitric acid
HSCs	Haemopoietic stem cells
IgG	Immunoglobulin
IL	Interleukin
IL-10	Interleukin-10
IL-1 β	Interleukin-1 beta
IL-6	Interleukin-6
LFC	Lateral femoral condyle
LPS	Lipopolysaccharides
Lrp5	Lipoprotein receptor-related protein 5
LTP	Lateral tibial plateau
MCP1	Monocyte Chemoattractant Protein-1
M-CSF	Macrophage colony-stimulating factor
MFC	Medial femoral condyle
MMA	Methyl methacrylate
MMPs	Matrix metalloproteases
MSCs	Mesenchymal stem cells
MTP	Medial tibial plateau
NaOH	Sodium hydroxide
NFATc1	Nuclear factor of activated T cells, cytoplasmic, calcineurin dependent 1
OA	Osteoarthritis
OARSI	Osteoarthritis research society international

Ob.N/B.Pm	Number of osteoblasts per bone perimeter
Ob.S/BS	Osteoblast surface per bone surface
Oc.N/B.Pm	Osteoclasts per bone perimeter
Oc.S/BS	Osteoclast surface per bone surface
OPG	Osteoprotegerin
Osx	Osterix
OVX	Ovariectomy
PCT	Procalcitonin
PROOF	Prevent Recurrence of Osteoporotic Fractures
Prrx1	Paired related homeobox 1
PTH	Parathyroid hormone
ptOA	Post traumatic osteoarthritis
PCR	Polymerase chain reaction
qRT-PCR	Real-time quantitative reverse transcription polymerase chain reaction
RAMP	Receptor activity-modifying proteins
RANK	Receptor activator of NF- κ B
RANKL	Receptor activator of NF- κ B ligand
Runx2	Runt-related transcription factor 2
S1P	Sphingosine-1-phosphate
SB	Subchondral bone
SBP	Subchondral bone plate
sCT	Salmon calcitonin
SGLT2	Sodium-glucose Cotransporter-2
Socs3	Suppressor of cytokine signaling 3
Sp7	Transcription factor Sp7
Sphk1	Sphingosine kinase 1
SPNS2	Sphingolipid transporter 2
STB	Subchondral trabecular bone
T1D	Type 1 diabetes
T2D	Type 2 diabetes
Tb.N	Trabecular number
Tb.sp	Trabecular separation
Tb.Th	Trabecular thickness

Tcf/Lef	Transcription factors T-cell factor/lymphoid enhancer factor
TNF α	Tumor necrosis factor- α
TNF α	Tumor necrosis factor alpha
TRAP	Tartrate-resistant acid phosphatase
VEGF-A	Vascular endothelial growth factor
VOI	Volume of interest
WOMAC	Western Ontario and McMaster Universities Osteoarthritis scores
WT	Wild type
α CGRP	Calcitonin gene-related peptide alpha
α -MEM	Minimum Essential Medium Alpha modification

9. References

9. Pharmacologic Approaches to Glycemic Treatment: Standards of Medical Care in Diabetes-2022. (2022). *Diabetes Care*, 45 (Suppl 1), S125-s143. doi:10.2337/dc22-S009
- Abdallah, B. M., Stilgren, L. S., Nissen, N., Kassem, M., Jørgensen, H. R., & Abrahamsen, B. (2005). Increased RANKL/OPG mRNA ratio in iliac bone biopsies from women with hip fractures. *Calcif Tissue Int*, 76 (2), 90-97. doi:10.1007/s00223-004-0074-4
- Adachi, J., Bensen, W., Bell, M., Bianchi, F., Cividino, A., Craig, G., . . . Gordon, M. J. B. j. o. r. (1997). Salmon calcitonin nasal spray in the prevention of corticosteroid-induced osteoporosis. 36 (2), 255-259.
- Aikawa, J., Uchida, K., Takano, S., Inoue, G., Iwase, D., Miyagi, M., . . . Takaso, M. (2018). Regulation of calcitonin gene-related peptide expression through the COX-2/mPGES-1/PGE2 pathway in the infrapatellar fat pad in knee osteoarthritis. *Lipids in Health and Disease*, 17.
- Ali, R., Hammad, A., El-Nahrery, E., Hamdy, N., Elhawary, A. K., & Eid, R. (2019). Serum RANKL, osteoprotegerin (OPG) and RANKL/OPG ratio in children with systemic lupus erythematosus. *Lupus*, 28 (10), 1233-1242. doi:10.1177/0961203319867129
- Anderson, H. C. (2003). Matrix vesicles and calcification. *Curr Rheumatol Rep*, 5 (3), 222-226. doi:10.1007/s11926-003-0071-z
- Anderson, H. C., Garimella, R., & Tague, S. E. (2005). The role of matrix vesicles in growth plate development and biomineralization. *Front Biosci*, 10, 822-837. doi:10.2741/1576
- Appelt, J., Baranowsky, A., Jahn, D., Yorgan, T., Kohli, P., Otto, E., . . . Keller, J. (2020). The neuropeptide calcitonin gene-related peptide alpha is essential for bone healing. *EBioMedicine*, 59, 102970. doi:10.1016/j.ebiom.2020.102970
- Arifin, W. N., & Zahiruddin, W. M. (2017). Sample Size Calculation in Animal Studies Using Resource Equation Approach. *Malays J Med Sci*, 24 (5), 101-105. doi:10.21315/mjms2017.24.5.11
- Assicot, M., Gendrel, D., Carsin, H., Raymond, J., Guilbaud, J., & Bohuon, C. (1993). High serum procalcitonin concentrations in patients with sepsis and infection. *Lancet*, 341 (8844), 515-518. doi:10.1016/0140-6736 (93)90277-n
- Atkins, G. J., & Findlay, D. M. (2012). Osteocyte regulation of bone mineral: a little give and take. *Osteoporos Int*, 23 (8), 2067-2079. doi:10.1007/s00198-012-1915-z
- Bagger, Y. Z., Tanko, L. B., Alexandersen, P., Karsdal, M. A., Olson, M., Mindeholm, L., . . . Christiansen, C. (2005). Oral salmon calcitonin induced suppression of urinary collagen type II degradation in postmenopausal women: a new potential treatment of osteoarthritis. *Bone*, 37 (3), 425-430. doi:10.1016/j.bone.2005.04.032
- Bailey, R. J., Walker, C. S., Ferner, A., Loomes, K. M., Prijic, G., Halim, A., . . . Hay, D. L. J. B. J. o. P. (2012). Pharmacological characterization of rat amylin receptors: implications for the identification of amylin receptor subtypes. 166.
- Ballica, R., Valentijn, K. M., Khachatryan, A., Guerder, S., Kapadia, S. E., Gundberg, C., . . . Vignery, A. s. (1999). Targeted Expression of Calcitonin Gene - Related Peptide to Osteoblasts Increases Bone Density in Mice. *Journal of Bone and Mineral Research*, 14.
- Bannuru, R. R., Osani, M. C., Vaysbrot, E. E., Arden, N. K., Bennell, K., Bierma-Zeinstra, S. M. A., . . . McAlindon, T. E. (2019). OARSI guidelines for the non-surgical

- management of knee, hip, and polyarticular osteoarthritis. *Osteoarthritis Cartilage*, 27 (11), 1578-1589. doi:10.1016/j.joca.2019.06.011
- Baranowsky, A., Appelt, J., Kleber, C., Lange, T., Ludewig, P., Jahn, D., . . . Keller, J. (2021). Procalcitonin Exerts a Mediator Role in Septic Shock Through the Calcitonin Gene-Related Peptide Receptor. *Crit Care Med*, 49 (1), e41-e52. doi:10.1097/ccm.0000000000004731
- Baranowsky, A., Jahn, D., Jiang, S., Yorgan, T., Ludewig, P., Appelt, J., . . . Keller, J. (2022). Procalcitonin is expressed in osteoblasts and limits bone resorption through inhibition of macrophage migration during intermittent PTH treatment. *Bone Res*, 10 (1), 9. doi:10.1038/s41413-021-00172-y
- Bartoletti, M., Antonelli, M., Bruno Blasi, F. A., Casagrande, I., Chierigato, A., Fumagalli, R., . . . Pea, F. (2018). Procalcitonin-guided antibiotic therapy: an expert consensus. *Clin Chem Lab Med*, 56 (8), 1223-1229. doi:10.1515/cclm-2018-0259
- Becker, K. L., Nylen, E. S., Snider, R. H., Müller, B., & White, J. C. (2003). Immunoneutralization of procalcitonin as therapy of sepsis. *Journal of Endotoxin Research*, 9, 367 - 374.
- Becker, K. L., Snider, R., & Nylen, E. S. (2010). Procalcitonin in sepsis and systemic inflammation: a harmful biomarker and a therapeutic target. *Br J Pharmacol*, 159 (2), 253-264. doi:10.1111/j.1476-5381.2009.00433.x
- Bettica, P., Cline, G., Hart, D. J., Meyer, J., & Spector, T. D. (2002). Evidence for increased bone resorption in patients with progressive knee osteoarthritis: longitudinal results from the Chingford study. *Arthritis Rheum*, 46 (12), 3178-3184. doi:10.1002/art.10630
- Bonewald, L. F. (2011). The amazing osteocyte. *J Bone Miner Res*, 26 (2), 229-238. doi:10.1002/jbmr.320
- Borm, A. K., Klevesath, M. S., Borcea, V., Kasperk, C., Seibel, M. J., Wahl, P., . . . Naworth, P. P. (1999). The effect of pramlintide (amylin analogue) treatment on bone metabolism and bone density in patients with type 1 diabetes mellitus. *Horm Metab Res*, 31 (8), 472-475. doi:10.1055/s-2007-978777
- Borst, S. E. (2004). The role of TNF-alpha in insulin resistance. *Endocrine*, 23 (2-3), 177-182. doi:10.1385/endo:23:2-3:177
- Botter, S. M., van Osch, G. J., Clockaerts, S., Waarsing, J. H., Weinans, H., & van Leeuwen, J. P. (2011). Osteoarthritis induction leads to early and temporal subchondral plate porosity in the tibial plateau of mice: an in vivo microfocal computed tomography study. *Arthritis Rheum*, 63 (9), 2690-2699. doi:10.1002/art.30307
- Bronský, J., & Průsa, R. (2004). Amylin fasting plasma levels are decreased in patients with osteoporosis. *Osteoporos Int*, 15 (3), 243-247. doi:10.1007/s00198-003-1538-5
- Bullock, C., Wookey, P. J., Bennett, A., Mobasheri, A., Dickerson, I., & Kelly, S. (2014). Peripheral Calcitonin Gene-Related Peptide Receptor Activation and Mechanical Sensitization of the Joint in Rat Models of Osteoarthritis Pain. *Arthritis & Rheumatology (Hoboken, N.j.)*, 66, 2188 - 2200.
- Camozzi, V., Tossi, A., Simoni, E., Pagani, F., Francucci, C. M., & Moro, L. (2007). Role of biochemical markers of bone remodeling in clinical practice. *J Endocrinol Invest*, 30 (6 Suppl), 13-17.
- Chambers, T. J., & Magnus, C. J. (1982). Calcitonin alters behaviour of isolated osteoclasts. *J Pathol*, 136 (1), 27-39. doi:10.1002/path.1711360104
- Chen, M., Hu, X., Wu, M., Yang, J., Han, R., Ma, Y., . . . Pan, F. (2019). Serum Levels of OPG, RANKL, and RANKL/OPG Ratio in Patients with Ankylosing Spondylitis: A Systematic Review and Meta-analysis. *Immunol Invest*, 48 (5), 490-504. doi:10.1080/08820139.2019.1567531
- Cheng, T., Zhang, L., Fu, X., Wang, W., Xu, H., Song, H., & Zhang, Y. (2013). The potential protective effects of calcitonin involved in coordinating chondrocyte response,

- extracellular matrix, and subchondral trabecular bone in experimental osteoarthritis. *Connect Tissue Res*, 54 (2), 139-146. doi:10.3109/03008207.2012.760549
- Chesnut, C. H. I., Silverman, S. L., Andriano, K., Genant, H. K., Gimona, A., Harris, S. T., . . . Baylink, D. J. P. (2000). A randomized trial of nasal spray salmon calcitonin in postmenopausal women with established osteoporosis: the prevent recurrence of osteoporotic fractures study. PROOF Study Group. *The American journal of medicine*, 109 4, 267-276.
- Chou, C. H., Jain, V., Gibson, J., Attarian, D. E., Haraden, C. A., Yohn, C. B., . . . Kraus, V. B. (2020). Synovial cell cross-talk with cartilage plays a major role in the pathogenesis of osteoarthritis. *Sci Rep*, 10 (1), 10868. doi:10.1038/s41598-020-67730-y
- Christopoulos, G. A., Perry, K. J., Morfis, M. M., Tilakaratne, N., Gao, Y., Fraser, N. J., . . . Sexton, P. M. J. M. p. (1999). Multiple amylin receptors arise from receptor activity-modifying protein interaction with the calcitonin receptor gene product. *56 1*, 235-242.
- Connor, J. R., LePage, C., Swift, B. A., Yamashita, D., Bendele, A. M., Maul, D., & Kumar, S. (2009). Protective effects of a cathepsin K inhibitor, SB-553484, in the canine partial medial meniscectomy model of osteoarthritis. *Osteoarthritis Cartilage*, 17 (9), 1236-1243. doi:10.1016/j.joca.2009.03.015
- Cornish, J., Callon, K. E., Bava, U., Kamona, S. A., Cooper, G. J., & Reid, I. R. (2001). Effects of calcitonin, amylin, and calcitonin gene-related peptide on osteoclast development. *Bone*, 29 (2), 162-168. doi:10.1016/s8756-3282 (01)00494-x
- Cornish, J., Callon, K. E., Bava, U., Kamona, S. A., Cooper, G. J. S., & Reid, I. R. (2001). Effects of calcitonin, amylin, and calcitonin gene-related peptide on osteoclast development. *Bone*, 29 2, 162-168.
- Cornish, J., Callon, K. E., Cooper, G. J. S., Reid, I. R. J. B., & communications, b. r. (1995). Amylin stimulates osteoblast proliferation and increases mineralized bone volume in adult mice. *207 1*, 133-139.
- Cornish, J., Callon, K. E., Gasser, J. A., Bava, U., Gardiner, E. M., Coy, D. H., . . . Reid, I. R. (2000). Systemic administration of a novel octapeptide, amylin- (1—8), increases bone volume in male mice. *American Journal of Physiology-Endocrinology and Metabolism*, 279 (4), E730-E735. doi:10.1152/ajpendo.2000.279.4.E730
- Cornish, J., Callon, K. E., King, A. R., Cooper, G. J. S., & Reid, I. R. (1998). Systemic administration of amylin increases bone mass, linear growth, and adiposity in adult male mice. *American Journal of Physiology-Endocrinology and Metabolism*, 275 (4), E694-E699. doi:10.1152/ajpendo.1998.275.4.E694
- Cornish, J., Callon, K. E., King, A. R., Cooper, G. J. S., & Reid, I. R. J. T. A. j. o. p. (1998). Systemic administration of amylin increases bone mass, linear growth, and adiposity in adult male mice. *275 4*, E694-699.
- Cornish, J., Callon, K. E., Lin, C. Q.-X., Xiao, C. L., Mulvey, T. B., Coy, D. H., . . . Reid, I. R. (1998). Dissociation of the effects of amylin on osteoblast proliferation and bone resorption. *American Journal of Physiology-Endocrinology and Metabolism*, 274 (5), E827-E833. doi:10.1152/ajpendo.1998.274.5.E827
- Cornish, J., Grey, A., Callon, K. E., Naot, D., Hill, B. L., Lin, C. Q., . . . Reid, I. R. (2004). Shared pathways of osteoblast mitogenesis induced by amylin, adrenomedullin, and IGF-1. *Biochem Biophys Res Commun*, 318 (1), 240-246. doi:10.1016/j.bbrc.2004.04.020
- Cui, A., Li, H., Wang, D., Zhong, J., Chen, Y., & Lu, H. (2020). Global, regional prevalence, incidence and risk factors of knee osteoarthritis in population-based studies. *EClinicalMedicine*, 29-30, 100587. doi:10.1016/j.eclinm.2020.100587
- Cui, Y., Niziolek, P. J., MacDonald, B. T., Zylstra, C. R., Alenina, N., Robinson, D. R., . . . Robling, A. G. (2011). Lrp5 functions in bone to regulate bone mass. *Nat Med*, 17 (6), 684-691. doi:10.1038/nm.2388

- Dacquin, R., Davey, R. A., Laplace, C., Levasseur, R., Morris, H. A., Goldring, S. R., . . . Karsenty, G. (2004). Amylin inhibits bone resorption while the calcitonin receptor controls bone formation in vivo. *J Cell Biol*, *164* (4), 509-514. doi:10.1083/jcb.200312135
- Delaisse, J. M. (2014). The reversal phase of the bone-remodeling cycle: cellular prerequisites for coupling resorption and formation. *Bonekey Rep*, *3*, 561. doi:10.1038/bonekey.2014.56
- Dempster, D. W., Compston, J. E., Drezner, M. K., Glorieux, F. H., Kanis, J. A., Malluche, H., . . . Parfitt, A. M. (2013). Standardized nomenclature, symbols, and units for bone histomorphometry: a 2012 update of the report of the ASBMR Histomorphometry Nomenclature Committee. *J Bone Miner Res*, *28* (1), 2-17. doi:10.1002/jbmr.1805
- Denger, S., Reid, G., & Gannon, F. (2008). Expression of the estrogen receptor during differentiation of human osteoclasts. *Steroids*, *73* (7), 765-774. doi:10.1016/j.steroids.2008.02.013
- Dong, X. N., Qin, A., Xu, J., & Wang, X. (2011). In situ accumulation of advanced glycation endproducts (AGEs) in bone matrix and its correlation with osteoclastic bone resorption. *Bone*, *49* (2), 174-183. doi:10.1016/j.bone.2011.04.009
- Everts, V., Delaissé, J. M., Korper, W., Jansen, D. C., Tigchelaar-Gutter, W., Saftig, P., & Beertsen, W. (2002). The bone lining cell: its role in cleaning Howship's lacunae and initiating bone formation. *J Bone Miner Res*, *17* (1), 77-90. doi:10.1359/jbmr.2002.17.1.77
- Fan, Y., Wei, F., Lang, Y., & Liu, Y. (2016). Diabetes mellitus and risk of hip fractures: a meta-analysis. *Osteoporos Int*, *27* (1), 219-228. doi:10.1007/s00198-015-3279-7
- Felson, D. T., Niu, J., Neogi, T., Goggins, J., Nevitt, M. C., Roemer, F., . . . Guermazi, A. (2016). Synovitis and the risk of knee osteoarthritis: the MOST Study. *Osteoarthritis Cartilage*, *24* (3), 458-464. doi:10.1016/j.joca.2015.09.013
- Fong, Y., Edelstein, D., Wang, E. A., & Brownlee, M. (1993). Inhibition of matrix-induced bone differentiation by advanced glycation end-products in rats. *Diabetologia*, *36* (9), 802-807. doi:10.1007/bf00400353
- Franz-Odenaal, T. A., Hall, B. K., & Witten, P. E. (2006). Buried alive: how osteoblasts become osteocytes. *Dev Dyn*, *235* (1), 176-190. doi:10.1002/dvdy.20603
- Frost, H. M. (1994). Wolff's Law and bone's structural adaptations to mechanical usage: an overview for clinicians. *Angle Orthod*, *64* (3), 175-188. doi:10.1043/0003-3219(1994)064<0175:Wlabsa>2.0.Co;2
- Fu, Q., Jilka, R. L., Manolagas, S. C., & O'Brien, C. A. (2002). Parathyroid Hormone Stimulates Receptor Activator of NFκB Ligand and Inhibits Osteoprotegerin Expression via Protein Kinase A Activation of cAMP-response Element-binding Protein*. *The Journal of Biological Chemistry*, *277*, 48868 - 48875.
- Gaur, T., Lengner, C. J., Hovhannisyan, H., Bhat, R. A., Bodine, P. V., Komm, B. S., . . . Lian, J. B. (2005). Canonical WNT signaling promotes osteogenesis by directly stimulating Runx2 gene expression. *J Biol Chem*, *280* (39), 33132-33140. doi:10.1074/jbc.M500608200
- Gerwin, N., Bendele, A. M., Glasson, S., & Carlson, C. S. (2010). The OARSI histopathology initiative - recommendations for histological assessments of osteoarthritis in the rat. *Osteoarthritis Cartilage*, *18 Suppl 3*, S24-34. doi:10.1016/j.joca.2010.05.030
- Gingell, J. J., Burns, E. R., & Hay, D. L. J. E. (2014). Activity of pramlintide, rat and human amylin but not Aβ1-42 at human amylin receptors. *155 I*, 21-26.
- Giuliani, N., Bataille, R., Mancini, C., Lazzaretti, M., & Barillé, S. (2001). Myeloma cells induce imbalance in the osteoprotegerin/osteoprotegerin ligand system in the human bone marrow environment. *Blood*, *98* (13), 3527-3533. doi:10.1182/blood.v98.13.3527

- Glass, D. A., 2nd, Bialek, P., Ahn, J. D., Starbuck, M., Patel, M. S., Clevers, H., . . . Karsenty, G. (2005). Canonical Wnt signaling in differentiated osteoblasts controls osteoclast differentiation. *Dev Cell*, 8 (5), 751-764. doi:10.1016/j.devcel.2005.02.017
- Glasson, S. S., Blanchet, T. J., & Morris, E. A. (2007). The surgical destabilization of the medial meniscus (DMM) model of osteoarthritis in the 129/SvEv mouse. *Osteoarthritis Cartilage*, 15 (9), 1061-1069. doi:10.1016/j.joca.2007.03.006
- Goldring, S. R. (2015). The osteocyte: key player in regulating bone turnover. *RMD Open*, 1 (Suppl 1), e000049. doi:10.1136/rmdopen-2015-000049
- Goodman, E. C., & Iversen, L. L. (1986). Calcitonin gene-related peptide: novel neuropeptide. *Life sciences*, 38 24, 2169-2178.
- Granhölm, S., Lundberg, P., & Lerner, U. H. (2007). Calcitonin inhibits osteoclast formation in mouse haematopoietic cells independently of transcriptional regulation by receptor activator of NF- κ B and c-Fms. *J Endocrinol*, 195 (3), 415-427. doi:10.1677/joe-07-0338
- Grimaud, E., Soubigou, L., Couillaud, S., Coipeau, P., Moreau, A., Passuti, N., . . . Heymann, D. (2003). Receptor activator of nuclear factor κ B ligand (RANKL)/osteoprotegerin (OPG) ratio is increased in severe osteolysis. *Am J Pathol*, 163 (5), 2021-2031. doi:10.1016/s0002-9440 (10)63560-2
- Gutiérrez-Rojas, I., Lozano, D., Lozano, D., Nuche-Berenguer, B., Moreno, P., Acitores, A. P., . . . Esbrit, P. (2013). Amylin exerts osteogenic actions with different efficacy depending on the diabetic status. *Molecular and Cellular Endocrinology*, 365, 309-315.
- Gutiérrez-Rojas, I., Lozano, D., Nuche-Berenguer, B., Moreno, P., Acitores, A., Ramos-Álvarez, I., . . . Esbrit, P. (2013). Amylin exerts osteogenic actions with different efficacy depending on the diabetic status. *Molecular and Cellular Endocrinology*, 365 (2), 309-315. doi:<https://doi.org/10.1016/j.mce.2012.11.013>
- Hauge, E. M., Qvesel, D., Eriksen, E. F., Mosekilde, L., & Melsen, F. (2001). Cancellous bone remodeling occurs in specialized compartments lined by cells expressing osteoblastic markers. *J Bone Miner Res*, 16 (9), 1575-1582. doi:10.1359/jbmr.2001.16.9.1575
- Hay, D. L., Chen, S., Lutz, T. A., Parkes, D. G., & Roth, J. D. (2015). Amylin: Pharmacology, Physiology, and Clinical Potential. *Pharmacol Rev*, 67 (3), 564-600. doi:10.1124/pr.115.010629
- Hellio, M. P., Peschard, M. J., Cohen, C., Richard, M., & Vignon, E. (1997). Calcitonin inhibits phospholipase A2 and collagenase activity of human osteoarthritic chondrocytes. *Osteoarthritis Cartilage*, 5 (2), 121-128. doi:10.1016/s1063-4584 (97)80005-2
- Henriksen, K., Byrjalsen, I., Andersen, J. R., Bihlet, A. R., Russo, L. A., Alexandersen, P., . . . Karsdal, M. A. (2016). A randomized, double-blind, multicenter, placebo-controlled study to evaluate the efficacy and safety of oral salmon calcitonin in the treatment of osteoporosis in postmenopausal women taking calcium and vitamin D. *Bone*, 91, 122-129. doi:10.1016/j.bone.2016.07.019
- Hidayat, K., Du, X., Wu, M. J., & Shi, B. M. (2019). The use of metformin, insulin, sulphonylureas, and thiazolidinediones and the risk of fracture: Systematic review and meta-analysis of observational studies. *Obes Rev*, 20 (10), 1494-1503. doi:10.1111/obr.12885
- Hoff, A. O., Catala-Lehnen, P., Thomas, P. M., Priemel, M., Rueger, J. M., Nasonkin, I., . . . Gagel, R. F. (2002). Increased bone mass is an unexpected phenotype associated with deletion of the calcitonin gene. *J Clin Invest*, 110 (12), 1849-1857. doi:10.1172/jci14218

- Horcajada-Molteni, M.-N., Chanteranne, B., Lebecque, P., Davicco, M.-J., Coxam, V., Young, A., & Barlet, J.-P. (2001). Amylin and Bone Metabolism in Streptozotocin-Induced Diabetic Rats. *Journal of Bone and Mineral Research*, *16* (5), 958-965. doi:<https://doi.org/10.1359/jbmr.2001.16.5.958>
- Horcajada-Molteni, M. N., Davicco, M. J., Lebecque, P., Coxam, V., Young, A. A., & Barlet, J. P. (2000). Amylin inhibits ovariectomy-induced bone loss in rats. *J Endocrinol*, *165* (3), 663-668. doi:10.1677/joe.0.1650663
- Hsia, A. W., Emami, A. J., Tarke, F. D., Cunningham, H. C., Tjandra, P. M., Wong, A., . . . Collette, N. M. (2018). Osteophytes and fracture calluses share developmental milestones and are diminished by unloading. *J Orthop Res*, *36* (2), 699-710. doi:10.1002/jor.23779
- Huang, J. C., Sakata, T., Pflieger, L. L., Bencsik, M., Halloran, B. P., Bikle, D. D., & Nissenson, R. A. (2003). PTH Differentially Regulates Expression of RANKL and OPG. *Journal of Bone and Mineral Research*, *19*.
- Huang, J. C., Sakata, T., Pflieger, L. L., Bencsik, M., Halloran, B. P., Bikle, D. D., & Nissenson, R. A. (2004). PTH differentially regulates expression of RANKL and OPG. *J Bone Miner Res*, *19* (2), 235-244. doi:10.1359/jbmr.0301226
- Hughes, D. E., Dai, A., Tiffie, J. C., Li, H. H., Mundy, G. R., & Boyce, B. F. (1996). Estrogen promotes apoptosis of murine osteoclasts mediated by TGF-beta. *Nat Med*, *2* (10), 1132-1136. doi:10.1038/nm1096-1132
- Hügler, T., & Geurts, J. (2017). What drives osteoarthritis?-synovial versus subchondral bone pathology. *Rheumatology (Oxford)*, *56* (9), 1461-1471. doi:10.1093/rheumatology/kew389
- Hunter, D. J., Pike, M. C., Jonas, B. L., Kissin, E., Krop, J., & McAlindon, T. (2010). Phase 1 safety and tolerability study of BMP-7 in symptomatic knee osteoarthritis. *BMC Musculoskelet Disord*, *11*, 232. doi:10.1186/1471-2474-11-232
- Ikegame, M., Rakopoulos, M., Zhou, H., Houssami, S., Martin, J. T., Moseley, J. M., & Findlay, D. M. (1995). Calcitonin receptor isoforms in mouse and rat osteoclasts. *Journal of Bone and Mineral Research*, *10*.
- Ishizuka, K., Hirukawa, K., Nakamura, H., & Togari, A. (2005). Inhibitory effect of CGRP on osteoclast formation by mouse bone marrow cells treated with isoproterenol. *Neurosci Lett*, *379* (1), 47-51. doi:10.1016/j.neulet.2004.12.046
- Iwanaga, T., Shikichi, M., Kitamura, H., Yanase, H., Nozawa - Inoue, K. J. A. o. h., & cytology. (2000). Morphology and functional roles of synoviocytes in the joint. *63* *1*, 17-31.
- Jacome-Galarza, C. E., Percin, G. I., Muller, J. T., Mass, E., Lazarov, T., Eitler, J., . . . Geissmann, F. (2019). Developmental origin, functional maintenance and genetic rescue of osteoclasts. *Nature*, *568* (7753), 541-545. doi:10.1038/s41586-019-1105-7
- Janghorbani, M., Van Dam, R. M., Willett, W. C., & Hu, F. B. (2007). Systematic review of type 1 and type 2 diabetes mellitus and risk of fracture. *Am J Epidemiol*, *166* (5), 495-505. doi:10.1093/aje/kwm106
- Jia, J., Zhou, H., Zeng, X., & Feng, S. (2017). Estrogen stimulates osteoprotegerin expression via the suppression of miR-145 expression in MG-63 cells. *Mol Med Rep*, *15* (4), 1539-1546. doi:10.3892/mmr.2017.6168
- Jiang, S., Xie, W., Knapstein, P. R., Donat, A., Albertsen, L. C., Sevecke, J., . . . Keller, J. (2024). Transcript-dependent effects of the CALCA gene on the progression of post-traumatic osteoarthritis in mice. *Commun Biol*, *7* (1), 223. doi:10.1038/s42003-024-05889-0
- Jilka, R. L., Hangoc, G., Girasole, G., Passeri, G., Williams, D. C., Abrams, J. S., . . . Manolagas, S. C. (1992). Increased osteoclast development after estrogen loss: mediation by interleukin-6. *Science*, *257* (5066), 88-91. doi:10.1126/science.1621100

- Jin, Y., Smith, C., Monteith, D., Brown, R., Camporeale, A., McNearney, T. A., . . . Schnitzer, T. J. (2018). CGRP blockade by galcanezumab was not associated with reductions in signs and symptoms of knee osteoarthritis in a randomized clinical trial. *Osteoarthritis Cartilage*, *26* (12), 1609-1618. doi:10.1016/j.joca.2018.08.019
- Kadri, A., Ea, H. K., Bazille, C., Hannouche, D., Lioté, F., & Cohen-Solal, M. E. (2008). Osteoprotegerin inhibits cartilage degradation through an effect on trabecular bone in murine experimental osteoarthritis. *Arthritis Rheum*, *58* (8), 2379-2386. doi:10.1002/art.23638
- Kameda, T., Mano, H., Yuasa, T., Mori, Y., Miyazawa, K., Shiokawa, M., . . . Kumegawa, M. (1997). Estrogen inhibits bone resorption by directly inducing apoptosis of the bone-resorbing osteoclasts. *J Exp Med*, *186* (4), 489-495. doi:10.1084/jem.186.4.489
- Kanatsuka, A., Makino, H., Ohsawa, H., Tokuyama, Y., Yamaguchi, T., Yoshida, S., & Adachi, M. (1989). Secretion of islet amyloid polypeptide in response to glucose. *FEBS Lett*, *259* (1), 199-201. doi:10.1016/0014-5793 (89)81527-3
- Kanis, J. A., Oden, A., Johnell, O., De Laet, C., Jonsson, B., & Oglesby, A. K. (2003). The components of excess mortality after hip fracture. *Bone*, *32* (5), 468-473. doi:10.1016/s8756-3282 (03)00061-9
- Karner, C. M., & Long, F. (2017). Wnt signaling and cellular metabolism in osteoblasts. *Cell Mol Life Sci*, *74* (9), 1649-1657. doi:10.1007/s00018-016-2425-5
- Karsdal, M. A., Byrjalsen, I., Alexandersen, P., Bihlet, A., Andersen, J. R., Riis, B. J., . . . Christiansen, C. (2015). Treatment of symptomatic knee osteoarthritis with oral salmon calcitonin: results from two phase 3 trials. *Osteoarthritis Cartilage*, *23* (4), 532-543. doi:10.1016/j.joca.2014.12.019
- Karsdal, M. A., Sondergaard, B. C., Arnold, M., & Christiansen, C. (2007). Calcitonin affects both bone and cartilage: a dual action treatment for osteoarthritis? *Annals of the New York Academy of Sciences*, *1117*, 181-195.
- Karsdal, M. A., Tankó, L. B., Riis, B. J., Sondergaard, B. C., Henriksen, K., Altman, R. D., . . . Christiansen, C. (2006). Calcitonin is involved in cartilage homeostasis: is calcitonin a treatment for OA? *Osteoarthritis Cartilage*, *14* 7, 617-624.
- Kato, M., Patel, M. S., Levasseur, R., Lobov, I., Chang, B. H., Glass, D. A., 2nd, . . . Chan, L. (2002). Cbfa1-independent decrease in osteoblast proliferation, osteopenia, and persistent embryonic eye vascularization in mice deficient in Lrp5, a Wnt coreceptor. *J Cell Biol*, *157* (2), 303-314. doi:10.1083/jcb.200201089
- Katsuki, A., Sumida, Y., Murashima, S., Murata, K., Takarada, Y., Ito, K., . . . Yano, Y. (1998). Serum levels of tumor necrosis factor-alpha are increased in obese patients with noninsulin-dependent diabetes mellitus. *J Clin Endocrinol Metab*, *83* (3), 859-862. doi:10.1210/jcem.83.3.4618
- Kawamoto, T., & Kawamoto, K. (2014). Preparation of thin frozen sections from nonfixed and undecalcified hard tissues using Kawamoto's film method (2012). *Methods Mol Biol*, *1130*, 149-164. doi:10.1007/978-1-62703-989-5_11
- Keller, J., Catala-Lehnen, P., Huebner, A. K., Jeschke, A., Heckt, T., Lueth, A., . . . Amling, M. (2014). Calcitonin controls bone formation by inhibiting the release of sphingosine 1-phosphate from osteoclasts. *Nat Commun*, *5*, 5215. doi:10.1038/ncomms6215
- Kenkre, J. S., & Bassett, J. (2018). The bone remodelling cycle. *Ann Clin Biochem*, *55* (3), 308-327. doi:10.1177/0004563218759371
- Kim, A. S., Girgis, C. M., & McDonald, M. M. (2022). Osteoclast Recycling and the Rebound Phenomenon Following Denosumab Discontinuation. *Curr Osteoporos Rep*, *20* (6), 505-515. doi:10.1007/s11914-022-00756-5
- Klose-Jensen, R., Hartlev, L. B., Boel, L. W. T., Laursen, M. B., Stengaard-Pedersen, K., Keller, K. K., & Hauge, E. M. (2015). Subchondral bone turnover, but not bone

- volume, is increased in early stage osteoarthritic lesions in the human hip joint. *Osteoarthritis Cartilage*, 23 (12), 2167-2173. doi:10.1016/j.joca.2015.06.001
- Knowles, H. J., Cleton-Jansen, A.-M., Korsching, E., & Athanasou, N. A. (2010). Hypoxia-inducible factor regulates osteoclast-mediated bone resorption: role of angiopoietin-like 4. *The FASEB Journal*, 24, 4648 - 4659.
- Kobayashi, S., Takahashi, H. E., Ito, A., Saito, N., Nawata, M., Horiuchi, H., . . . Takaoka, K. (2003). Trabecular minimodeling in human iliac bone. *Bone*, 32 (2), 163-169. doi:10.1016/s8756-3282 (02)00947-x
- Komori, T. (2018). Runx2, an inducer of osteoblast and chondrocyte differentiation. *Histochem Cell Biol*, 149 (4), 313-323. doi:10.1007/s00418-018-1640-6
- Komori, T. (2019). Regulation of Proliferation, Differentiation and Functions of Osteoblasts by Runx2. *Int J Mol Sci*, 20 (7). doi:10.3390/ijms20071694
- Komori, T., Yagi, H., Nomura, S., Yamaguchi, A., Sasaki, K., Deguchi, K., . . . Kishimoto, T. (1997). Targeted disruption of Cbfa1 results in a complete lack of bone formation owing to maturational arrest of osteoblasts. *Cell*, 89 (5), 755-764. doi:10.1016/s0092-8674 (00)80258-5
- Kostenuik, P. J. (2005). Osteoprotegerin and RANKL regulate bone resorption, density, geometry and strength. *Curr Opin Pharmacol*, 5 (6), 618-625. doi:10.1016/j.coph.2005.06.005
- Krzeski, P., Buckland-Wright, C., Balint, G., Cline, G. A., Stoner, K., Lyon, R., . . . Spector, T. D. (2007). Development of musculoskeletal toxicity without clear benefit after administration of PG-116800, a matrix metalloproteinase inhibitor, to patients with knee osteoarthritis: a randomized, 12-month, double-blind, placebo-controlled study. *Arthritis Res Ther*, 9 (5), R109. doi:10.1186/ar2315
- Langdahl, B., Ferrari, S., & Dempster, D. W. (2016). Bone modeling and remodeling: potential as therapeutic targets for the treatment of osteoporosis. *Ther Adv Musculoskelet Dis*, 8 (6), 225-235. doi:10.1177/1759720x16670154
- LeBoff, M. S., Greenspan, S. L., Insogna, K. L., Lewiecki, E. M., Saag, K. G., Singer, A. J., & Siris, E. S. (2022). The clinician's guide to prevention and treatment of osteoporosis. *Osteoporos Int*, 33 (10), 2049-2102. doi:10.1007/s00198-021-05900-y
- Lewis, J. S., Hembree, W. C., Furman, B. D., Tippets, L., Cattell, D., Huebner, J. L., . . . Olson, S. A. (2011). Acute joint pathology and synovial inflammation is associated with increased intra-articular fracture severity in the mouse knee. *Osteoarthritis Cartilage*, 19 (7), 864-873. doi:10.1016/j.joca.2011.04.011
- Liang, W., Zhuo, X., Tang, Z., Wei, X., & Li, B. (2015). Calcitonin gene-related peptide stimulates proliferation and osteogenic differentiation of osteoporotic rat-derived bone mesenchymal stem cells. *Mol Cell Biochem*, 402 (1-2), 101-110. doi:10.1007/s11010-014-2318-6
- Liappis, A. P., Gibbs, K. W., Nysten, E. S., Yoon, B., Snider, R. H., Gao, B., & Becker, K. L. (2011). Exogenous procalcitonin evokes a pro-inflammatory cytokine response. *Inflamm Res*, 60 (2), 203-207. doi:10.1007/s00011-010-0255-8
- Little, C. B., Barai, A., Burkhardt, D., Smith, S. M., Fosang, A. J., Werb, Z., . . . Thompson, E. W. (2009). Matrix metalloproteinase 13-deficient mice are resistant to osteoarthritic cartilage erosion but not chondrocyte hypertrophy or osteophyte development. *Arthritis Rheum*, 60 (12), 3723-3733. doi:10.1002/art.25002
- Liu, F., Lee, S. K., Adams, D. J., Gronowicz, G. A., & Kream, B. E. (2007). CREM deficiency in mice alters the response of bone to intermittent parathyroid hormone treatment. *Bone*, 40 (4), 1135-1143. doi:10.1016/j.bone.2006.12.003
- Logerstedt, D. S., Ebert, J. R., MacLeod, T. D., Heiderscheidt, B. C., Gabbett, T. J., & Eckenrode, B. J. (2022). Effects of and Response to Mechanical Loading on the Knee. *Sports Med*, 52 (2), 201-235. doi:10.1007/s40279-021-01579-7

- Lou, H., Gagel, R. F., & Berget, S. M. (1996). An intron enhancer recognized by splicing factors activates polyadenylation. *Genes Dev*, *10* (2), 208-219. doi:10.1101/gad.10.2.208
- Lu, J. T., Son, Y. J., Lee, J., Jetton, T. L., Shiota, M., Moscoso, L., . . . Emeson, R. B. (1999). Mice lacking alpha-calcitonin gene-related peptide exhibit normal cardiovascular regulation and neuromuscular development. *Mol Cell Neurosci*, *14* (2), 99-120. doi:10.1006/mcne.1999.0767
- Ma, Y. L., Cain, R. L., Halladay, D. L., Yang, X., Zeng, Q., Miles, R. R., . . . Onyia, J. E. (2001). Catabolic effects of continuous human PTH (1--38) in vivo is associated with sustained stimulation of RANKL and inhibition of osteoprotegerin and gene-associated bone formation. *Endocrinology*, *142* (9), 4047-4054. doi:10.1210/endo.142.9.8356
- Maeda, Y., Miwa, Y., & Sato, I. (2017). Expression of CGRP, vasculogenesis and osteogenesis associated mRNAs in the developing mouse mandible and tibia. *Eur J Histochem*, *61* (1), 2750. doi:10.4081/ejh.2017.2750
- Maeno, T., Moriishi, T., Yoshida, C. A., Komori, H., Kanatani, N., Izumi, S., . . . Komori, T. (2011). Early onset of Runx2 expression caused craniosynostosis, ectopic bone formation, and limb defects. *Bone*, *49* (4), 673-682. doi:10.1016/j.bone.2011.07.023
- Maleitzke, T., Dietrich, T., Hildebrandt, A., Weber, J., Appelt, J., Jahn, D., . . . Keller, J. (2023). Inactivation of the gene encoding procalcitonin prevents antibody-mediated arthritis. *Inflamm Res*, *72* (5), 1069-1081. doi:10.1007/s00011-023-01719-x
- Maleitzke, T., Hildebrandt, A., Dietrich, T., Appelt, J., Jahn, D., Otto, E., . . . Keller, J. (2021). The calcitonin receptor protects against bone loss and excessive inflammation in collagen antibody-induced arthritis. *iScience*, *25*.
- Maleitzke, T., Hildebrandt, A., Weber, J., Dietrich, T., Appelt, J., Jahn, D., . . . Keller, J. (2020). Proinflammatory and bone protective role of calcitonin gene-related peptide alpha in collagen antibody-induced arthritis. *Rheumatology*.
- Mancini, L., Paul-Clark, M. J., Rosignoli, G., Hannon, R., Martin, J. E., Macintyre, I., & Perretti, M. (2007). Calcitonin and prednisolone display antagonistic actions on bone and have synergistic effects in experimental arthritis. *Am J Pathol*, *170* (3), 1018-1027. doi:10.2353/ajpath.2007.060830
- Manicourt, D. H., Azria, M., Mindeholm, L., Thonar, E. J., & Devogelaer, J. P. (2006). Oral salmon calcitonin reduces Lequesne's algofunctional index scores and decreases urinary and serum levels of biomarkers of joint metabolism in knee osteoarthritis. *Arthritis Rheum*, *54* (10), 3205-3211. doi:10.1002/art.22075
- Manolagas, S. C. (2000). Birth and death of bone cells: basic regulatory mechanisms and implications for the pathogenesis and treatment of osteoporosis. *Endocr Rev*, *21* (2), 115-137. doi:10.1210/edrv.21.2.0395
- Mapp, P. I., McWilliams, D. F., Turley, M. J., Hargin, E., & Walsh, D. A. (2012). A role for the sensory neuropeptide calcitonin gene-related peptide in endothelial cell proliferation in vivo. *Br J Pharmacol*, *166* (4), 1261-1271. doi:10.1111/j.1476-5381.2012.01848.x
- Martínez, J. M., Wagner, K. E., Snider, R. H., Nylen, E. S., Müller, B., Sarani, B., . . . White, J. C. (2001). Late immunoneutralization of procalcitonin arrests the progression of lethal porcine sepsis. *Surgical infections*, *2* 3, 193-202; discussion 202-193.
- Matera, G., Quirino, A., Giancotti, A., Pulicari, M. C., Rametti, L., Rodríguez, M. L., . . . Focà, A. (2012). Procalcitonin neutralizes bacterial LPS and reduces LPS-induced cytokine release in human peripheral blood mononuclear cells. *BMC Microbiol*, *12*, 68. doi:10.1186/1471-2180-12-68

- Mathiessen, A., & Conaghan, P. G. (2017). Synovitis in osteoarthritis: current understanding with therapeutic implications. *Arthritis Res Ther*, *19* (1), 18. doi:10.1186/s13075-017-1229-9
- Mazzuoli, G. F., Passeri, M., Gennari, C., Minisola, S., Antonelli, R., Valtorta, C., . . . Francini, G. (1986). Effects of salmon calcitonin in postmenopausal osteoporosis: a controlled double-blind clinical study. *Calcif Tissue Int*, *38* (1), 3-8. doi:10.1007/bf02556587
- Mcsheehy, P. M. J., & Chambers, T. J. (1986). Osteoblastic cells mediate osteoclastic responsiveness to parathyroid hormone. *Endocrinology*, *118* 2, 824-828.
- Messerer, D. A. C., Datzmann, T., Baranowsky, A., Peschel, L., Hoffmann, A., Gröger, M., . . . Keller, J. (2022). Systemic calcitonin gene-related peptide receptor antagonism decreases survival in a porcine model of polymicrobial sepsis: blinded randomised controlled trial. *Br J Anaesth*, *128* (5), 864-873. doi:10.1016/j.bja.2021.11.042
- Mi, J., Xu, J., Yao, H., Li, X., Tong, W., Li, Y., . . . Qin, L. (2021). Calcitonin Gene-Related Peptide Enhances Distraction Osteogenesis by Increasing Angiogenesis. *Tissue Eng Part A*, *27* (1-2), 87-102. doi:10.1089/ten.TEA.2020.0009
- Minatani, A., Uchida, K., Inoue, G., Takano, S., Aikawa, J., Miyagi, M., . . . Takaso, M. (2016). Activation of calcitonin gene-related peptide signaling through the prostaglandin E2-EP1/EP2/EP4 receptor pathway in synovium of knee osteoarthritis patients. *Journal of Orthopaedic Surgery and Research*, *11*.
- Motiur Rahman, M., Takeshita, S., Matsuoka, K., Kaneko, K., Naoe, Y., Sakaue-Sawano, A., . . . Ikeda, K. (2015). Proliferation-coupled osteoclast differentiation by RANKL: Cell density as a determinant of osteoclast formation. *Bone*, *81*, 392-399. doi:10.1016/j.bone.2015.08.008
- Muff, R., Bühlmann, N., Fischer, J. A., & Born, W. J. E. (1999). An amylin receptor is revealed following co-transfection of a calcitonin receptor with receptor activity modifying proteins-1 or -3. *140* 6, 2924-2927.
- Murshed, M. (2020). Corrigendum: Mechanism of Bone Mineralization. *Cold Spring Harb Perspect Med*, *10* (8). doi:10.1101/cshperspect.a040667
- Muthuri, S. G., McWilliams, D. F., Doherty, M., & Zhang, W. (2011). History of knee injuries and knee osteoarthritis: a meta-analysis of observational studies. *Osteoarthritis Cartilage*, *19* (11), 1286-1293. doi:10.1016/j.joca.2011.07.015
- Nakamura, T., Imai, Y., Matsumoto, T., Sato, S., Takeuchi, K., Igarashi, K., . . . Kato, S. (2007). Estrogen prevents bone loss via estrogen receptor alpha and induction of Fas ligand in osteoclasts. *Cell*, *130* (5), 811-823. doi:10.1016/j.cell.2007.07.025
- Nakashima, K., Zhou, X., Kunkel, G., Zhang, Z., Deng, J. M., Behringer, R. R., & de Crombrughe, B. (2002). The novel zinc finger-containing transcription factor osterix is required for osteoblast differentiation and bone formation. *Cell*, *108* (1), 17-29. doi:10.1016/s0092-8674(01)00622-5
- Naot, D., Bava, U., Matthews, B., Callon, K. E., Gamble, G. D., Black, M., . . . Reid, I. R. (2007). Differential gene expression in cultured osteoblasts and bone marrow stromal cells from patients with Paget's disease of bone. *J Bone Miner Res*, *22* (2), 298-309. doi:10.1359/jbmr.061108
- Naot, D., & Cornish, J. (2008). The role of peptides and receptors of the calcitonin family in the regulation of bone metabolism. *Bone*, *43* (5), 813-818. doi:10.1016/j.bone.2008.07.003
- Nishii, T., Tamura, S., Shiomi, T., Yoshikawa, H., & Sugano, N. (2013). Alendronate treatment for hip osteoarthritis: prospective randomized 2-year trial. *Clin Rheumatol*, *32* (12), 1759-1766. doi:10.1007/s10067-013-2338-8

- Niu, P., Zhong, Z., Wang, M., Huang, G., Xu, S., Hou, Y., . . . Wang, H. (2017). Zinc finger transcription factor Sp7/Osterix acts on bone formation and regulates coll10a1a expression in zebrafish. *Sci Bull (Beijing)*, 62 (3), 174-184. doi:10.1016/j.scib.2017.01.009
- Nylen, E. S., Whang, K. T., Snider, R. H., Jr., Steinwald, P. M., White, J. C., & Becker, K. L. (1998). Mortality is increased by procalcitonin and decreased by an antiserum reactive to procalcitonin in experimental sepsis. *Crit Care Med*, 26 (6), 1001-1006. doi:10.1097/00003246-199806000-00015
- Ogawa, A., Harris, V., McCorkle, S. K., Unger, R. H., & Luskey, K. L. (1990). Amylin secretion from the rat pancreas and its selective loss after streptozotocin treatment. *J Clin Invest*, 85 (3), 973-976. doi:10.1172/jci114528
- Ominsky, M. S., Li, X., Asuncion, F. J., Barrero, M., Warmington, K. S., Dwyer, D., . . . Kostenuik, P. J. (2008). RANKL inhibition with osteoprotegerin increases bone strength by improving cortical and trabecular bone architecture in ovariectomized rats. *J Bone Miner Res*, 23 (5), 672-682. doi:10.1359/jbmr.080109
- Ono, N., Ono, W., Nagasawa, T., & Kronenberg, H. M. (2014). A subset of chondrogenic cells provides early mesenchymal progenitors in growing bones. *Nat Cell Biol*, 16 (12), 1157-1167. doi:10.1038/ncb3067
- Oreffo, R. O., Kusec, V., Viridi, A. S., Flanagan, A. M., Grano, M., Zamboni-Zallone, A., & Triffitt, J. T. (1999). Expression of estrogen receptor-alpha in cells of the osteoclastic lineage. *Histochem Cell Biol*, 111 (2), 125-133. doi:10.1007/s004180050342
- Ortuño, M. J., Susperregui, A. R., Artigas, N., Rosa, J. L., & Ventura, F. (2013). Osterix induces Colla1 gene expression through binding to Sp1 sites in the bone enhancer and proximal promoter regions. *Bone*, 52 (2), 548-556. doi:10.1016/j.bone.2012.11.007
- Osteoporosis prevention, diagnosis, and therapy. (2001). *Jama*, 285 (6), 785-795. doi:10.1001/jama.285.6.785
- Overman, R. A., Borse, M., & Gourlay, M. L. (2013). Salmon calcitonin use and associated cancer risk. *Ann Pharmacother*, 47 (12), 1675-1684. doi:10.1177/1060028013509233
- Phinney, D. G., & Prockop, D. J. (2007). Concise review: mesenchymal stem/multipotent stromal cells: the state of transdifferentiation and modes of tissue repair--current views. *Stem Cells*, 25 (11), 2896-2902. doi:10.1634/stemcells.2007-0637
- Ponzetti, M., & Rucci, N. (2021). Osteoblast Differentiation and Signaling: Established Concepts and Emerging Topics. *Int J Mol Sci*, 22 (13). doi:10.3390/ijms22136651
- Prkno, A., Wacker, C., Brunkhorst, F. M., & Schlattmann, P. (2013). Procalcitonin-guided therapy in intensive care unit patients with severe sepsis and septic shock--a systematic review and meta-analysis. *Crit Care*, 17 (6), R291. doi:10.1186/cc13157
- Revell, P. A., Al-Saffar, N., Fish, S., & Osei, D. J. A. o. t. R. D. (1995). Extracellular matrix of the synovial intimal cell layer. 54, 404 - 407.
- Ringe, J.-D., & Welzel, D. J. E. J. o. C. P. (2004). Salmon calcitonin in the therapy of corticoid-induced osteoporosis. 33, 35-39.
- Rodrigues, T. A., de Oliveira Freire, A., Carvalho, H. C. O., Silva, G. E. B., Vasconcelos, J. W., Guerra, R. N. M., . . . Garcia, J. B. S. (2018). Prophylactic and Therapeutic Use of Strontium Ranelate Reduces the Progression of Experimental Osteoarthritis. *Front Pharmacol*, 9, 975. doi:10.3389/fphar.2018.00975
- Roemer, F. W., Guermazi, A., Felson, D. T., Niu, J., Nevitt, M. C., Crema, M. D., . . . Zhang, Y. (2011). Presence of MRI-detected joint effusion and synovitis increases the risk of cartilage loss in knees without osteoarthritis at 30-month follow-up: the MOST study. *Ann Rheum Dis*, 70 (10), 1804-1809. doi:10.1136/ard.2011.150243
- Rosenfeld, M. G., Mermod, J. J., Amara, S. G., Swanson, L. W., Sawchenko, P. E., Rivier, J., . . . Evans, R. M. (1983). Production of a novel neuropeptide encoded by the

- calcitonin gene via tissue-specific RNA processing. *Nature*, 304 (5922), 129-135. doi:10.1038/304129a0
- Russell, F. A., King, R., Smillie, S. J., Kodji, X., & Brain, S. D. (2014). Calcitonin gene-related peptide: physiology and pathophysiology. *Physiol Rev*, 94 (4), 1099-1142. doi:10.1152/physrev.00034.2013
- Rutkovskiy, A., Stenslkken, K. O., & Vaage, I. J. (2016). Osteoblast Differentiation at a Glance. *Med Sci Monit Basic Res*, 22, 95-106. doi:10.12659/msmbr.901142
- Ryu, J., Kim, H. J., Chang, E.-J., Huang, H., Banno, Y., & Kim, H.-H. (2006). Sphingosine 1 - phosphate as a regulator of osteoclast differentiation and osteoclast - osteoblast coupling. *The EMBO Journal*, 25.
- Scanzello, C. R., & Goldring, S. R. (2012). The role of synovitis in osteoarthritis pathogenesis. *Bone*, 51 (2), 249-257. doi:10.1016/j.bone.2012.02.012
- Schacter, G. I., & Leslie, W. D. (2017). DXA-Based Measurements in Diabetes: Can They Predict Fracture Risk? *Calcif Tissue Int*, 100 (2), 150-164. doi:10.1007/s00223-016-0191-x
- Schinke, T., Liese, S., Priemel, M., Haberland, M., Schilling, A. F., Catala-Lehnen, P., . . . Amling, M. (2004). Decreased bone formation and osteopenia in mice lacking alpha-calcitonin gene-related peptide. *J Bone Miner Res*, 19 (12), 2049-2056. doi:10.1359/jbmr.040915
- Schuetz, P., Bolliger, R., Merker, M., Christ-Crain, M., Stolz, D., Tamm, M., . . . Mueller, B. (2018). Procalcitonin-guided antibiotic therapy algorithms for different types of acute respiratory infections based on previous trials. *Expert Rev Anti Infect Ther*, 16 (7), 555-564. doi:10.1080/14787210.2018.1496331
- Sexton, P. M., Christopoulos, G., Christopoulos, A., Nylen, E. S., Snider, R. H., Jr., & Becker, K. L. (2008). Procalcitonin has bioactivity at calcitonin receptor family complexes: potential mediator implications in sepsis. *Crit Care Med*, 36 (5), 1637-1640. doi:10.1097/CCM.0b013e318170a554
- Shah, V. N., Harrall, K. K., Shah, C. S., Gallo, T. L., Joshee, P., Snell-Bergeon, J. K., & Kohrt, W. M. (2017). Bone mineral density at femoral neck and lumbar spine in adults with type 1 diabetes: a meta-analysis and review of the literature. *Osteoporos Int*, 28 (9), 2601-2610. doi:10.1007/s00198-017-4097-x
- Shah, V. N., Shah, C. S., & Snell-Bergeon, J. K. (2015). Type 1 diabetes and risk of fracture: meta-analysis and review of the literature. *Diabet Med*, 32 (9), 1134-1142. doi:10.1111/dme.12734
- Silver, I. A., Murrills, R. J., & Etherington, D. J. (1988). Microelectrode studies on the acid microenvironment beneath adherent macrophages and osteoclasts. *Exp Cell Res*, 175 (2), 266-276. doi:10.1016/0014-4827 (88)90191-7
- Simonet, W. S., Lacey, D. L., Dunstan, C. R., Kelley, M., Chang, M. S., Lthy, R., . . . Boyle, W. J. (1997). Osteoprotegerin: a novel secreted protein involved in the regulation of bone density. *Cell*, 89 (2), 309-319. doi:10.1016/s0092-8674 (00)80209-3
- Smit, T. H., Burger, E. H., & Huyghe, J. M. (2002). A case for strain-induced fluid flow as a regulator of BMU-coupling and osteonal alignment. *J Bone Miner Res*, 17 (11), 2021-2029. doi:10.1359/jbmr.2002.17.11.2021
- Sondergaard, B. C., Catala-Lehnen, P., Huebner, A. K., Bay-Jensen, A. C., Schinke, T., Henriksen, K., . . . Karsdal, M. A. (2012). Mice over-expressing salmon calcitonin have strongly attenuated osteoarthritic histopathological changes after destabilization of the medial meniscus. *Osteoarthritis Cartilage*, 20 (2), 136-143. doi:10.1016/j.joca.2011.11.004
- Sondergaard, B. C., Wulf, H., Henriksen, K., Schaller, S., Oestergaard, S., Qvist, P., . . . Karsdal, M. A. (2006). Calcitonin directly attenuates collagen type II degradation by inhibition of matrix metalloproteinase expression and activity in articular

- chondrocytes. *Osteoarthritis Cartilage*, *14* (8), 759-768.
doi:10.1016/j.joca.2006.01.014
- Starup-Linde, J., Eriksen, S. A., Lykkeboe, S., Handberg, A., & Vestergaard, P. (2014). Biochemical markers of bone turnover in diabetes patients--a meta-analysis, and a methodological study on the effects of glucose on bone markers. *Osteoporos Int*, *25* (6), 1697-1708. doi:10.1007/s00198-014-2676-7
- Starup-Linde, J., Hygum, K., Harsløf, T., & Langdahl, B. (2019). Type 1 Diabetes and Bone Fragility: Links and Risks. *Diabetes Metab Syndr Obes*, *12*, 2539-2547.
doi:10.2147/dms0.S191091
- Takahashi, I., Takeda, K., Matsuzaki, T., Kuroki, H., & Hosono, M. (2021). Reduction of knee joint load suppresses cartilage degeneration, osteophyte formation, and synovitis in early-stage osteoarthritis using a post-traumatic rat model. *PLoS One*, *16* (7), e0254383. doi:10.1371/journal.pone.0254383
- Takano, S., Uchida, K., Inoue, G., Minatani, A., Miyagi, M., Aikawa, J., . . . Takaso, M. (2017). Increase and regulation of synovial calcitonin gene-related peptide expression in patients with painful knee osteoarthritis. *Journal of Pain Research*, *10*, 1099 - 1104.
- Tamura, T., Miyaura, C., Owan, I., & Suda, T. (1992). Mechanism of action of amylin in bone. *J Cell Physiol*, *153* (1), 6-14. doi:10.1002/jcp.1041530103
- Tatsumi, S., Ishii, K., Amizuka, N., Li, M., Kobayashi, T., Kohno, K., . . . Ikeda, K. (2007). Targeted ablation of osteocytes induces osteoporosis with defective mechanotransduction. *Cell Metab*, *5* (6), 464-475. doi:10.1016/j.cmet.2007.05.001
- Teodorescu, A. C., Martu, I., Teslaru, S., Kappenberg-Nitescu, D. C., Goriuc, A., Luchian, I., . . . Mârțu, S. (2019). Assessment of Salivary Levels of RANKL and OPG in Aggressive versus Chronic Periodontitis. *J Immunol Res*, *2019*, 6195258.
doi:10.1155/2019/6195258
- Tian, G., Zhang, G., & Tan, Y. H. (2013). Calcitonin gene-related peptide stimulates BMP-2 expression and the differentiation of human osteoblast-like cells in vitro. *Acta Pharmacol Sin*, *34* (11), 1467-1474. doi:10.1038/aps.2013.41
- Tolar, J., Teitelbaum, S. L., & Orchard, P. J. (2004). Osteopetrosis. *N Engl J Med*, *351* (27), 2839-2849. doi:10.1056/NEJMra040952
- Tu, Q., Valverde, P., & Chen, J. (2006). Osterix enhances proliferation and osteogenic potential of bone marrow stromal cells. *Biochem Biophys Res Commun*, *341* (4), 1257-1265. doi:10.1016/j.bbrc.2006.01.092
- Udagawa, N., Koide, M., Nakamura, M., Nakamichi, Y., Yamashita, T., Uehara, S., . . . Tsuda, E. (2021). Osteoclast differentiation by RANKL and OPG signaling pathways. *J Bone Miner Metab*, *39* (1), 19-26. doi:10.1007/s00774-020-01162-6
- Valentijn, K., Gutow, A. P., Troiano, N., Gundberg, C., Gilligan, J. P., & Vignery, A. (1997). Effects of calcitonin gene-related peptide on bone turnover in ovariectomized rats. *Bone*, *21* (3), 269-274. doi:10.1016/s8756-3282(97)00142-7
- Valentijn, K. M., Gutow, A. P., Troiano, N. W., Gundberg, C. M., Gilligan, J. P., & Vignery, A. s. (1997). Effects of calcitonin gene-related peptide on bone turnover in ovariectomized rats. *Bone*, *21* 3, 269-274.
- Vestergaard, P. (2007). Discrepancies in bone mineral density and fracture risk in patients with type 1 and type 2 diabetes--a meta-analysis. *Osteoporos Int*, *18* (4), 427-444.
doi:10.1007/s00198-006-0253-4
- Vilaca, T., Schini, M., Harnan, S., Sutton, A., Poku, E., Allen, I. E., . . . Eastell, R. (2020). The risk of hip and non-vertebral fractures in type 1 and type 2 diabetes: A systematic review and meta-analysis update. *Bone*, *137*, 115457.
doi:<https://doi.org/10.1016/j.bone.2020.115457>

- Villa, I., Rubinacci, A., Ravasi, F., Ferrara, A. F., & Guidobono, F. (1997). Effects of amylin on human osteoblast-like cells. *Peptides*, *18* (4), 537-540. doi:10.1016/s0196-9781(97)00056-9
- Wacker, C., Prkno, A., Brunkhorst, F. M., & Schlattmann, P. (2013). Procalcitonin as a diagnostic marker for sepsis: a systematic review and meta-analysis. *Lancet Infect Dis*, *13* (5), 426-435. doi:10.1016/s1473-3099(12)70323-7
- Wakita, T., Mogi, M., Kurita, K., Kuzushima, M., & Togari, A. (2006). Increase in RANKL: OPG ratio in synovia of patients with temporomandibular joint disorder. *J Dent Res*, *85* (7), 627-632. doi:10.1177/154405910608500709
- Walsh, D. A., Mapp, P. I., & Kelly, S. (2015). Calcitonin gene-related peptide in the joint: contributions to pain and inflammation. *Br J Clin Pharmacol*, *80* (5), 965-978. doi:10.1111/bcp.12669
- Wang, H., Ba, Y., Xing, Q., & Du, J.-L. (2019). Diabetes mellitus and the risk of fractures at specific sites: a meta-analysis. *9* (1), e024067. doi:10.1136/bmjopen-2018-024067 %J BMJ Open
- Wang, L., Shi, X., Zhao, R., Halloran, B. P., Clark, D. J., Jacobs, C. R., & Kingery, W. S. (2010). Calcitonin-gene-related peptide stimulates stromal cell osteogenic differentiation and inhibits RANKL induced NF-kappaB activation, osteoclastogenesis and bone resorption. *Bone*, *46* (5), 1369-1379. doi:10.1016/j.bone.2009.11.029
- Wang, M., Tan, G., Jiang, H., Liu, A., Wu, R., Li, J., . . . Shi, D. (2022). Molecular crosstalk between articular cartilage, meniscus, synovium, and subchondral bone in osteoarthritis. *Bone Joint Res*, *11* (12), 862-872. doi:10.1302/2046-3758.1112.Bjr-2022-0215.R1
- Wang, X. J., Bai, X., Miu, Y., Chen, P., Yan, P. J., & Jiang, C. X. (2023). The assessment value of pathological condition of serum adiponectin and amylin in primary osteoporosis and its correlation analysis with bone metabolism indexes. *J Med Biochem*, *42* (1), 86-93. doi:10.5937/jomb0-35877
- Watts, N. B., Bilezikian, J. P., Usiskin, K., Edwards, R., Desai, M., Law, G., & Meininger, G. (2016). Effects of Canagliflozin on Fracture Risk in Patients With Type 2 Diabetes Mellitus. *The Journal of Clinical Endocrinology & Metabolism*, *101* (1), 157-166. doi:10.1210/jc.2015-3167
- Wee, N. K. Y., Novak, S., Ghosh, D., Root, S. H., Dickerson, I. M., & Kalajzic, I. (2023). Inhibition of CGRP signaling impairs fracture healing in mice. *J Orthop Res*, *41* (6), 1228-1239. doi:10.1002/jor.25474
- Wei, J. X., Verity, A., Garle, M., Mahajan, R., & Wilson, V. (2008). Examination of the effect of procalcitonin on human leucocytes and the porcine isolated coronary artery. *Br J Anaesth*, *100* (5), 612-621. doi:10.1093/bja/aen073
- Wen, Z.-H., Tang, C.-C., Chang, Y. C., Huang, S.-Y., Lin, Y.-Y., Hsieh, S.-P., . . . Jean, Y. H. (2016). Calcitonin attenuates cartilage degeneration and nociception in an experimental rat model of osteoarthritis: role of TGF- β in chondrocytes. *Sci Rep*, *6*.
- Whittaker, J. L., Woodhouse, L. J., Nettel-Aguirre, A., & Emery, C. A. (2015). Outcomes associated with early post-traumatic osteoarthritis and other negative health consequences 3-10 years following knee joint injury in youth sport. *Osteoarthritis Cartilage*, *23* (7), 1122-1129. doi:10.1016/j.joca.2015.02.021
- Wong, P. K., Egan, P. J., Croker, B. A., O'Donnell, K., Sims, N. A., Drake, S., . . . Wicks, I. P. (2006). SOCS-3 negatively regulates innate and adaptive immune mechanisms in acute IL-1-dependent inflammatory arthritis. *J Clin Invest*, *116* (6), 1571-1581. doi:10.1172/jci25660
- Wronski, T. J., Cintrón, M., & Dann, L. M. (1988). Temporal relationship between bone loss and increased bone turnover in ovariectomized rats. *Calcif Tissue Int*, *43* (3), 179-183. doi:10.1007/bf02571317

- Yang, X., Mostafa, A. J., Appleford, M., Sun, L. W., & Wang, X. (2016). Bone Formation is Affected by Matrix Advanced Glycation End Products (AGEs) In Vivo. *Calcif Tissue Int*, 99 (4), 373-383. doi:10.1007/s00223-016-0153-3
- Yang, Y., Huang, Y., Zhang, L., & Zhang, C. (2016). Transcriptional regulation of bone sialoprotein gene expression by Osx. *Biochem Biophys Res Commun*, 476 (4), 574-579. doi:10.1016/j.bbrc.2016.05.164
- Yasuda, H., Shima, N., Nakagawa, N., Yamaguchi, K., Kinosaki, M., Mochizuki, S., . . . Suda, T. (1998). Osteoclast differentiation factor is a ligand for osteoprotegerin/osteoclastogenesis-inhibitory factor and is identical to TRANCE/RANKL. *Proc Natl Acad Sci U S A*, 95 (7), 3597-3602. doi:10.1073/pnas.95.7.3597
- Yuan, Y., Chen, X., Zhang, L., Wu, J., Guo, J., Zou, D., . . . Zou, J. (2016). The roles of exercise in bone remodeling and in prevention and treatment of osteoporosis. *Prog Biophys Mol Biol*, 122 (2), 122-130. doi:10.1016/j.pbiomolbio.2015.11.005
- Zaki, S., Blaker, C. L., & Little, C. B. (2022). OA foundations - experimental models of osteoarthritis. *Osteoarthritis Cartilage*, 30 (3), 357-380. doi:10.1016/j.joca.2021.03.024
- Zhang, S., Li, T., Feng, Y., Zhang, K., Zou, J., Weng, X., . . . Zhang, L. (2023). Exercise improves subchondral bone microenvironment through regulating bone-cartilage crosstalk. *Front Endocrinol (Lausanne)*, 14, 1159393. doi:10.3389/fendo.2023.1159393
- Zheng, S., Li, W., Xu, M., Bai, X., Zhou, Z., Han, J., . . . Wang, X. (2010). Calcitonin gene-related peptide promotes angiogenesis via AMP-activated protein kinase. *Am J Physiol Cell Physiol*, 299 (6), C1485-1492. doi:10.1152/ajpcell.00173.2010
- Zhou, H., Chernenky, R., & Davies, J. E. (1994). Deposition of cement at reversal lines in rat femoral bone. *J Bone Miner Res*, 9 (3), 367-374. doi:10.1002/jbmr.5650090311

10. Acknowledgements

I hereby would like to express my deepest gratitude to the individuals who in one way or another contributed and extended their valuable assistance in the preparation and completion of this study.

First of all, I sincerely appreciate my supervisor Prof. Dr. Dr. Johannes Keller, who offered me great opportunities to study in Germany and work on these fantastic projects. His mentoring is of great value in guiding me through my academic journey. He also supported me to present my work at several international congresses, which allowed me to exchange ideas with excellent researchers around the world. It has been truly a pleasure and an honor to have Prof. Keller as my supervisor. I also would like to express my deepest gratitude to my co-supervisor Dr. Anke Baranowsky, who showed me all the experiment details with great patience, helped me organize my projects and managed all the different aspects of the experiments. In addition, I would like to thank Prof. Dr. Karl-Heinz Frosch for the opportunity to prepare this work at the Department of Trauma and Orthopedic Surgery. Furthermore, special thanks to Michael Amling for the substantial support from the Department of Osteology and Biomechanics.

I am immensely proud to be a part of our outstanding team at Experimentelle Unfallchirurgie. The atmosphere within our group is always motivating and uplifting. We actively support each other with experiments and exchange scientific insights and ideas. Moreover, my colleagues have provided me with massive help for my daily life in Germany, broadening my perspective of different cultures and making me feel more at ease during my life abroad. I am very happy to work with them and enjoy the nice time together.

Finally, many thanks also to my parents and family, it was a hard decision to go abroad but your supports have made me invincible. Special thanks to my girlfriend Xinyue Wang and all my friends for their maximal support. Cheers!

11. Curriculum Vitae

Personal information

Name: **Shan Jiang**

Date of birth: 23.04.1993

Place of birth: Zibo, China

Academic career

11/2019-07/2023	PhD promotion in Experimental Trauma Surgery, Department of Trauma and Orthopedic Surgery, University Medical Center Hamburg-Eppendorf, Hamburg, Germany
09/2016-06/2019	Research Assistant, Lingnan Medical Research Center, The First Affiliated Hospital of Guangzhou University of Chinese, Guangzhou, China

Education background

11/2019-07/2023	Non-Medical PhD program, UKE, University of Hamburg, Hamburg, Germany
09/2016-06/2019	Graduate program of Chinese Medicine (Orthopedics), Guangzhou University of Chinese Medicine, Guangzhou, China
09/2011-06/2016	Bachelor's degree of Chinese Medicine, Guangzhou University of Chinese Medicine, Guangzhou, China

Publications

1. Xie W, **Jiang S**, Donat A, Knapstein PR, Albertsen LC, Kokot JL, Erdmann C, Rolvien T, Frosch KH, Baranowsky A, et al. Tranexamic Acid Attenuates the Progression of Posttraumatic Osteoarthritis in Mice. *Am J Sports Med* 2024: 3635465231220855.
2. Xie W, Donat A, **Jiang S**, Baranowsky A, Keller J. The emerging role of tranexamic acid and its principal target, plasminogen, in skeletal health. *Acta Pharmaceutica Sinica B* 2024.
3. **Jiang S**, Xie W, Knapstein PR, Donat A, Albertsen LC, Sevecke J, Erdmann C, Appelt J, Fuchs M, Hildebrandt A, et al. Transcript-dependent effects of the CALCA gene on the progression of post-traumatic osteoarthritis in mice. *Commun Biol* 2024; 7: 223.

4. Jahn D, Knapstein PR, Otto E, Köhli P, Sevecke J, Graef F, Graffmann C, Fuchs M, **Jiang S**, Rickert M, et al. Increased β (2)-adrenergic signaling promotes fracture healing through callus neovascularization in mice. *Sci Transl Med* 2024; 16: eadk9129.
5. Brylka LJ, Alimy AR, Tschaffon-Müller MEA, **Jiang S**, Ballhause TM, Baranowsky A, von Kroge S, Delsmann J, Pawlus E, Eghbalian K, et al. Piezo1 expression in chondrocytes controls endochondral ossification and osteoarthritis development. *Bone Res* 2024; 12: 12.
6. Maleitzke T, Dietrich T, Hildebrandt A, Weber J, Appelt J, Jahn D, Otto E, Zocholl D, **Jiang S**, Baranowsky A, et al. Inactivation of the gene encoding procalcitonin prevents antibody-mediated arthritis. *Inflamm Res* 2023; 72: 1069-1081.
7. Hildebrandt A, Dietrich T, Weber J, Günderoth MM, Zhou S, Fleckenstein FN, **Jiang S**, Winkler T, Duda GN, Tsitsilonis S, et al. The dual pro-inflammatory and bone-protective role of calcitonin gene-related peptide alpha in age-related osteoarthritis. *Arthritis Res Ther* 2023; 25: 244.
8. Donat A, **Jiang S**, Xie W, Knapstein PR, Albertsen LC, Kokot JL, Sevecke J, Augustin R, Jahn D, Yorgan TA, et al. The selective norepinephrine reuptake inhibitor reboxetine promotes late-stage fracture healing in mice. *iScience* 2023; 26: 107761.
9. Ballhause TM[#], **Jiang S**[#], Xie W, Sevecke J, Dowling C, Dust T, Brandt S, Mertens PR, Yorgan TA, Schinke T, et al. Fracture healing in a mouse model of Hajdu-Cheney-Syndromewith high turnover osteopenia results in decreased biomechanical stability. *Sci Rep* 2023; 13: 11418.
10. Messerer DAC, Datzmann T, Baranowsky A, Peschel L, Hoffmann A, Gröger M, Amling M, Wepler M, Nussbaum BL, **Jiang S**, et al. Systemic calcitonin gene-related peptide receptor antagonism decreases survival in a porcine model of polymicrobial sepsis: blinded randomised controlled trial. *Br J Anaesth* 2022; 128: 864-873.

11. Grewe JM, Knapstein PR, Donat A, **Jiang S**, Smit DJ, Xie W, Keller J. The role of sphingosine-1-phosphate in bone remodeling and osteoporosis. *Bone Res* 2022; 10: 34.
12. Baranowsky A, Jahn D, **Jiang S**, Yorgan T, Ludewig P, Appelt J, Albrecht KK, Otto E, Knapstein P, Donat A, et al. Procalcitonin is expressed in osteoblasts and limits bone resorption through inhibition of macrophage migration during intermittent PTH treatment. *Bone Res* 2022; 10: 9.
13. **Jiang S**, Knapstein P, Donat A, Tsitsilonis S, Keller J. An optimized protocol for a standardized, femoral osteotomy model to study fracture healing in mice. *STAR Protoc* 2021; 2: 100798.
14. Donat A, Knapstein PR, **Jiang S**, Baranowsky A, Ballhause TM, Frosch KH, Keller J. Glucose Metabolism in Osteoblasts in Healthy and Pathophysiological Conditions. *Int J Mol Sci* 2021; 22.
15. Baranowsky A, Appelt J, Tseneva K, **Jiang S**, Jahn D, Tsitsilonis S, Frosch KH, Keller J. Tranexamic Acid Promotes Murine Bone Marrow-Derived Osteoblast Proliferation and Inhibits Osteoclast Formation In Vitro. *Int J Mol Sci* 2021; 22.
16. Ballhause TM[#], **Jiang S**[#], Baranowsky A, Brandt S, Mertens PR, Frosch KH, Yorgan T, Keller J. Relevance of Notch Signaling for Bone Metabolism and Regeneration. *Int J Mol Sci* 2021; 22.
17. Appelt J, Tsitsilonis S, Otto E, Jahn D, Köhli P, Baranowsky A, **Jiang S**, Fuchs M, Bucher CH, Duda GN, et al. Mice Lacking the Calcitonin Receptor Do Not Display Improved Bone Healing. *Cells* 2021; 10.

(# co-first authors)

12. Eidesstattliche Erklärung

Ich versichere ausdrücklich, dass ich die Arbeit selbständig und ohne fremde Hilfe verfasst, andere als die von mir angegebenen Quellen und Hilfsmittel nicht benutzt und die aus den benutzten Werken wörtlich oder inhaltlich entnommenen Stellen einzeln nach Ausgabe (Auflage und Jahr des Erscheinens), Band und Seite des benutzten Werkes kenntlich gemacht habe.

Ferner versichere ich, dass ich die Dissertation bisher nicht einem Fachvertreter an einer anderen Hochschule zur Überprüfung vorgelegt oder mich anderweitig um Zulassung zur Promotion beworben habe.

Ich erkläre mich einverstanden, dass meine Dissertation vom Dekanat der Medizinischen Fakultät mit einer gängigen Software zur Erkennung von Plagiaten überprüft werden kann.

Unterschrift: